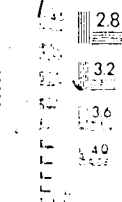


1



Mercid



National Library
of Canada

Bibliothèque nationale
du Canada

Canadian Theses Service

Service des thèses canadiennes

Ottawa, Canada
K1A 0N4

NOTICE

The quality of this microform is heavily dependent upon the quality of the original thesis submitted for microfilming. Every effort has been made to ensure the highest quality of reproduction possible.

If pages are missing, contact the university which granted the degree.

Some pages may have indistinct print especially if the original pages were typed with a poor typewriter ribbon or if the university sent us an inferior photocopy.

Previously copyrighted materials (journal articles, published tests, etc.) are not filmed.

Reproduction in full or in part of this microform is governed by the Canadian Copyright Act, R.S.C. 1970, c. C-30.

AVIS

La qualité de cette microforme dépend grandement de la qualité de la thèse soumise au microfilmage. Nous avons tout fait pour assurer une qualité supérieure de reproduction.

S'il manque des pages, veuillez communiquer avec l'université qui a conféré le grade.

La qualité d'impression de certaines pages peut laisser à désirer, surtout si les pages originales ont été dactylographiées à l'aide d'un ruban usé ou si l'université nous a fait parvenir une photocopie de qualité inférieure.

Les documents qui font déjà l'objet d'un droit d'auteur (articles de revue, tests publiés, etc.) ne sont pas microfilmés.

La reproduction, même partielle, de cette microforme est soumise à la Loi canadienne sur le droit d'auteur, 1970, c. C-30.

THE UNIVERSITY OF ALBERTA

MAGNETIC STABILIZATION OF LASER GAS DISCHARGES

by

RAJENDER RAZDAN

A THESIS

SUBMITTED TO THE FACULTY OF GRADUATE STUDIES AND RESEARCH
IN PARTIAL FULFILMENT OF THE REQUIREMENTS FOR THE DEGREE
OF DOCTOR OF PHILOSOPHY

DEPARTMENT OF ELECTRICAL ENGINEERING

EDMONTON, ALBERTA

Fall 1987

Permission has been granted to the National Library of Canada to microfilm this thesis and to lend or sell copies of the film.

The author (copyright owner) has reserved other publication rights, and neither the thesis nor extensive extracts from it may be printed or otherwise reproduced without his/her written permission.

L'autorisation a été accordée à la Bibliothèque nationale du Canada de microfilmer cette thèse et de prêter ou de vendre des exemplaires du film.

L'auteur (titulaire du droit d'auteur) se réserve les autres droits de publication; ni la thèse ni de longs extraits de celle-ci ne doivent être imprimés ou autrement reproduits sans son autorisation écrite.

ISBN 0-315-41058-2

THE UNIVERSITY OF ALBERTA

RELEASE FORM

NAME OF AUTHOR : RAJENDER RAZDAN
TITLE OF THESIS : MAGNETIC STABILIZATION OF LASER GAS DISCHARGES
DEGREE FOR WHICH THESIS WAS PRESENTED : DOCTOR OF PHILOSOPHY
YEAR THIS DEGREE GRANTED : Fall 1987

Permission is hereby granted to THE UNIVERSITY OF ALBERTA LIBRARY to reproduce single copies of this thesis and to lend or sell such copies for private, scholarly or scientific research purposes only.

The author reserves other publication rights, and neither the thesis nor extensive extracts from it may be printed or otherwise reproduced without the author's written permission.

(SIGNED)

PERMANENT ADDRESS:

Rajender Razdan
.....
c/o DR. H. RAZDAN

.....
NRL, ZAKURA

.....
SRINAGAR, KASHMIR

.....
INDIA 190006

DATED *May 11* 1987

THE UNIVERSITY OF ALBERTA
FACULTY OF GRADUATE STUDIES AND RESEARCH

The undersigned certify that they have read, and recommend to the Faculty of Graduate Studies and Research, for acceptance, a thesis entitled MAGNETIC STABILIZATION OF LASER GAS DISCHARGES submitted by RAJENDER RAZIDAN in partial fulfilment of the requirements for the degree of DOCTOR OF PHILOSOPHY.

P. P. Casjani

Supervisor

M. J. ...

Supervisor

J. ...

M. J. ...

External Examiner

Date... May 11, 1987.....

DEDICATION

*To my mother and father who encouraged me to follow the path of knowledge and to my gurus
who guided me along the way.*

ABSTRACT

Many techniques have been used over the years to enhance the stability of CO₂ laser discharges and thereby increase their power output. These include the use of rapid gas flow, external ionization sources and multi-element electrode systems. A new technique, using magnetic stabilization, has recently received attention and has been shown to enhance laser discharge performance. The mechanism of stabilization was initially believed to be due to a bulk gas motion, but recent experiments and computer simulations seem to suggest that other mechanisms play a greater role.

It is the purpose of the present research to gain a better understanding of the magnetic stabilization mechanism, in order that the technique be more fruitfully utilized in practical systems. In this thesis, the CO₂ laser gas discharge has been simulated taking into account the influence of external magnetic and electric fields. The Monte Carlo technique, suitable for analyzing large number of particles, has been employed. This involves following the three dimensional trajectories of electrons and ions, taking into account anisotropic scattering collisions. Instead of calculating the phase space parameters at regularly spaced grid points, or alternatively at regular time intervals, a new approach has been used in this thesis to describe inelastic scattering within a nonuniform space-charge sheath of a magnetized cathode fall region. The particle trajectories are determined using a hybrid analytical-computational technique, whereby the phase space points are calculated only at the points of collision. This approach results in a reduction in the number of computations and is more accurate; since round-off errors are reduced.

The technique described above, has been used to model the cathode fall region of a glow discharge, for gases such as He, N₂ and CO₂, and at pressures of 5, 10 and 30 torr. A mixture of these gases, at pressures typical of high power CO₂ lasers, has also been studied. The results show that cathode glow electrons move a considerable distance in the Hall ($\vec{J} \times \vec{B}$) direction, transverse to the electric field. This motion results in secondary ionizations which are far from their origin. The magnetic field, therefore, effectively sweeps these charge

carriers through distances which are several orders of magnitude greater than typical instability scale sizes; thereby effectively reducing instability growth. These results confirm experimental observations that modest strength magnetic fields can indeed be used to enhance the stability of laser gas discharges.

It is hoped that the increased understanding of gas discharge physics and magnetic stabilization processes, gained from the work in this thesis, will help in the development of new, higher efficiency electrode designs for higher power laser systems.

ACKNOWLEDGEMENTS

The author extends his appreciation to all the people who have, in some way or the other, helped in the completion of this thesis. A special note of gratitude is extended to the author's supervisors, Mr. Herb Seguin and Dr. Clarence Capjack, who initially suggested this project and provided invaluable guidance. Their kindness, enthusiasm, encouragement and stimulating discussions have helped immensely.

To all the members of the laser research group, the author gives his sincere thanks for their many helpful suggestions and interesting discussions. In particular, it has been a great pleasure interacting with fellow co-workers: Mr. Ron Willis, Dr. Vern Seguin, Dr. Suwas Nikumb, Dr. Ashish Nath, Mr. Andrew Labun, Mr. Walter Bilida, Mr. Warren Finlay and Dr. Farouk Soliman. The author has also shared many enjoyable moments with the laboratory technicians: Mr. Hugo Reshef, Mr. Vladimir Pohnert and Mr. Don Presakarchuk. To all these people, the author would like to offer his warm, heart-felt appreciation.

The financial support of the Electrical Engineering department and the Students Awards Office at the University of Alberta and the funding of the National Research Council are all gratefully acknowledged.

Finally, the author would like to express his deepest appreciation to his entire family and his friends, for their patience and encouragement during the course of these studies. A special note of gratitude is in order to the author's wife, Pamposh, who provided constant moral support and encouragement; and to the author's mother and father whose foresight and sacrifices enabled the author to continue his education to this point. To all of them the author will forever be indebted.

Table of Contents

<u>Chapter</u>		<u>Page</u>
1.	INTRODUCTION	1
1.1	PROJECT MOTIVATION	1
1.2	HISTORICAL REVIEW	3
1.2.1	CO ₂ Laser Discovery	3
1.2.2	Gas-cooling Techniques	3
1.2.3	High-Pressure Lasers	4
1.2.4	Pre-Ionization Techniques	8
1.2.5	Other Major Developments	8
1.3	EXCITATION MECHANISMS IN THE CO ₂ LASER	9
1.3.1	Transition States for a CO ₂ molecule	9
1.3.2	Role of Nitrogen	12
1.3.3	Role of Helium	12
1.3.4	The Lasing Process	13
1.3.5	Relaxation Processes	14
1.4	GAS-DISCHARGE PROCESS	14
1.4.1	The Glow Discharge	17
1.4.2	Instability Formation	22
1.4.3	Auxillary Ionization	25
1.4.4	Co-Axial Discharges	28
1.4.5	Mag. Field Stabilization	30
2.	DISCHARGE INSTABILITY ANALYSIS	35
2.1	INTRODUCTION	35
2.2	STEADY STATE CONDITIONS	38
2.2.1	Self Sustained Discharge: No Detachment	39
2.2.2	Self Sustained Discharge: Strong Detachment	41
2.2.3	Externally Sustained Discharge	41

2.3	GLOW DISCHARGE INSTABILITIES	42
2.3.1	Striations	42
2.3.2	Thermal Instabilities	45
2.4	CONCLUSION	50
3.	MONTE CARLO SIMULATION OF MAGNETIC FIELD EFFECT ON GROWTH OF INSTABILITIES IN LASER GASES	53
3.1	INTRODUCTION	53
3.2	MODELLING CONSIDERATIONS	54
3.3	THE SIMULATION ALGORITHM	55
3.3.1	Tracking Electron Motion	56
3.3.2	Determination of electron path length	58
3.3.3	Determination of electron motion between collisions	58
3.3.4	Determination of collision type	60
3.3.5	Determining Scattering Parameters	70
3.3.6	Termination Parameters	74
3.3.7	Motion of Ions	74
3.4	RESULTS	76
4.	SUMMARY AND CONCLUSIONS	92
4.1	Summary of thesis	92
4.2	Results	93
4.3	Future Considerations	94
	REFERENCES	98
	APPENDIX I: DIRECTION OF AN ELECTRON AFTER SCATTERING	106
	APPENDIX II: LISTING OF THE PROGRAM MAGSIM	108

List of Tables

Table	Page
3.1 References used for the Various Cross Sections of Helium, Nitrogen and Carbon-Dioxide.	61
3.2 Differential cross-sections ($d\sigma/d\Omega$), for elastic electron-helium scattering. The units of ($d\sigma/d\Omega$) are $10^{-18} \text{ cm}^2/\text{s}$ [54].	66
3.3 Differential cross-sections ($d\sigma/d\Omega$), for elastic electron-nitrogen scattering. The units of ($d\sigma/d\Omega$) are $10^{-18} \text{ cm}^2/\text{s}$ [56].	67
3.4 Differential cross-sections ($d\sigma/d\Omega$), for elastic electron-carbon dioxide scattering. ($d\sigma/d\Omega$) are in arbitrary units [63].	68
3.5 Swarm parameters for Helium, Nitrogen, Carbon-Dioxide and CO_2 laser mixture gas discharges at various magnetic fields and pressures.	78

List of Figures

<u>Figure</u>	<u>Page</u>
1.1 Resistive pin cathode TEA laser used by Beaulieu [8].	6
1.2 LaFlamme's double discharge TEA laser configuration [11].	6
1.3 Energy level diagram of the CO ₂ :N ₂ :He laser.	11
1.4 Schematic diagram of a self-sustained pumped laser apparatus.	16
1.5 Typical V-I characteristics for a gas discharge [17].	16
1.6 Regions of a gas discharge. The luminous zones are shown shaded [17].	18
1.7 Calculated ionization and attachment coefficients vs. E/N. The E/N units are Townsends (1 Td = 10 ⁻¹⁷ V/cm ²).	21
1.8 (a) Schematic of a coaxial CO ₂ laser and (b) Cross-sectional diagram of the coaxial laser [38].	29
1.9 Schematic of gas flow channel, electrical discharge and transverse magnetic field in a magnetically stabilized CO ₂ laser [39].	32
1.10 Magnetically stabilized transverse discharge CO ₂ laser structure used by Capjack <i>et. al.</i> [41].	33
1.11 Magnetically stabilized co-axial discharge CO ₂ laser structure used by Seguin <i>et. al.</i> [40].	33
2.1 Comparison of ionization, attachment and recombination coefficients for a typical CO ₂ laser discharge.	40
2.2 Ionization instability boundary computed by Nighan and Wiegand [43] for a 20-Torr CO ₂ :N ₂ :He = 1:7:12 mixture. The electron density, n _e and CO fraction, f, are the variable parameters from which the negative-ion concentration n _n /n _e , the electron temperature T _e , and the stability criteria are computed.	46
2.3 Fractional response of the electron density to a perturbation in gas density computed for a 20 Torr CO ₂ -N ₂ -He (1:7:12) mixture. From Nighan and Wiegand [27].	49
2.4 Computed thermal instability growth time in the direction normal to the direction of J and E ($\phi = 90^\circ$) for a self sustained CO ₂ -N ₂ -He (1:7:12) laser discharge at a gas temperature of 300°K (From Nighan and Wiegand [27]).	51
3.1 Electron phase-space co-ordinate system. The magnetic field is assumed to have only an x-component. (a) Space co-ordinates. (b) Velocity co-ordinates.	57
3.2 Various collisional cross-sections for Helium [64].	63

3.3	Various collisional cross-sections for Nitrogen [46].	64
3.4	Various collisional cross-sections for Carbon Dioxide [46].	65
3.5	Scattering probability densities for electrons in Helium, for energies ranging from 0 eV to 100 eV. The cross-sections are in units of 10^{-18} cm ² /s.	71
3.6	Cumulative distribution function for scattering of electrons in different gas species for energies between 0 and 100 eV: (a) Helium gas (b) Nitrogen gas (c) Carbon-Dioxide gas	73
3.7	Flowchart of the Monte-Carlo simulation program	75
3.8	Discharge parameters for a 10 Torr Helium discharge with a magnetic field of 500 Gauss (a) Position of ions formed as a result of ionization from primary and secondary electrons. (b) Discharge velocity distribution in the $\vec{E} \times \vec{B}$ direction (i.e. y direction).	82
3.9	Histogram of the transverse discharge velocity distribution	83
3.10	Plot of transverse discharge velocity as a function of the applied magnetic field for a Helium gas discharge at 5, 10 and 30 Torr.	86
3.11	Plot of transverse discharge velocity as a function of the applied magnetic field for a Nitrogen gas discharge at 5, 10 and 30 Torr.	87
3.12	Plot of transverse discharge velocity as a function of the applied magnetic field for a Carbon-Dioxide gas discharge at 5, 10 and 30 Torr.	88
3.13	Plot of transverse discharge velocity as a function of the applied magnetic field for a CO ₂ Laser gas discharge at 30 Torr.	89
3.14	Variation of Lorentz mixing velocity with total gas pressure for a typical medium pressure CO ₂ laser mixture assuming a magnetic field strength of 500 Gauss	90

CHAPTER I

INTRODUCTION

1.1 PROJECT MOTIVATION

The carbon dioxide laser is today one of the most widely used industrial gas lasers. The reason for this is that the CO₂ laser possesses a number of distinct advantages over most other laser devices; the two most important of these being, their high conversion efficiency and their capability for continuous high power operation.

In particular, whereas most laser efficiencies are measured in the range of 1% or less, the CO₂ laser's efficiency is regularly specified in the 10% category. Also, the CO₂ laser has achieved, by far, the highest continuous average power output; reaching well into the 20 kW range.

Some additional features possessed by the CO₂ laser systems are as follows: the capability for very short pulse operation; good frequency stability and narrow linewidth; long lifetime; the feasibility of Q switched operation; the possibility of many different pumping schemes and ease of operation over a wide range of pressures.

These, and many other equally desirable operational characteristics, have translated into numerous scientific and industrial applications, some of these being; welding, cutting, cladding, heat treatment, isotope separation, medical surgery, communications and weaponry.

Over the last decade, considerable research has been undertaken to increase the output power, and thus the usefulness, of these CO₂ laser systems. Such work has generally involved some method of increasing the electrical power input to the device. Unfortunately, experience has shown that at elevated input power densities, electro-thermal instabilities invariably become manifest; often resulting in glow-to-arc transitions that effectively terminate laser action. As a consequence, these instability problems have gradually become the focus of large scale investigations world wide.

One of the more recently proposed methods to circumvent these difficulties in gas lasers is the use of magnetic field discharge stabilization. Lasers utilizing external magnetic fields have already been built and have proven to be excellent in providing a highly stable discharge at acceptable power loading and within a reasonable size system. Despite this early success, however, the exact mechanism of magnetic stabilization has not been clearly understood. Consequently, the full potential of the process has remained unexploited. This situation has persisted because previous laser discharge studies have been restricted to an analytical approach, using Boltzmann's equations. Experience has shown, however, that such methods are hopelessly complicated when inelastic collisions in nonuniform electric and magnetic fields have to be modelled. As a consequence of this fact, many of the essential aspects and important parameters of the magnetic stabilization process have remained undiscovered. In an effort to ameliorate this situation an alternative approach was developed. This method, which forms the subject matter of this thesis, investigates individual single particle motion within the laser discharge using the well known Monte Carlo simulation technique. In particular, in this work, the Monte Carlo technique has been applied to the cathode fall region of a laser gas discharge, taking into account both non-uniform electric fields and transverse magnetic fields. The results obtained, as a result of these more comprehensive and accurate simulations, provide a much better understanding and insight into the magnetic stabilization process.

This thesis, therefore, progresses in the following fashion: The first chapter gives a historical review of CO₂ lasers. Various excitation mechanisms are explained; with special emphasis given to gas discharge excitation. Chapter 2 describes the various instability modes inherent in laser gas discharges, and the methods used thus far, to overcome these instabilities. The magnetic stabilization process, used for reducing such instability growth, is explained in Chapter 3. A Monte Carlo simulation of a laser gas discharge, under the influence of transverse electric and magnetic fields is then presented. The results of these simulations, for various gases such as helium, nitrogen, carbon dioxide and a laser containing

a typical mixture of these three gases; are analyzed with respect to discharge stability. On the basis of these results, conclusions are drawn in Chapter 4, regarding the magnetic stabilization process. A detailed derivation of the direction of an electron after a scattering collision, is given in Appendix I. Finally, the code used in all these simulations, termed MAGSIM (short for magnetically stabilized laser simulation), has been listed in Appendix II.

1.2 HISTORICAL REVIEW

1.2.1 CO₂ Laser Discovery

The discovery, in 1961, by Javan and co-workers [1] of laser oscillations in a Helium-Neon glow discharge heralded the advent of gas lasers. This spurred research into other higher efficiency gas laser systems. In 1964, Patel [2] discovered laser action in the CO₂ molecule; producing the most important molecular laser operated thus far.

After the first report of cw laser action in a CO₂ discharge at 10.6 and 9.4 μm , by Patel, the next important development was the addition of N₂. This addition resulted in an increase in the average power output available with the system from a few milliwatts to several tens of watts [3]. Moeller and Rigden [4] subsequently showed that the laser's output power and efficiency could be still further increased by the addition of helium to the laser mixture. The exact mechanisms by which many of these important improvements were achieved were not, however, well understood in those early times.

1.2.2 Gas-cooling Techniques

During the early development of the CO₂ laser, it was soon documented that both the power and the efficiency of the laser could be increased by cooling the laser discharge. Subsequent investigations revealed that the removal of waste heat was necessary to prevent the gas mixture from overheating; which would in turn populate the lower vibrational levels of the CO₂ molecule and thus 'thermally bottle-neck' the lasing process. Early cooling techniques

involved the circulation of cold air or water through cooling jackets to remove the waste heat through conduction across the outer jacket walls. Forced air cooling and water cooling of the discharge tube were utilized by Moeller and Rigden [4] and Patel *et. al.* [5]. The use of fast-flowing gas, to provide convective cooling in CO₂ lasers, was first reported by Deutsch *et. al.* [6] in 1969. This form of convective cooling was soon demonstrated to be much more effective than the earlier diffusion cooling used in sealed and slow-flow systems. As a result of the improved cooling of the laser plasma, the output power per unit length of the laser increased by several orders of magnitude, and made possible for the first time, multikilowatt electrically excited lasers of reasonable size.

1.2.3 High-Pressure Lasers

All early CO₂ lasers operated at low gas pressures. Subsequently, higher pressure lasers were developed, so as to provide a higher density of lasing molecules within the optical cavity. These high-pressure CO₂ devices thereby generated considerably higher output powers as compared to similar sized low-pressure devices. In general, large volume atmospheric pressure lasers were found to be easier to construct than large volume low-pressure lasers; because they did not have to be as well sealed or capable of withstanding the large pressure differentials typical of low pressure devices. Unfortunately however, experience soon revealed that higher pressure discharges were much more difficult to produce than those at low pressure.

Numerous tests have established the fact that the excitation efficiency of CO₂ lasers is maximum at an electric field to pressure ratio (E/p) of 10 to 50 V/torr-cm, and falls rapidly away from this optimum E/p value. Effective high pressure operation, therefore, meant working with very high voltages; particularly for longitudinally excited plasmas. For a 1 m. discharge at 800 torr, voltages on the order of 10⁵ to 10⁶ V were necessary for the proper operation of the laser. Since C.W. discharges at such high pressures are difficult to maintain, without the discharge degenerating into an arc, high pressure CO₂ lasers have generally operated under pulse mode conditions. In addition, voltages in the MV region are much easier

to obtain under pulsed conditions. To lessen the requirements for such extremely high applied voltages, French and Canadian scientists introduced the concept of transverse excitation (*i.e.* a discharge across the laser tube rather than along the axis of the laser device). This arrangement reduces the electrode spacing from meters, as is typical in axially excited lasers, to centimeter dimensions. These *transversely excited atmospheric* pressure lasers have come to be known as TEA lasers.

A high-pressure (450-torr) pulsed CO₂ laser was first reported by Dumanchin and Rocca-Serra [7] in Nov. 1969 and atmospheric pressure operation was reported by Beaulieu [8] in June 1970. Most of the early TEA-CO₂ lasers used an excitation technique which was originally developed by Beaulieu. This technique involved the use of very short high-voltage pulses applied to a transverse discharge electrode structure [9-11]. The electrode system consisted of a long tubular anode, spaced by a few centimeters from an array of carbon resistors, which served as the cathode. When a high voltage, short rise time electrical pulse of short duration is applied to this electrode structure, there results a shower or conical shaped brush discharge emanating simultaneously out from each resistor-cathode. As a consequence, the excited volume becomes a linear array of overlapping discharges, as shown in Fig. 1.1.

As the pressure of the gases is increased in the TEA-laser described above, a transition point is reached when the uniform glow constricts into a narrow arc. Such a transition is marked by an increase in the plasma current, a decrease in the voltage drop across the gas and the appearance of a bright white arc in the discharge. The voltage collapse that occurs when an arc forms effectively terminates laser pumping. Effective laser pumping occurs when the E/p ratio is fairly high, a condition satisfied by the laser plasma only when it operates in a uniform glow mode. The formation of an arc, however, takes a characteristic finite time. The simple excitation method used by Beaulieu avoided the problem of arc-formation by arranging that the discharge duration be short as compared to this arc formation time. The array of cathode resistors also serves to limit the discharge current and spread it uniformly over the entire discharge area. Subsequent improvements were made on

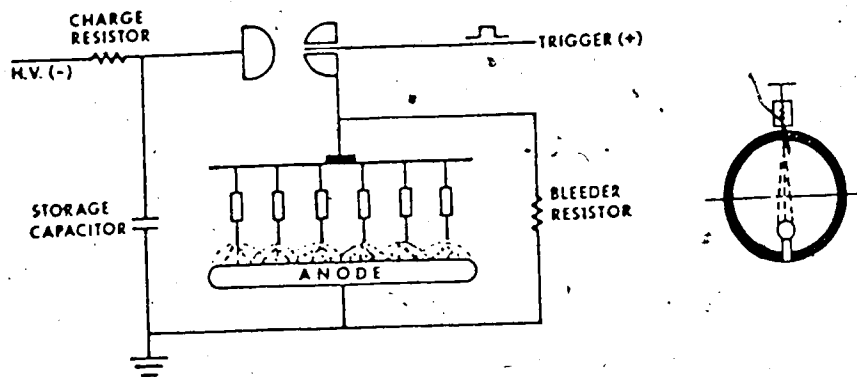


Fig. 1.1: Resistive pin cathode TEA laser used by Beaulieu [8].

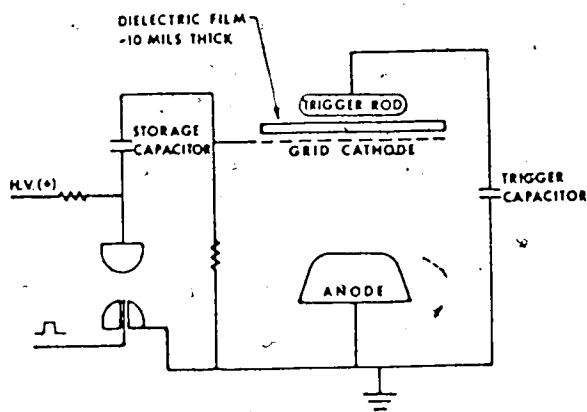


Fig. 1.2: LaFlamme's double discharge TEA laser configuration [11].

the Beaulieu system by using inductors or capacitors instead of resistors and by using electrode arrays instead of a single row. The elimination of resistors resulted in an improvement in the operational efficiency, due to the reduction of the ohmic losses. Extended electrode arrays were used to enlarge the discharge volume and improve the uniformity of the discharge.

The Beaulieu system works well for small TEA lasers; but at the volumes, electrode areas and input energies of current interest in high power laser devices, the discharge time becomes too long when using conventional circuitry. Consequently arcs do have time to form. In addition, a fast discharge time does not correspond to the most efficient pumping rate of CO₂ lasers [9]. A fast discharge rate is, therefore, not a particularly good method of arc suppression, even if it could be achieved at high energies.

An alternate solution to this problem is to prevent the current density from reaching a large enough value to initiate an arc. One such device is the Double-Discharge laser developed by Dumanchin *et al.* [10] and by Laflamme [11]. This system, as shown in Fig. 1.2, uses a mesh or grid cathode with a third electrode placed in close proximity, on the side opposite the anode. A fast low-energy discharge is triggered between the cathode and the third electrode, thereby producing a cloud of electrons around the cathode. These electrons greatly improve the quality of the main discharge to the anode by effectively increasing the discharge area and thereby reducing the current density sufficiently to prevent the formation of a constricted arc. Laflamme obtained 9 J per pulse with a peak power of 12 MW and an output energy density of 5.5 J/l, from a 3-8 m. long laser.

Nichols and Brandenburg [12] used a similar electrode structure, but produced a cloud of electrons with an 11 MHz. rf generator connected between the grid and the cathode. The device operated very well at a total pressure of 160 torr and with a volume flow ratio of CO₂:N₂:He = 1:1:8. With gas flow transverse to the optical axis at supersonic speeds, a 17 kHz. pulsed laser output was obtained.

1.2.4 Pre-Ionization Techniques

Parallel with the developments outlined above was the introduction of preionization techniques and the use of specially shaped electrodes, in order to increase the area of atmospheric pressure uniform discharges. Preionization refers to the presence of charged particles in the gas volume prior to the initiation of the discharge. These charges aid in the production of large volume glow discharges having high spatial uniformity. Preionization has been used in TEA type lasers for pumping large active volumes, thereby providing more laser power.

The double discharge lasers, discussed earlier, basically employed a low-energy preionizing discharge from the trigger to the cathode. This is sufficient to cause an ionization cloud to be uniformly distributed around the cathode. Such preionization helps to initiate the main anode-to-cathode discharge in a very uniform fashion, thereby reducing the effects of electrode surface irregularities and also the tendency to generate a bright arc. Dumanchin *et al.* [13] used a cathode made of parallel fins and insulated trigger wires running between the fins. They reported the attainment of 20 J/litre of laser energy.

Other preionizing techniques that have been investigated are: the use of electron beams, ultra-violet radiation and plasma jets. All these preionizing techniques utilize the fact that a discharge can be stabilized if the volume electron-ion production mechanism in the plasma is made independent of the applied electric field, through the use of external ionization sources. In such externally controlled plasmas, the applied electric field can be much lower than that required for self-sustaining discharges.

1.2.5 Other Major Developments

CO₂ lasers have already demonstrated improved performance at high pressures due to increased pulse energies, peak powers and high repetition rates. CO₂ lasers operating at very high pressures (above 1 atm.) and having broadened vibrational-rotational lines (which may eventually merge into continuous emission bands) have already been built. Such lasers can be

used to produce ultra-short pulses ($\approx 10^{-12}$ s.) by mode-locking techniques. They can also be tuned continuously over a broad spectral range. Though the goals of tunability and ultra-short pulse generation have yet to be fully realized, pulsed CO_2 - N_2 -He lasers have already been operated at pressures as high as 50 atm. [13].

Some of the other major advancements made in the development of CO_2 laser include:

- the introduction of seedants like water vapour and xenon to improve the laser performance.
- the use of fast pumping techniques to increase pulse energies.
- the introduction of new excitation methods such as those used in optically pumped and chemical reaction initiated CO_2 lasers.
- the advancement of new CO_2 systems such as gas-dynamic and waveguide lasers.

The details of these systems is beyond the scope of this modest summary. More exhaustive reviews can be found in [14-16].

1.3 EXCITATION MECHANISMS IN THE CO_2 LASER

1.3.1 Transition States for a CO_2 molecule

The CO_2 molecule can be visualized as 3 atoms which usually lie in a straight line, the outer atoms being oxygen with a carbon atom in between. There are three possible modes of vibration; in each case the center of gravity remains fixed.

1. The oxygen atoms can vibrate in opposition to each other along a straight line- this mode is called *the symmetric mode*, and is denoted by ν_1 .
2. The oxygen atoms may oscillate at right angles to the straight line- this is called *the bending mode*, and is denoted by ν_2 .
3. The two oxygen atoms may vibrate about the central carbon atom in such a way that they are each always moving in the same direction- this is known as the *asymmetric mode*, and

is denoted by ν_3 .

1.3 shows diagrammatically the 3 modes. Each possible vibrational state is called as follows:

Symmetric mode (ν_1) 000, 100, 200, 300...

Bending mode (ν_2) 000, 010, 020, 030.....

Asymmetric mode (ν_3) 000, 001, 002, 003.....

In addition to these vibrational modes the molecules can rotate and therefore quantized rotational energies are possible: A set of rotational levels is associated with each vibrational level: these are labelled in order of increasing energies by J values; each value being either a zero or a positive integer. The rotational energy per molecule is:

$$E_{\text{rot}} = hcB_e J(J+1) \quad (1.1)$$

where $B_e = h/8\pi^2 cI$ is the rotational constant ($B_e = 0.387 \text{ cm}^{-1}$ at 400°K) and 'I' is the moment of inertia of the molecule, 'h' is Planck's constant and 'c' is the velocity of light.

The population N_j at the rotational level j, assuming local thermodynamic equilibrium, can be estimated by using the Boltzmann's distribution equation:

$$N_j = N_v (2J + 1) (hcB_e/kT) [\exp(-E_{\text{rot}}/kT)] \quad (1.2)$$

where N_v is the population density of vibrational level v.

Transitions between different rotational levels in a given vibrational state are forbidden for the CO_2 molecule since it does not have a permanent dipole moment. However, a transition from one rotational level to another is allowed if it is to a different vibrational state. Quantum mechanical selection rules require that the rotational state, J, either increase (denoted by P branch) or decrease (denoted by R branch) by 1. Laser transitions have been obtained from both the P and R branch and these transitions tend to compete with one another. For example, the strongest transition is the P(20) transition from rotational level

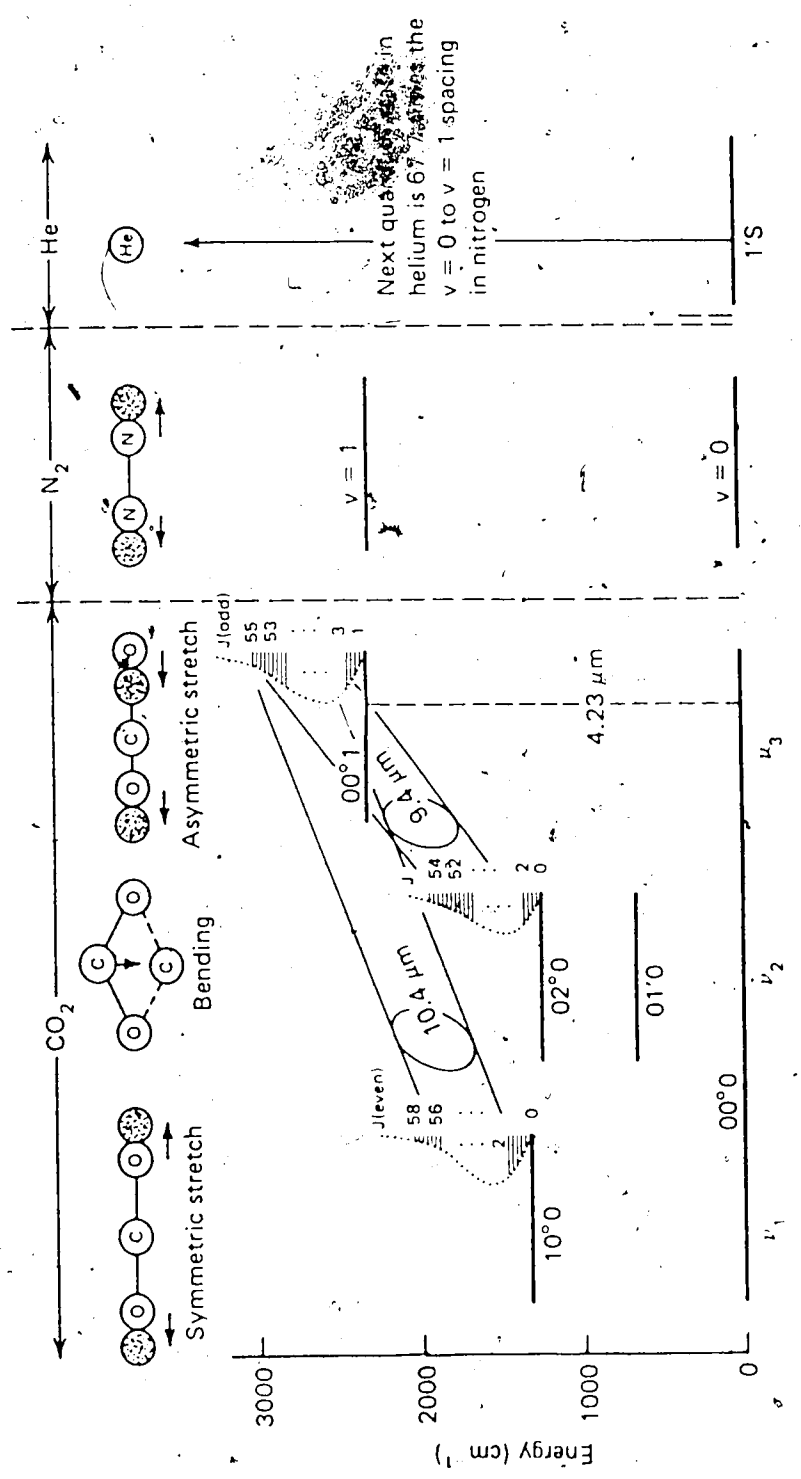


Fig. 1.3: Energy level diagram of the CO₂:N₂:He laser.

$J=19$ at the higher vibrational level (001) to $J=20$ at the lower vibrational level (100) (occurring at $10.6 \mu\text{m}$). This line competes with the R(20) transition from $J=21$ (001) to $J=20$ (100). In accordance with the Boltzmann distribution the population at $J=21$ level is less than that at $J=19$. Hence, there is a greater population inversion for the P branch as compared to the R branch. Consequently P branch transitions tend to dominate over R branch transitions.

1.3.2 Role of Nitrogen

The energy level spacing, for the CO_2 molecule, increases with J as shown on an expanded scale in Fig. 1.3. This figure also depicts the energy levels associated with each mode of vibration together with a set of rotational levels for the 001 and 100 modes. The ground state and the first excited state of the N_2 molecule are also shown. As only two atoms are involved, the N_2 molecule can have just one vibrational mode. Notice that the $\nu = 1$ level of N_2 is in close coincidence with the upper laser level (001) of CO_2 . The many desirable properties of CO_2 lasers can be attributed to this near-perfect match of levels. In addition, the N_2 molecule has a large cross-section for electron excitation of its vibrational levels. The N_2 molecules can hence be vibrationally excited by means of electron collisions and they can then transfer their trapped energy directly to the upper laser level of the CO_2 molecule. Because N_2 is a metastable molecule, it can only go to the ground state via a transfer of energy to the CO_2 molecule.

1.3.3 Role of Helium

It was not possible to place the excited-state energy levels of He in Fig. 1.3 because the first excited state of He occurs at $159,850 \text{ cm}^{-1}$, whereas the upper laser level (001) is only at 2349 cm^{-1} . This contrast explains why the CO_2 laser is more efficient than the He-Ne laser. One needs to supply only 0.5 eV to excite the (001) state of CO_2 , whereas more than 19.8 eV is required to excite the upper state of the He-Ne laser. The role of He in the CO_2 laser is as

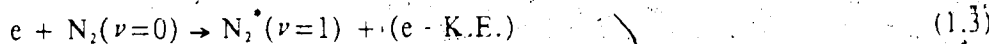
follows:

1. Helium helps in transporting the heat generated by the discharge onto the walls of the container for cooling.
2. Helium indirectly helps in depletion of the lower laser level (100), which is linked through resonant collisions with the (020) and (010) levels, the latter being directly depleted by helium.
3. Helium helps in controlling the E/p ratio and thus the electron "temperature" of the discharge.

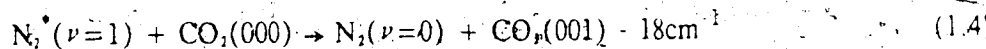
1.3.4 The Lasing Process

The pumping sequence for an electrical discharge in a mixture of CO₂/N₂/He can be described as follows:

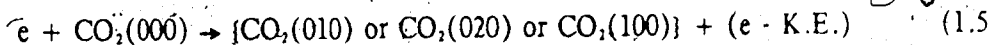
1. Electrical power is transferred to the electrons from the electric field.
2. The electrons transfer this power by collisions with neutral gas atoms. The inelastic collision process (of first kind) is represented by:



The excited N₂ molecule cannot drop directly to the ground state (due to its metastable property) but it can do so indirectly by transfer of energy to the CO₂ (000) state and raising it to the (001) state. This collision of the second kind is represented by:



This reaction is highly favourable because the CO₂ (001) energy level is very close to the N₂ (ν=1) level. Another possible, but less probable, mechanism is the excitation of the CO₂ molecules by collisions with high-energy electrons:



3. Since the (100) vibrational state is of much lower energy than the $\nu = 1$ state of N_2 , it cannot be populated by excited N_2 molecules. As a consequence, there is a build-up of population in the (001) state and it soon exceeds the population of the (100) level. This is the so called population inversion which is necessary for laser action to take place.

1.3.5 Relaxation Processes

In addition to creating a population inversion, it is necessary to maintain this inversion for a sufficient time, in order that laser action take place. Thus, it is important to know the relaxation times associated with the various levels. For a typical 15 torr CO_2 laser mixture, the natural lifetime of the (001) state of CO_2 is of the order of seconds, but due to collisional effects, this lifetime is in practice effectively reduced to the order of milliseconds [16]. The (100), (020) levels are closely spaced on the energy level diagram, and so are in Fermi resonance. Transitions from (100) \rightarrow (010) and (020) \rightarrow (010) are very fast (less than 1 μ sec). Therefore, the three levels (100), (020) and (010), reach thermal equilibrium quickly. This leaves only the decay rate of the (010) level to ground, to be examined. If this decay rate were slow (as is the case with a gas mixture containing just CO_2 and N_2), the (010) level would build up in population, thus creating a thermal bottleneck for laser action. Fortunately, the presence of Helium speeds up the decay rate of (010) symmetric mode to the order of 20 μ sec.

1.4 GAS-DISCHARGE PROCESS

Carbon Dioxide lasers commonly employ electrical discharges for pumping the laser medium. The reason for this is that the gas discharge technique is the simplest method of producing a low temperature plasma. Parameters such as the temperature of charged and neutral species, degree of atomic and molecular excitation and ionization can all be controlled over broad limits by varying the gas composition, electric field strength and the discharge current.

A typical gas discharge apparatus, used as a laser pumping medium, is shown schematically in Fig. 1.4. It consists of two electrodes separated by some distance, d , and driven by a power supply with a series ballast resistor. The ballast resistor limits the current through the discharge, protecting the power supply and stabilizing the operation of the tube. By adjusting the ballast resistance and/or the source voltage one may obtain the V-I (voltage-current) characteristics of the discharge. The various operating regimes of a discharge, as identified by these V-I characteristics, are shown in Fig. 1.5. One can easily recognize two distinct regions: *the glow regime*, characterized by high voltages and low currents and *the arc regime*, characterized by low voltages and large currents.

In the glow-discharge regime of operation, the voltage across the plasma column is fairly large (above 100 V), and remains constant over a 2 to 3 order range of current variation. At relatively low currents, the cross-sectional area of the cathode glow will be less than the total available cathode area. This arises because the glow discharge requires a minimum current density in order to produce sufficient secondary electrons to maintain itself. When only a small amount of current is available, the cross sectional area of the glow is reduced until this minimum current density condition is attained. The glow adjusts to any additional current by increasing the cross sectional area of the discharge, in order to maintain a constant current density. When the current to the discharge is increased beyond the point where the discharge occupies the whole cathode area, the voltage across the discharge tends to increase. This is known as the abnormal glow regime. A further increase in current will usually result in a sudden transition of the discharge into an arc. An arc discharge has a much higher conductivity than a glow-discharge and therefore operates at a much lower voltage. The arc effectively "shorts out" the discharge electrodes. Once an arc is formed, the self-sustained glow is terminated and no further pumping of the laser gas is possible. The currents involved in this mode are often large enough to damage the cathode material.

The glow discharge regime is preferred for laser operation since it can result in excitation of gas molecules over a large cross-sectional area (especially if operated in

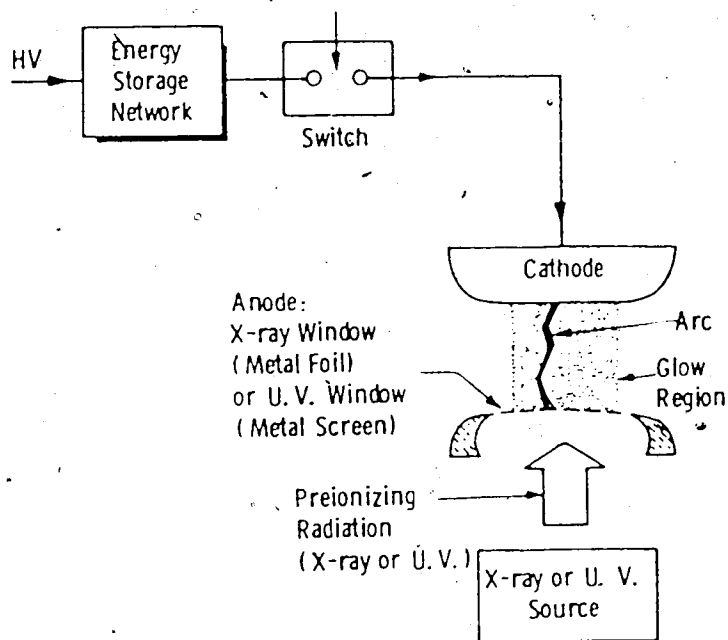


Fig. 1.4: Schematic diagram of a self-sustained pumped laser apparatus.

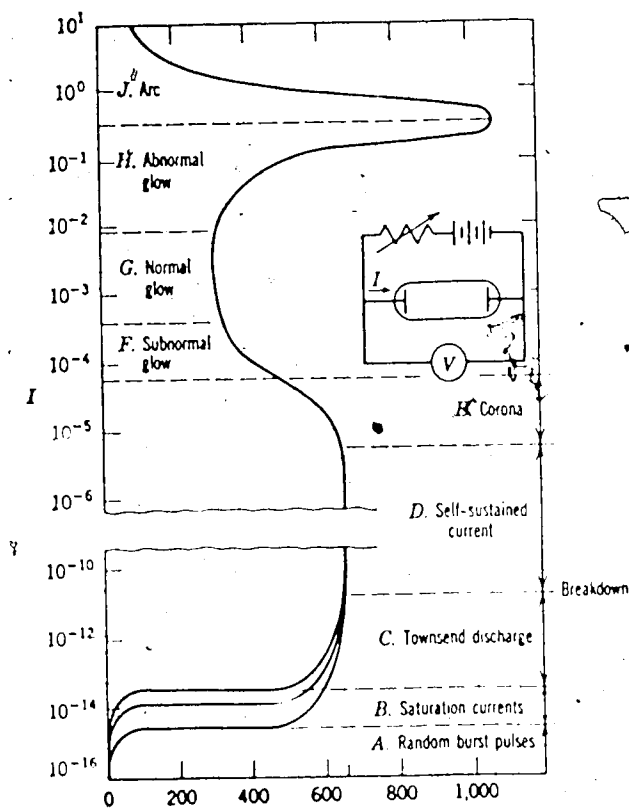


Fig. 1.5: Typical V-I characteristics for a gas discharge [17].

abnormal glow). Consequently, the glow discharge regime needs to be studied in greater detail.

1.4.1 The Glow Discharge

The glow discharge, when carefully scrutinized, is seen to consist of a number of distinct regions, such as: the cathode region, consisting of a cathode "dark" space, where a disproportionate amount of voltage is dropped; the negative glow, where hardly any voltage is dropped; the positive column, which occupies the major portion of the discharge and the anode fall, located in the immediate vicinity of the anode. These various regions and their corresponding current and voltage variations are shown in Fig. 1.6. The most important of these regions, so far as maintaining the discharge is concerned, is the cathode fall region. As is seen in Fig. 1.6, there is a large voltage drop across the cathode fall; typically 100 to 400 V. This results in a large electric field close to the cathode, which accelerates positive ions towards the cathode, giving them enough energy to cause secondary emission from the cathode surface. These emitted electrons are accelerated by the high electric fields and acquire a sufficiently high energy to cause ionization as they cross the cathode fall region. In the cathode fall region the current is mainly carried by the ions, which outnumber by far the electrons. However, if the cathode emits large quantities of electrons, for e.g. through thermionic emission, the ions do not have to carry as much of the current. Consequently, the cathode fall voltage drops to roughly the ionization potential of the gas.

The product of the cathode fall distance and gas pressure (pd_c) has been experimentally seen to be constant over a wide range of pressures. Since pd_c is constant, there must be a constant number of mean free paths in d_c . This implies that the number of ionizing collisions made by each emitted electron tends to remain constant. As such, this fact supports the contention that the primary function of the cathode fall region is to produce a specific number of ions per emitted electron. Clearly, if this number of ions is, on average, enough to produce one electron through secondary emission, the discharge becomes self-sustaining.

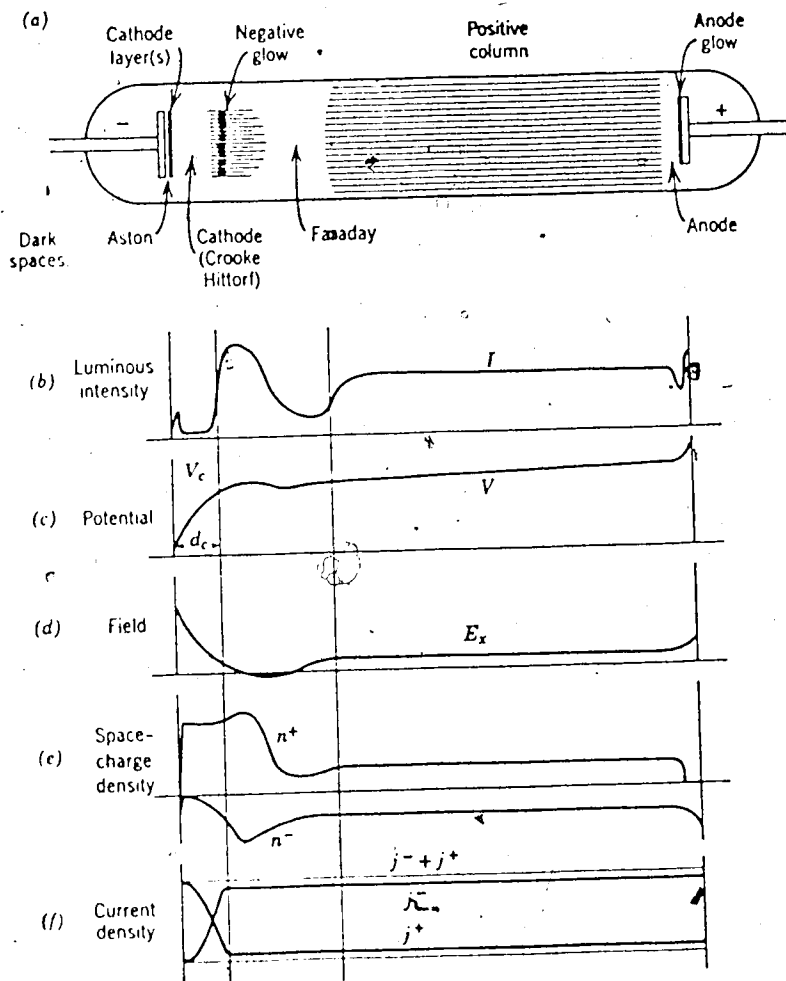


Fig. 1.6: Regions of a gas discharge. The luminous zones are shown shaded [17].

The negative glow is caused by those electrons that have gained a kinetic energy corresponding to a significant fraction of the cathode fall voltage. Energetic electrons are slowed down in this region by exciting and ionizing collisions; some of which result in visible light emission.

By the time these electrons reach the positive column, the densities of ions and electrons are approximately equal; and the electric field falls to a low value to produce just enough ionization to balance diffusion losses to the walls, thereby maintaining the plasma column. The electrons, being considerably lighter than the positive ions, respond much faster to the electric field. Consequently, almost all the electrical power enters through the electrons; which in turn later excite the remaining neutral atoms and molecules. It is these excited atoms and molecules, which generate coherent radiation within the laser's active medium.

The last region of the discharge, close to the anode, is the anode fall. This region consists of a negative space charge close to the anode, formed by electrons as they are accelerated towards the anode surface by the steep voltage gradient. On their way, these electrons produce, by collision, negative ions which then move into the positive column.

In addition to these considerations, it is important to take into account the time dependence of the discharge process. It takes a time T_f (known as the formative time lag) before the voltage across the electrodes will reach a quasi-equilibrium condition at the self-sustained glow-discharge voltage, V_g . In this phase, the ionization and attachment processes in the laser are in equilibrium and the gas will behave as a voltage regulator; with the voltage between the electrodes fixed at V_g independent of current as long as the current density is not too high (*i.e.* $< 100 \text{ amp/cm}^2\text{-atm}!$). When a large power density is applied to a laser gas discharge, the plasma often degenerates into an arc. If the arc occurs late in the pumping cycle, the laser intensity will be reduced and generally vary from shot to shot. If, however, the arc occurs before the self-sustained glow discharge can be established, then the gas will not lase. It is therefore critical that the formative time lag, T_f , be minimized if arc-free laser operation is to be achieved.

In order to calculate the self-sustained voltage, V_g and the formative time lag, T_f , use is made of the continuity equation for electrons:

$$\left(\frac{\partial n_e}{\partial t}\right) = \text{production of new electrons by ionization} + \text{production of new electrons by an externally connected source (eg. an e-beam, uv-ionization)} - \text{loss of electrons due to recombination and attachment.} \quad (1.6)$$

Neglecting the external ionization source, this reduces to:

$$\left(\frac{dn_e}{dt}\right) = \left[\frac{\partial n_e}{\partial t} + \frac{\partial(n_e u)}{\partial x}\right] = \alpha n_e - a n_e \quad (1.7)$$

where n_e is the electron density, t is time, x is distance from the cathode measured parallel to the uniform applied field, u is the electron drift velocity, and ' α ' and ' a ' are the electron ionization and attachment coefficients, respectively. Only when α is larger than a , can the discharge grow. The resulting electron avalanche process builds up the electron density from its initial preionization value (typically 10^6 to 10^8 electrons/cm³) to the levels which exist in the pulsed glow discharge phase (typically 10^{12} to 10^{15} electrons/cm³).

Neglecting the spatial variation in (1.7) and defining $\tau_e = [(\alpha - a)u]^{-1}$ as the time constant for electron growth or decay, we get:

$$\left(\frac{\partial n_e}{\partial t}\right) = (n_e / \tau_e) \quad (1.8)$$

The time constant, τ_e , can be calculated from the Boltzmann transportation equation using numeric cross-section data to determine the electron energy distribution and the resulting variation of α and a as a function of the electric field-to-gas density ratio, E/N . These tedious calculations have already been attempted in references [18-19] and the results are reproduced here in Fig. 1.7. Note that there is a limiting value of E/N , denoted by $(E/N)^*$, below which the discharge will not be self-sustained. $(E/N)^*$ corresponds to the case where $\alpha = a$. When a constant impedance power supply is used to operate the glow-discharge, the

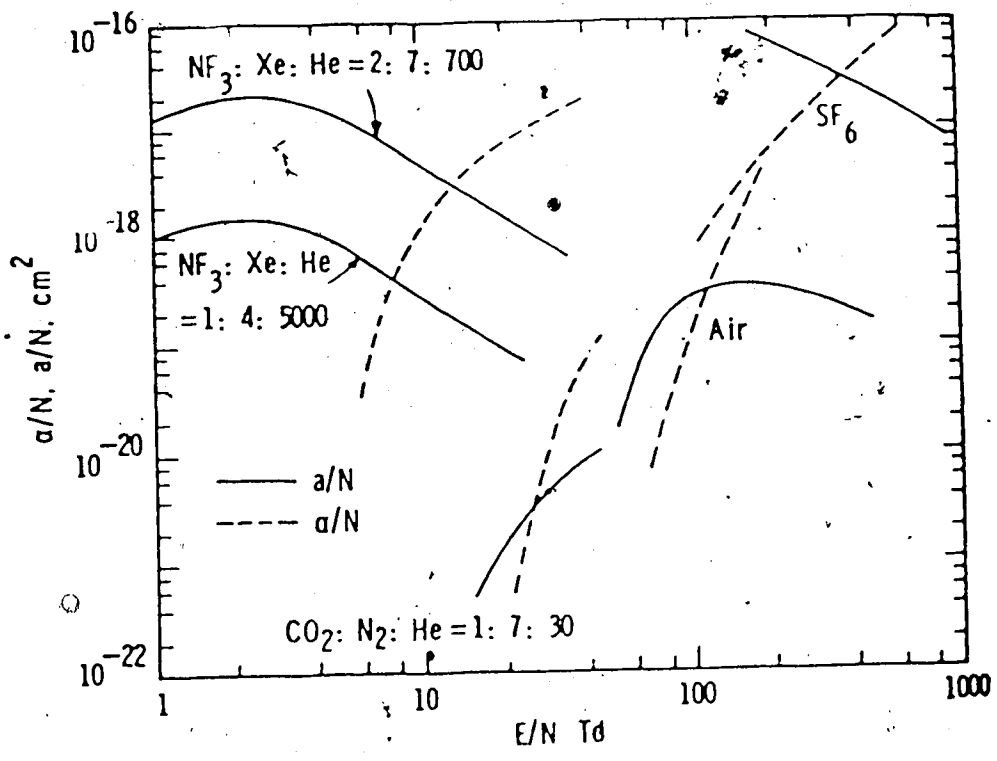


Fig. 1.7: Calculated ionization and attachment coefficients vs. E/N. The E/N units are Townsends (1 Td = 10^{-17} V/cm²).

measured voltage is given by:

$$V_g = V^* = N d (E/N)^* \quad (1.9)$$

where d is the length of the electrode gap. Eq. (1.9) implies that the glow discharge operates at a voltage where electron production and loss are equal, *i.e.* at $(E/N)^*$

Simplified expressions for V_g and T_f at room temperature using conventional $CO_2:N_2:He$ gas mixes are given below [20]:

$$\begin{aligned} V_g &= 20 D P R^{2/3} \\ T_f &= (0.2/PR^{2/3}) \exp [10.5 V_g / V_a] \end{aligned} \quad (1.10)$$

where V_g is the self sustained discharge voltage (kV), T_f is the formative time lag (ns), D is the electrode separation (cm), P is the laser gas pressure (atm), R is the ratio of non-helium gas partial pressure to total gas pressure and V_a is the voltage applied to the electrodes by the main discharge circuits (kV)

It can also be shown that the steady state electron density is given by [18]:

$$n_e = I / (e u A) = (V_a - V_g) / (e u A Z_0) \quad (1.11)$$

where A is the cross-sectional area of the discharge, e is the electron charge, u is the electron drift velocity at $(E/N)^*$; and Z_0 is the characteristic impedance of the power supply. These equations agree well with experimental results obtained by George and Denes [21].

1.4.2 Instability Formation

There is a tendency for high pressure glow discharges to degenerate, with time, into arcs. In laser applications, the glow discharge mode is essential because effective laser pumping occurs only with the high E/N values which are obtained in the glow mode. The voltage collapse that occurs when an arc forms, effectively terminates laser pumping and

additionally destroys the optical homogeneity of the laser medium; often resulting in damage to the system components.

The most commonly accepted theory for arcing has been formulated by Turner [22]. Turner has shown that the key factor influencing arc formation is the appearance of hot-spots on the cathode surface. These hot spots result in a thermally driven cathode-sheath instability. This is explained as follows: The break-up of the cathode sheath produces local concentrations of current on the cathode which in turn leads to the formation of multiple streamers in the gas. As the repetition rate is increased, the temperature of the gas near the cathode increases, thereby increasing the electron density, so that the streamers become fewer, but more intense. The process becomes regenerative, resulting in even higher gas temperatures, until finally a single arc results.

In addition to these simple thermal considerations, instabilities in laser gas discharges can also result in arc formation. Haas [23] studied the mechanisms influencing molecular discharge stability and his calculations indicated that small amplitude fluctuations present within these discharges excite several different wave modes with different characteristic times. The major unstable modes for high-power, electrically-excited CO₂ lasers are; the ionization, the negative-ion production and the vibrational-relaxation modes. The stability of these modes is seen to be critically dependent on the electron and gas temperature, the type of gas mixture and the degree of ionization.

The most common manifestations of plasma instabilities in electrically excited medium-pressure gas lasers are the occurrence of striations and glow collapse.

1. **Striations:** Moving striations in CO₂ laser mixtures were first observed in a self-sustained convection discharge by Nighan *et. al.* [24], and in electron-beam sustained discharges by Douglas-Hamilton and Mani [25-26]. Striations have been shown to be the result of charge particle production modes (which include ionization, negative-ion production and excited species production modes) of instabilities. These instabilities are generally not directly visible to the eye. However, oscilloscope monitoring of the plasma potential

measured using electrostatic probes, and display of the sidelight fluctuations as measured by light detectors, reveals periodic fluctuations in such discharges with wave growth along the direction of current flow. The occurrence of moving striations has been shown to be independent of laser gas pressure and electric power density. Consequently, striations can be detected for a wide range of experimental conditions. Nighan *et. al.* [24] reported that for conditions typical of electrically excited CO₂ laser mixtures, the existence of striations (due to ionization instability) requires a negative ion concentration greater than one-tenth that of the electrons, combined with an electron temperature value below 1.5 eV. These instabilities are generally of a less serious nature than thermal constrictions because laser action often persists despite the presence of striations.

2. **Thermal constriction (glow collapse):** In contrast to striations, the occurrence of plasma glow collapse is clearly visible and invariably occurs when the current density reaches a critical level. The occurrence of thermal constriction usually accompanies increases in pressure, electric power density, or both. The study of glow collapse (i.e. plasma constriction) is of paramount importance in laser discharge studies since it sets a limit to the maximum attainable power from these devices. Whereas a laser discharge can operate for long periods of time under striated conditions, it can operate for only very short times under glow collapse conditions. Nighan and Wiegand [27] analyzed the factors causing glow-to-arc transitions in high power CW lasers, in terms of the collisional processes taking place in the plasma. According to their theory, arcing can be initiated by the growth of disturbances, in either vibrational or translational electron temperature. The formation time of these instabilities is of the order of a millisecond. If one flushes away the locally unstable plasma inside the laser within this time range, say by convection cooling, then the stability of the discharge can be greatly increased.

Jacob and Mani [28] have also investigated the thermal and acoustic instabilities that could possibly cause arcing in high power pulsed and CW lasers. They arrived at a very simple description of the thermal instability process. An initial localized temperature

rise in a uniform plasma results in a local pressure rise, which creates gas expansion and thereby a drop in the local gas density. This region of low gas density will have higher electrical conductivity, which in turn will result in a higher local current density and a further temperature rise. A regenerative feedback effect proceeds rapidly and eventually causes the plasma to constrict into an arc.

A large number of methods have been used to stabilize the glow discharge, in order to maintain high output power from the laser. These include the use of internal ionization sources, the use of gas-cooling and turbulence, the use of specially shaped electrode profiles, and finally the use of magnetic fields. These methods will be reviewed briefly in the next few pages.

1.4.3 Auxillary Ionization

An auxillary source of ionization, such as high energy electron beams or UV radiation, applied independent of the main discharge, can be used to produce a large volume glow-discharge at high pressure. Such a process eventually translates into the attainment of even higher powered laser systems. Nighan *et. al.* [27] have shown that ionization and neutral particle instabilities are the most probable causes of discharge instability. These instabilities depend essentially on the response of the electron density to a disturbance in the laser medium. Haas [23] has pointed out that by using an external control of the electron density one can enhance discharge stability. The use of an external source of ionization reduces the sensitivity of electron-density fluctuations to electron temperature, gas temperature and gas density fluctuations. Thus arc formation is suppressed by auxillary ionization, thereby permitting scaling of both the volume and pulse length of high-pressure glow discharges. Two commonly used auxillary ionization techniques are: high energy electron beams and UV-radiation. These are discussed separately.

Electron-Beam Controlled Discharge

The concept of an electron-beam-controlled discharge (EBCD) appeared early in 1965 [29]. It was first applied to the production of uniform discharges for gas lasers in 1971. To date, the EBCD has produced the most impressive results in the preionization of CO₂ lasers for high pulsed energy. An energy density of 50 J/litre, corresponding to a total output of 2 kJ, has been obtained from a 40 litre EBCD laser by Daugherty *et. al.* [30]. The EBCD utilizes a high-energy beam of electrons to ionize the gas. A field across the gas accelerates the resulting charges and provides electrical excitation of the laser molecule. In the EBCD the separation of the source of ionization from the excitation process avoids the problems of self-sustained breakdown and arc formation. This can be explained as follows:

In self-sustained discharges, the ionization process is dominated by direct impact ionization of the molecules. Only electrons in the high energy portion of the electron distribution, *i.e.* in the range 10 - 20 eV, participate in this process. The ionization coefficient α depends upon E/N , as is shown in Fig. 1.6. It is seen, in this figure, that a small disturbance in E/N leads to a large fluctuation in α/N , and correspondingly in the electron density. This has a dominant effect on discharge stability. The discharge stabilizes at values of E/N which are generally too high to achieve good conversion efficiency. In e-beam sustained discharges, the applied field does not sustain the plasma, as in self-sustained discharges, so that E/N can be independently adjusted to optimize vibrational excitation of the upper laser levels. Thus, by employing an e-beam to control the discharge, a drift field lower than that required for self-sustained discharge operation can be applied. In addition, the electric field can be tailored for a particular electron velocity distribution and molecular pumping efficiency.

E-beam controlled discharges have also achieved uniform plasmas in large cross-sectional volumes (about 30 cm x 30 cm). To date, no other discharge technique, permits uniform discharges in so large a cross-section, at moderate pressure. Furthermore, operation at pressures as high as 20 atm. has been achieved by Basov *et. al.* [31] using a beam

of very fast electrons at 700 keV.

Though the EBCD process appears attractive, it has a number of drawbacks:

1. The electron gun can be very expensive and complicated; requiring high voltage supplies to generate electrons of sufficiently high energy.
2. The EBCD process tends to damage the foil separating the electron-beam vacuum chamber from the lasing gas chamber, due to heating.
3. Without the use of rapid gas circulation, the EBCD has a maximum permissible duration (approximately 100 μ s.) for current pulses. Using longer pulses causes the gas to overheat thereby bottle-necking the lasing process.

Ultra-Violet Preionization

Another preionization technique, which produces almost as dramatic results as the EBCD technique and yet does not suffer from the above drawbacks, is the ultra-violet photo-ionization system. Since the uv-source can operate within the laser gas medium there is no need for high vacuum construction. The uv-system can be scaled to pressures of many atmospheres, since a delicate foil window is no longer needed. High voltage sources needed to accelerate electrons in electron guns are not required in uv control. Ultra-violet sources can be readily constructed in large arrays, giving rise to uniform illumination over a large aperture. The uv-system is thus relatively cheap and considerably less complicated than the e-beam system.

Initial u.v. preionization techniques were developed by Richardson *et. al.* [32] and Seguin and Tulip [33] for use in pulsed CO₂ TEA lasers. These TEA lasers consisted of a number of pin-electrodes which when subjected to high voltage pulses, result in intense flashes of ultraviolet radiation. The high energy photons served to dissociate the electrons from the gas molecules, thus preionizing the system. After a certain delay, the main discharge is fed onto the pin electrodes. It is important that this delay is not too long, otherwise the electrons will have time to recombine with molecular oxygen. Denes and Kline [34] have shown, by means of computer modelling, that to obtain a uniform glow discharge with a

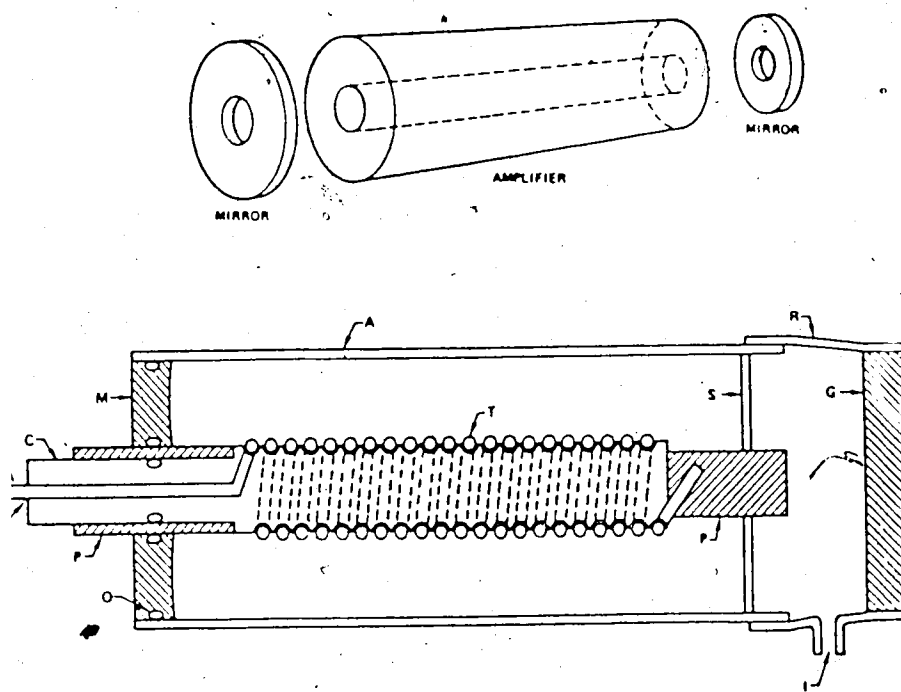
uniformly applied electric field, the initial preionization must be uniform in the plane parallel to the electrodes and its density must be orders of magnitude greater than the background preionization (≈ 100 electrons/cm³).

1.4.4 Co-Axial Discharges

The earliest lasers used longitudinal d.c. discharges to create a plasma for the required laser action: With the need for higher power and more compact lasers, the longitudinal discharge laser has given way to the more effective transverse discharge lasers. Initial transverse lasers used a discrete number of electrode pins to produce a glow discharge. These devices had a tendency to arc and so new electrode profiles were developed. The main aim of these electrode profiles was to maintain a uniform field configuration. Thus one had the Rogowski profiled electrode which was so shaped in order to avoid field concentrations at the ends of the electrodes. Though these transverse devices performed very well, there has been a need for even more compact TEA CO₂ structures. Arcing problems are more pronounced for small scale TEA discharges. This is partly due to the increase in field gradients associated with small electrodes which are fabricated to the same tolerance as larger electrodes. A compact and feasible transverse laser discharge system that can overcome these problems and thereby achieve high power, is a coaxial system.

The coaxial system consists of two cylindrical electrodes, one inside the other, enclosing a narrow annular discharge laser medium. This is shown in Fig. 1.8. Such a system has the following advantages:

1. The laser can be built into a grounded metal pipe (*i.e.* the outer electrode can be grounded). This provides compactness, ruggedness and safety characteristics not possible for conventional laser geometries. Also, whenever the need arises, the dimensions of the laser structure can be consistently reduced.
2. The symmetry of current distribution reduces the possibility of arcing.
3. One can use comparatively lower voltages.



Cross sectional drawing of a coaxial CO₂ laser showing A, aluminum anode pipe; C, machined aluminum cathode rod; M, machined and polished aluminum mirror; S, steel support pins; P, Plexiglas insulators; T, trigger wire; O, o rings; R, rubber diaphragm; I, gas inlet; and E, gas exhaust around trigger wire. Laser length is not to scale.

Fig. 1.8: (a) Schematic of a coaxial CO₂ laser and (b) Cross-sectional diagram of the coaxial laser [38].

4. The heat conduction through the walls, is improved because of the large outer surface.
5. One can use a relatively small gas blower for high repetition rate operation. This is because the recirculating gas flow is proportional to the width of the discharge region.

The earliest coaxial TEA CO₂ laser was built by Garnsworthy *et. al.* [35], using an outer cathode and an inner anode rod. Casperson and Shekani [36] designed a co-axial double discharge TEA CO₂ laser similar to the one designed by Garnsworthy except with the electrodes reversed. They also used a trigger wire, spiralled around the inside surface of the cathode pipe, to serve as the preionizer. Oche and Sontag [37] constructed a cylindrical discharge system, for low energy applications, having a small diameter wire as the central electrode. Earlier systems employed large diameter rods, as the central electrodes. The advantage gained by using a thin central electrode is that it can be used simultaneously as a preionizing electrode. The extension of the coaxial discharge to cw lasers was made by Cheng and Casperson [38]. They found that the overall efficiency of the coaxial system is the same as that for conventional longitudinal discharge, but with the added advantage of low voltage operation, better cooling and a rugged construction.

1.4.5 Magnetic Field Stabilization

The coaxial discharge CO₂ lasers, though very promising, seem to suffer from the same electrothermal instabilities that plague other CO₂ laser systems. There is, fortunately, yet another method by which one can stabilize a discharge, *i.e.* the use of a properly profiled magnetic field.

The effect of a magnetic field on breakdown is determined by its influence on the drift motion of charged particles, particularly electrons. An electron moving freely through a uniform magnetic field of flux density B gyrates about the field lines with a frequency

$$\omega_c = \frac{|e|\hbar}{m} B \quad (1.12)$$

known as the cyclotron frequency.

The radius of gyration a , depends upon v_{\perp} (the electron's velocity component perpendicular to B) and is given by:

$$a = \left(\frac{m}{e}\right)(v_{\perp}/B) = (v_{\perp}/\omega_c) \quad (1.13)$$

so that the electron velocity in the B direction is unaffected, while velocity perpendicular to B produces rotation. Free electrons are therefore effectively anchored to flux lines. If an electric field E also acts on the electron, then the component of E parallel to B produces acceleration in the same direction, while the component perpendicular to B produces helical motion along an axis perpendicular to both. Hence electron flow is severely restricted by a transverse magnetic field and only by virtue of collisions can a net flow of electrons be achieved across the field direction. It may be shown that if ν is the electron collision frequency, both the mobility and the diffusion are reduced by factors of $[\nu^2/(\nu^2 + \omega_c^2)]$ and $[1/(1 + \omega_c^2 \lambda^2)]$ respectively, for flow across the magnetic field. Here λ is the mean free path.

The gyrations of electrons in a transverse magnetic field causes an increased path length in spanning a given distance and hence results in a greater number of collisions. The effect is equivalent to an increase in pressure, with a corresponding change in α .

Buczek *et. al.* [39] were the first to apply magnetic fields to laser systems. In a convectively cooled crossflow CO_2 laser discharge an unmagnetized plasma column is bowed strongly downstream under the force of the transverse gas flow. This effect is illustrated in Fig. 1.9. In order to obtain efficient laser operation it is necessary to straighten and maintain the positive column within the confines of the optical resonator geometry. A tapered magnetic field, mutually perpendicular to the axial electric field and the gas flow velocity, is used to push back electrons into the optical axis by means of the $\vec{J} \times \vec{B}$ force.

Recently, magnetic fields have been used by Seguin *et. al.* [40-42] to suppress the growth of electrothermal plasma instabilities and to increase the power loading in high power laser discharges. Figs. 1.10 and 1.11 show the structure of the magnetically stabilized transverse and co-axial discharge systems. Profiled magnetic fields, which interact with the

SCHEMATIC OF A CROSS - FIELD LASER

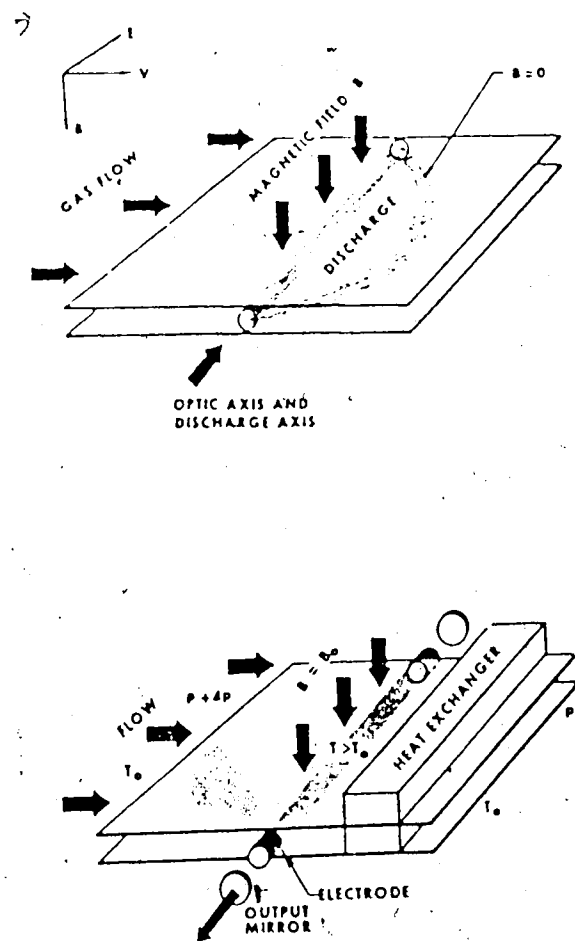


Fig. 1.9: Schematic of gas flow channel, electrical discharge and transverse magnetic field in a magnetically stabilized CO_2 laser [39].

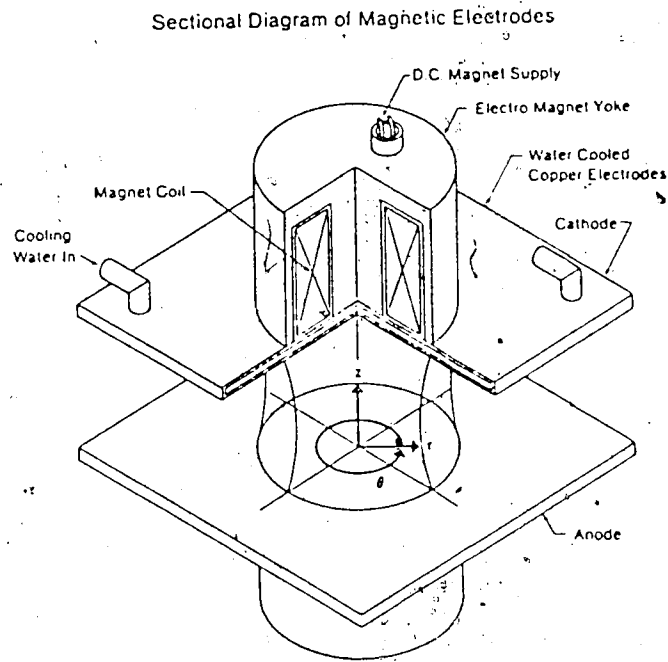


Fig. 1.10: Magnetically stabilized transverse discharge CO_2 laser structure used by Capjack *et. al.* [41].

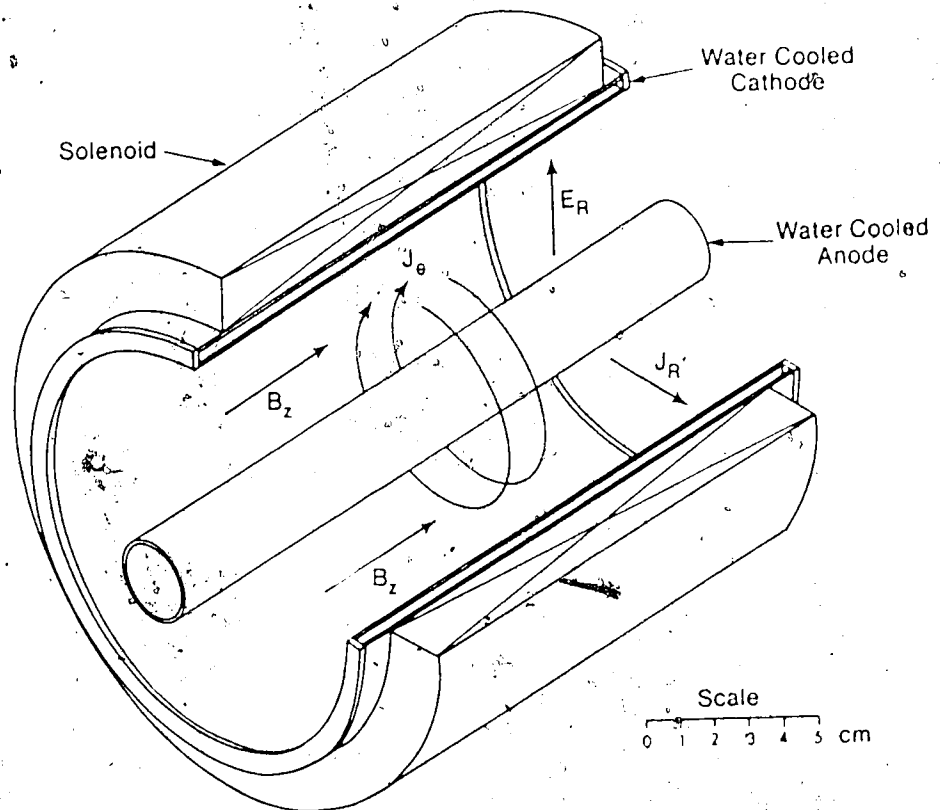


Fig. 1.11: Magnetically stabilized co-axial discharge CO_2 laser structure used by Seguin *et. al.* [40].

electron and ion sheaths at or near the electrode surface are used. Any potential current filament occurring in the discharge will be accelerated by a force of $\vec{J} \times \vec{B}$ in a direction orthogonal to both E and B . This filament will quickly spread out into a diffuse rotating plasma cylinder (*i.e.* the filament will follow a helicoidal motion). This results in a strongly sheared flow system near the electrode surfaces, which further helps in suppressing the formation of arcs.

Initially, the mechanism by which these magnetic fields stabilize laser discharges was thought to be due to the $\vec{J} \times \vec{B}$ drift velocity of the ions and neutral molecules. Subsequent analysis of these drift velocities showed that they were far too small to account for the observed stability effects. Clearly, the stabilization mechanism must involve the motion of electrons, which move 1000 times faster than the ions and neutral molecules. It is the purport of this thesis that magnetic stabilization of laser gas discharges results primarily from the sweeping of charge carrier instabilities over the cathode region through distances larger than characteristic instability scale lengths. In order to prove this hypothesis, it is necessary to have a clear understanding of the various instability modes that occur in CO_2 lasers, their scale lengths and the conditions leading to their occurrence. The next chapter addresses precisely these points.

CHAPTER II

DISCHARGE INSTABILITY ANALYSIS

2.1 INTRODUCTION

In Chapter 1, the various instability modes that can perturb uniform glow operation within a laser gas discharge were briefly described. It was shown that large-volume convection lasers are subject to the occurrence of plasma instabilities which prevent the attainment of the elevated electrical power density levels dictated solely from thermal considerations. Such instability modes are often manifest as striations or as contractions within the discharge. Eventually, the process can result in a glow-to-arc transition, thereby effectively terminating laser action. It is, therefore, important to analyze these instability modes in greater detail; so that these unfavorable conditions can be avoided; or alternatively, appropriate methods to circumvent them can be formulated.

Discharge instabilities arise basically as a result of local fluctuations in the plasma variables; (such as species type, concentration, density and vibrational temperature). Noise generated by flow turbulence and power supply ripple can also be contributing factors. However, not all fluctuations lead to instabilities. Typically, there are three ways a system can respond to small perturbations:

1. The perturbations can be attenuated in time. Under these conditions the system is said to be stable.
2. The perturbations are amplified in time, but within the same time frame are 'transported' out of the system (e.g. by gas flow).
3. The perturbations are amplified in time and remain within the system.

Obviously, case (3) is the most serious since it could eventually result in permanent damage to the system. For example, arcing of the discharge could cause catastrophic electrode failure.

Stability analysis attempts to predict the conditions which will result in the system becoming unstable. The amplitude of the initial fluctuations in plasma properties are usually

small enough so that one can use first-order perturbation theory for stability analysis. Perturbation theory allows all plasma properties, $\psi(x,t)$, to be considered as the sum of two components; the spatially invariant, steady state value ψ_0 and a small spatially and temporally varying component $\tilde{\psi}(x,t)$. Thus:

$$\psi(x,t) = \psi + \tilde{\psi}(x,t) \quad (2.1)$$

where ψ denotes a complete set of fundamental plasma properties, *i.e.*, $\psi \equiv \{n, n_e, n_p, \dots, T_e, T, T_v\}$. The temporally varying component, $\tilde{\psi}(x,t)$, is assumed to have a space and time dependence given by:

$$\tilde{\psi}(x,t) = \psi_k \exp [i(k \cdot x - \omega t)] \quad (2.2)$$

where ω is the complex frequency ($\omega = \omega_r + i\omega_i$), k is the wavevector, x is the spatial variable and ψ_k is the amplitude of the perturbations.

These perturbed variables are substituted into the fundamental conservation equations for the plasma (continuity, momentum and energy equations) and decomposed into their zero (for steady state) and first-order linear components (for fluctuating quantities). The solution of both the zeroth and first-order conservation equations is a formidable task, requiring accurate knowledge of various attachment, recombination and ionization coefficients. In addition, a host of positive and negative ions and neutral species are produced in the discharge as a result of numerous reactions. The behaviour of such a plasma is governed by a complex set of energy and particle conservation interactions. Considerable simplification is achieved by assuming only one species each of positive and negative ions (see Haas [23]). These conservation equations can also be partitioned into various time ranges with regard to different instability modes. Such an approach, apart from considerably simplifying the mathematical analysis, also provides a better physical insight into the different instability modes.

The various modes that exist within the discharge can be decoupled by assuming that the higher order terms, which consist of products of the amplitudes of two or more different modes, is of smaller magnitude than the individual mode amplitudes. Thus, one can eliminate the perturbation amplitude ψ_k from the first order equations and arrive at an equation for ω and k in terms of the steady-state plasma properties. The complex roots of such an equation (commonly referred to as a dispersion relation) can each be identified with a potential mode of unstable plasma behaviour. Haas [23] has shown that the characteristic time scales associated with these modes cover a wide time range (10^{-10} - 10^{-2} sec.). A significant simplification of the dispersion relation is possible by breaking it up into various time ranges. The complex roots of the resulting dispersion relations, each of which cover different time frames, are associated with various instability modes. Based on the physical processes associated with their evolution, these modes have been classified and ordered into their characteristic time scales by Haas [23] as follows:

1. Space-charge relaxation mode (10^{-10} - 10^{-8} sec.)
2. Electron thermal mode (10^{-8} - 10^{-7} sec.)
3. Ionization mode (10^{-6} - 10^{-5} sec.)
4. Negative-ion production mode (10^{-6} - 10^{-5} sec.)
5. Electronic-species production mode (10^{-6} - 10^{-4} sec.)
6. Sound mode (10^{-5} - 10^{-4} sec.)
7. Vibrational energy relaxation mode (10^{-4} - 10^{-3} sec.)
8. Heavy particle thermal mode (10^{-4} - 10^{-3} sec.)
9. Vorticity mode (10^{-3} - 10^{-2} sec.)

Haas [23] has shown that the space-charge relaxation, electron-thermal and vorticity modes are stable for high-power CO₂ laser plasmas. However, the stability of the other modes is critically dependent on the steady state plasma properties, such as gas-mixture, the degree of ionization, the discharge E/n (electric field to gas density ratio) or equivalently the electron temperature and the gas temperature.

2.2 STEADY STATE CONDITIONS

In order to determine the steady state plasma properties of interest, we start with the analysis of the continuity equations for various charged species in the laser plasma. If ' n_e ' denotes the electron density, ' n_n ' the negative ion density, ' n_p ' the positive ion density and ' n ' the total heavy-particle density; the charged particle continuity equations are:

$$\begin{aligned} \frac{\partial n_e}{\partial t} &= n_e n k_i - n_e n_p k_r^c - n_e n k_a + n_n n k_d + nS \\ \frac{\partial n_n}{\partial t} &= n_e n k_a - n_n n k_d - n_n n_p k_r^i \end{aligned} \quad (2.3)$$

where S is the rate of ionization due to an external source and the various k 's are the rate coefficients for the following processes:

- (i) k_i (electron impact ionization) e.g. $e + M \rightarrow M^+ + 2e$
- (ii) k_a (electron neutral attachment) e.g. $e + M \rightarrow M^-$
- (iii) k_r^c (electron-positive ion recombination) e.g. $e + M^+ \rightarrow M$
- (iv) k_d (negative ion detachment) e.g. $N + M^- \rightarrow N + M + e$
- (v) k_r^i (positive ion - negative ion recombination) e.g. $M^- + M^+ \rightarrow 2M$

Note that in (2.3) we have not written a separate equation for n_p . This is because one can assume charge neutrality in the laser plasma. So:

$$n_p = n_e + n_n \quad (2.4)$$

The rate coefficients, k_i , k_a and k_r^c are obtained by averaging the corresponding cross-sections over the electron density function, f , i.e.:

$$k_j\left(\frac{E}{n}\right) = \left(\frac{2e}{m}\right)^{1/2} \int_0^\infty u f\left(u, \frac{E}{n}\right) Q_j(u) du \quad (2.5)$$

where u is the electron energy in electron volts, e and m are the electron charge and mass, $Q_j(u)$ is the cross-section of the particular process in question, and E/n is the ratio of

electric field intensity to the total neutral particle number density. Since the electron energy density distribution function depends on E/n and the gas mixture, the rate coefficients are also dependent on these properties.

Nighan and Wiegand [43] have computed these electron rate coefficients for a representative CO_2 - N_2 -He mixture. Fig 2.1 presents the ionization and attachment rate coefficient as a function of this E/n ratio. Also shown is the electron-ion recombination rate, k_r^e , weighted by the fractional n_p/n . Note that this weighted recombination rate is only a slowly varying function of E/n , as compared to the ionization and attachment rates (which vary over many orders of magnitude for small changes in E/n). The operating value of E/n will depend on the type of laser discharge considered; *i.e.* whether it is externally sustained or self sustained and if self sustained whether it is detachment dominated or not. In any case, the sustaining value of E/n , *i.e.* $(E/n)^*$, for a specific gas mixture is determined by the condition that electron loss mechanisms (attachment and recombination) should be balanced by electron production mechanisms (ionization and detachment). We will consider these individual cases separately.

2.2.1 Self Sustained Discharge: No Detachment

When detachment is an unimportant process the steady state electron conservation equation (2.3) simplifies to:

$$n_e n k_i = n_e n k_a + n_e n_p k_r^e \quad \text{or} \\ k_i = k_a + (n_p/n) k_r^e \quad (2.6)$$

Fig. 2.1 shows the values of these coefficients for different E/n ratios. One can clearly note that $k_a \gg (n_p/n) k_r^e$ throughout the E/n range considered here. Therefore, for the no-detachment case the electron conservation equation simplifies finally to:

$$k_i = k_a \quad (2.7)$$

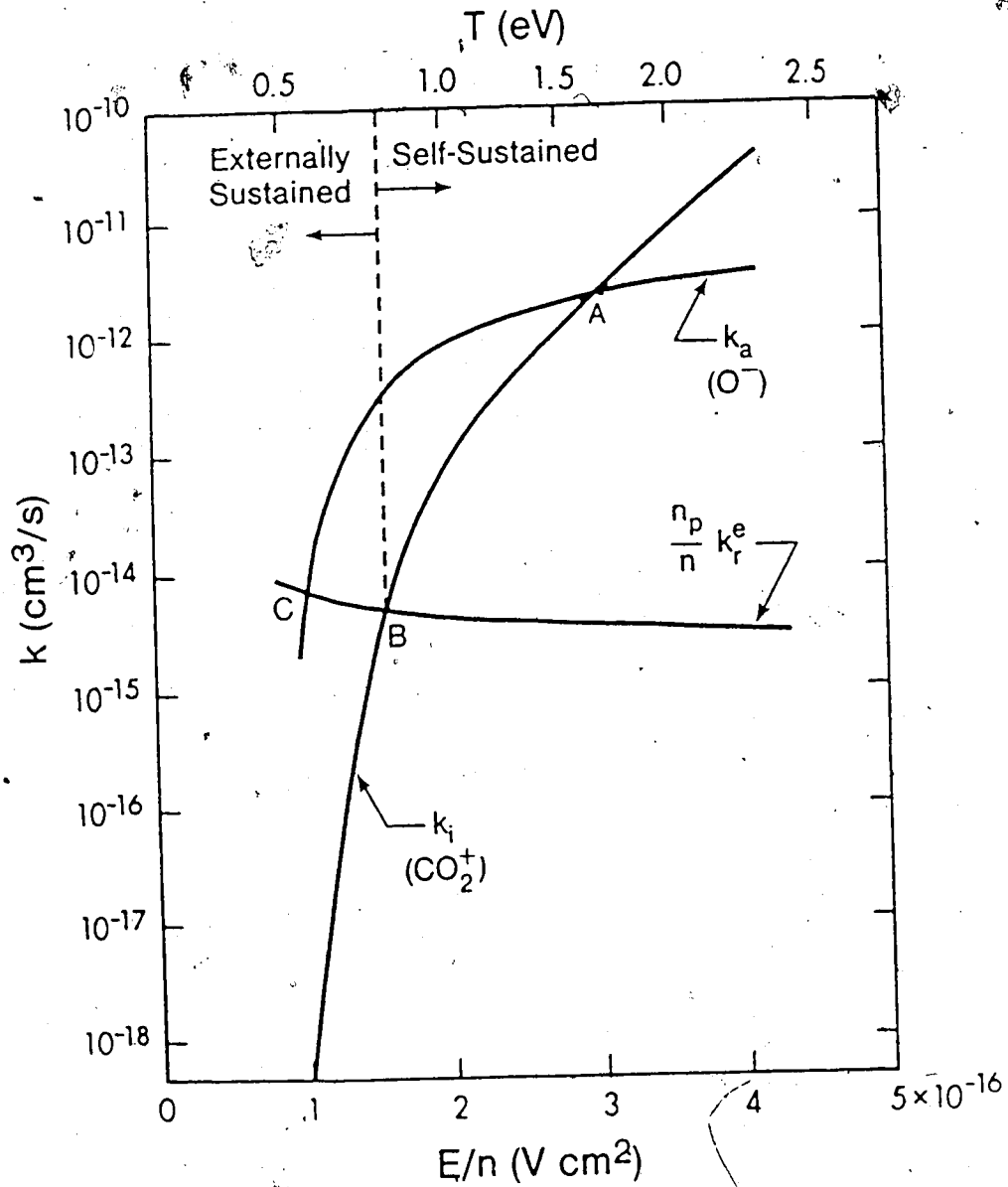


Fig. 2.1: Comparison of ionization, attachment and recombination coefficients for a typical CO_2 laser discharge.

This equality occurs at point (A) on Fig. 2.1 and the corresponding E/n value is the sustaining value for the glow discharge with little detachment.

2.2.2 Self Sustained Discharge: Strong Detachment

When the detachment rate is very high (for e.g. if there are large quantities of detaching species like CO), the charge conservation equation (2.3) simplifies to:

$$\begin{aligned} n_e n k_i &= n_e n k_a - n_n n k_d + n_e n_p k_r^e \text{ and} \\ n_e n k_a &= n_n n k_d \end{aligned} \quad (2.8)$$

Combining these two equations together results in:

$$k_i = (n_p/n) k_r^e \quad (2.9)$$

This equality occurs at point (B) on Fig. 2.1 and once again the corresponding E/n value gives us the sustaining value for the discharge operating in the glow mode with strong detachment.

In actual practice, one can operate at E/n values anywhere between the no detachment (A), and strong detachment (B), limits; depending on the concentration of the detaching species.

2.2.3 Externally Sustained Discharge

The introduction of an external, independently controlled, source of ionization, such as an electron-beam or uv-preionization, is equivalent to shifting the ionization rate coefficient, k_i , up above its value for the self-sustained case. This corresponds to a shift in the points (A) and (B) of Fig. 2.1 to the left. This further implies that lower E/n values are required to maintain the steady state glow operation for an externally sustained discharge.

For both self-sustained and externally sustained discharges, the region to the left of point (B) in Fig. 2.1 is seen to be a strongly dependent function of the E/n (and therefore of electron temperature, T_e) values. This strong dependence can lead to various instabilities as will be shown later.

2.3 GLOW-DISCHARGE INSTABILITIES

In a self-sustained CO_2 laser glow discharge there are two major manifestations of instabilities; namely striation of the plasma discharge and plasma constriction (or thermal instability). Striations occur in the time scales of 10^{-10} sec. to 10^{-4} sec., whereas plasma constrictions occur in 10^{-5} sec. to 10^{-2} sec. time scales.

2.3.1 Striations

Striations have been observed in the discharge positive column region from the times of the earliest gas-discharge studies. Striations are basically wave-like structures or regions within the discharge which have higher electron densities than elsewhere. These regions are sometimes visible to the naked eye, but more often are observable only by means of sophisticated measurement schemes. The electron density builds up at certain intervals due to the fact that the electrons gain enough energy for ionization only after travelling a certain distance. The electric field potential also shows sharp rises (resulting in large excitations) near the striations, followed by regions of flat potential between striations (where there are few excitations).

To determine whether or not striations will build up one has to first determine the dispersion relation for the striation mode. Since the characteristic time scales for these modes are between 10^{-8} sec. to 10^{-4} sec. one can neglect neutral particle properties which take longer time periods to respond to perturbations. Space-charge fluctuations respond on a much smaller time scale (10^{-10} sec. to 10^{-9} sec.) so that one can assume charge neutrality (*i.e.* $n_p \cong n_e + n_n$). One can then write the electron and negative-ion conservation equations and

substitute the perturbed variables in these equations. One then separates these equations into the first order and the zeroth order equations. There are two first order equations consisting of three coupled perturbed variables N_{ek} , N_{nk} and T_{ek} . If one adds to these equations, the quasi-steady electron energy equation given by Nighan [43], which relates the perturbed quantities N_{ek} and T_{ek} (generally N_{ek} and T_{ek} are negatively related); one can solve for N_{ek} , N_{nk} and T_{ek} in terms of unperturbed variables. This results in a quadratic equation for ' $i\omega$ ' in terms of the real, zeroth order (*i.e.* steady state) properties of the plasma. The corresponding dispersion relation for striation modes is of the form:

$$\omega = -\frac{b}{2} \pm (b^2 - 4c)^{1/2} > 0 \quad (2.10)$$

The full form of expressions 'b' and 'c' are given in [43]. The two roots of (2.10) are identifiable with the temporal growth or damping of disturbances in electron (ionization mode) and negative-ion densities (negative-ion mode). The ionization mode is unstable if $b < 0$, whereas the negative ion mode is unstable if b and c have opposite signs. For CO₂ laser conditions of interest, the coefficient c is always positive but b can change sign. The ionization instability then requires that $b < 0$. Under that condition the negative ion mode will also be unstable. The condition $b < 0$ is given by:

$$-b = \left[\left(\frac{-2 \cos^2 \phi}{\hat{\nu}'_u} \right) \left(1 - \frac{k_a \hat{k}_a}{k_i k_l} \right) nk_i \hat{k}_i \right] - \left(\frac{n_e}{n_p} n_p k_r^e + \frac{n_n}{n_e} nk_d + \frac{n_n}{n_p} n_p k_r^i + \frac{n_e}{n_n} nk_a + \frac{n}{n_e} S \right) > 0 \quad (2.11)$$

Here, ϕ is the angle between the wave propagation vector, k and the electric field E , *i.e.* $\cos \phi = k \cdot E$. The term $\hat{\nu}'_u$ is given by:

$$\hat{\nu}'_u \equiv 1 + \hat{\nu}_u - \hat{\nu}_m \cos 2\phi \quad (2.12)$$

where ν_u and ν_m are the total electron energy exchange and momentum transfer collision

frequencies. The *caret* notation refers to the logarithmic derivatives with respect to electron temperature, e.g.:

$$\hat{k} \equiv \frac{\partial \ln k}{\partial \ln T_e} = \frac{T_e}{k} \frac{\partial k}{\partial T_e} \quad (2.13)$$

To simplify (2.11) and to get a better physical insight into the striation instability modes, consider the case when the discharge is operated near condition (A), i.e. no negative ion limit of Fig. 2.1. In the absence of negative ions, $n_e = n_p$ and $nk_1 = n_e k_r^c$ (from equation 2.2) and all terms representing negative ion processes vanish. Therefore (2.11) reduces to

$$nk_1 \left[\frac{-2 \cos^2 \phi}{\hat{\nu}_u} \hat{k}_1 - 1 \right] > 0 \quad (2.14)$$

For most species of interest \hat{k}_1 is positive, with value between 10 to 30. Also $\hat{\nu}_u$ is almost always positive with values in the range of 2 to 5. Thus the left hand term is always negative; implying that no striation modes of instability are present.

However, if we do operate at regions between (A) and (B) or between (A) and (C) then the full form of (2.11) must be considered for stability analysis. The terms in the parenthesis act as stabilizing elements and are all positive. Thus the main stability criteria reduces to the quantity $(k_a \hat{k}_a / k_i \hat{k}_i)$ exceeding unity. This quantity, $(k_a \hat{k}_a / k_i \hat{k}_i)$ or $\delta k_a / \delta k_i$, represents the change in k_a associated with a change in k_i in response to a variation in the electron temperature. When $(k_a \hat{k}_a / k_i \hat{k}_i)$ is greater than 1, the loss of electrons due to attachment dominates over electron production due to ionizations, for an initial positive fluctuation in electron temperature. This results in an inverse relationship between electron density and electron temperature. The net result is that the initial disturbance is further reinforced. The sequence of events is summarized as follows:

$$n_e \downarrow \quad T_e \uparrow \quad \begin{matrix} k_i \uparrow \\ k_a \uparrow \uparrow \end{matrix} \quad n_e \downarrow \downarrow \quad (2.15)$$

Nighan and Wiegand [43] have evaluated inequality (2.10) in order to determine the electron

attachment instability (and ionization instability) conditions; with electron density, electron temperature and CO fractional concentration taken as variable parameters. Their results, reproduced in Fig. 2.2, shows the instability boundary regions for a 20 torr $\text{CO}_2:\text{N}_2:\text{He}$ (1:7:12) mixture. The minimum ratio of (n_n/n_e) , corresponding to the lower limit of the unstable region, is 0.1. Below this value, ionization and electron-positive ion recombination dominates plasma behaviour. The upper limit of (n_n/n_e) is ≈ 10 ; and although the plasma is attachment controlled, the electron temperature T_e is very high, resulting in $(k_a k_u / k_i k_r) < 1$. Thus, the presence of a large quantity of negative ions is not a necessary condition for negative-ion instability. Rather, it is the relative slopes or variations of k_a and k_i which are important. These parameters control the electron production and loss mechanisms during a disturbance in plasma properties.

An additional point worth noting, is the importance of ϕ being close to 0 (see equations 2.11 and 2.14) for attachment instability to occur. This means that the instability occurs only in the direction of the unperturbed electric field; and results from the nonisotropic coupling between electron temperature and electron density disturbance. Wave growth in the electric field direction often results in layering in plasma properties normal to the electric field. These are physically and experimentally observed as striations in the plasma column.

Finally, Fig 2.2 shows that larger CO concentrations (i.e. larger f values) result in lower electron temperatures, and correspondingly to detachment dominated discharges. Thus, the addition of large quantities of a detaching species, such as CO, can greatly reduce striation instabilities.

2.3.2 Thermal Instabilities

Unlike striations, thermal instabilities (also referred to as plasma constrictions) are present in all types of gas discharges and are often the limiting factor for determining the maximum power output from large CO_2 lasers.

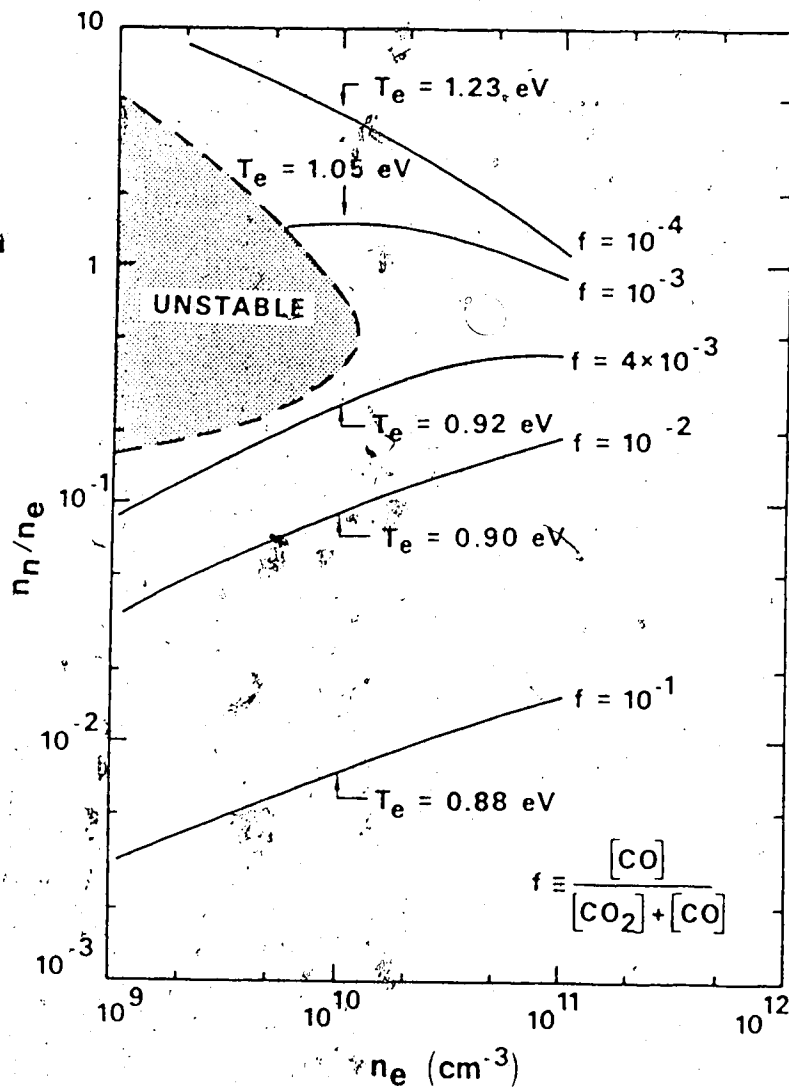


Fig. 2.2: Ionization instability boundary computed by Nighan and Wiegand [43] for a 20-Torr $\text{CO}_2:\text{N}_2:\text{He} = 1:7:12$ mixture. The electron density, n_e and CO fraction, f , are the variable parameters from which the negative-ion concentration n_n/n_e , the electron temperature T_e , and the stability criteria are computed.

The causes of thermal instabilities have been studied in great detail; and it is generally agreed that the primary cause of these instabilities is local overheating of the gas, due to plasma fluctuations. Thermal instabilities proceed in the following sequence: A local increase in the gas temperature (T) results in a decrease in the gas density (n), causing the (E/n) ratio to increase. This results in increased current density and thereby the E-J heating term increases, causing the local temperature to rise further. This sequence is summarized as follows:

$$T \uparrow \quad n \downarrow \quad \frac{E}{n} \uparrow \quad E \cdot J \uparrow \quad T \uparrow \uparrow \quad (2.16)$$

Since thermal instability requires heating of the gas molecules by fluctuating E-J power, it is much slower than the striation modes of instability. Thus, in order to derive the dispersion relation for the thermal modes of instability, one has to consider the conservation equations for neutral particles in addition to those for charged particles. Haas [23] and Nighan *et al.* [27] have solved the perturbed neutral density and energy conservation equations to determine the growth rate, ω , of thermal instability modes. The dispersion relation for thermal instability is of form:

$$\omega = -\frac{b}{2} \pm \frac{1}{2}(b^2 - 4c)^{1/2} > 0 \quad (2.17)$$

where:

$$b = \nu_{vt} + \frac{1}{nC_p T} \left[\frac{\kappa T}{\ell^2} + JEF_T \frac{n}{n_e} \frac{\delta n_e}{\delta n} + JEF_V (2 + \hat{\tau}_{VT}) \right] \text{ and}$$

$$c = \frac{\nu_{vt}}{nC_p T} \left[\frac{\kappa T}{\ell^2} + JEF_V \frac{n}{n_e} \frac{\delta n_e}{\delta n} \right] \quad (2.18)$$

where κ is the thermal conductivity and ℓ the scale length of the fluctuation, F_T and F_V the fraction of the input power, JE transmitted to translational and vibrational kinetic energy, ν_{vt} the frequency of energy exchange between vibrational and translational modes and τ_{VT} is the characteristic time for vibrational-translational relaxation. As before, the caret notation for

$\hat{\tau}_{VT}$ reflects the sensitivity of the rate coefficient for vibrational-translational relaxation to changes in the gas temperature *i.e.* $\hat{\tau}_{VT} \equiv d(\ln \tau_{VT})/d(\ln T)$.

Equation (2.17) gives two modes of instability; (i) if $b < 0$ translational energy grows (termed as thermal instability) or (ii) if $b > 0$ and $c < 0$ vibrational energy grows (termed as vibrational instability). Therefore, for at least one of these instabilities (thermal or vibrational) to occur, b or c must be negative. Inspecting the terms b and c in (2.18) we find that the thermal conduction term ($\kappa T/\lambda^2$) is always positive for both b and c , and, therefore, exerts a stabilizing influence. The term $(\delta n_e/n_e)(\delta n/n)^{-1}$ has been shown by Nigan *et al.* [27] to be always negative, thus exerting a destabilizing influence for both modes. Figure 2.3 shows $(\delta n_e/n_e)(\delta n/n)^{-1}$ evaluated for two different cases, *i.e.* attachment dominated and recombination dominated plasmas. As can be seen from this figure, $(\delta n_e/n_e)(\delta n/n)^{-1}$ is very strongly peaked in a direction perpendicular to the electric field ($\phi = 90^\circ$). Therefore, the coefficients b and c become negative and ω becomes positive in this direction. Thus, the resulting wave growth occurs in a direction normal to the electric field and thereby results in layering of plasma properties parallel to the direction of current flow. Such a condition can easily result in the plasma collapsing in the region of the layer having the highest electrical conductivity. The situation for thermal instability modes are, therefore, in direct contrast with the plasma striation modes of instability where wave growth occurs in the electric field direction.

Figure 2.3 also shows that the magnitude of $(\delta n_e/n_e)(\delta n/n)^{-1}$ can be 10 to 100 times larger in the attachment dominated case as compared to the recombination dominated case. Thus the presence of negative ions significantly affects thermal instabilities just as is the case for attachment instabilities. However, unlike attachment instabilities which are caused primarily due to the presence of large quantities of negative ions, thermal instabilities are not caused (but merely amplified) by the presence of negative ions. The use of an external ionization source has a very beneficial effect on thermal instability and results in the reduction of the $(\delta n_e/n_e)(\delta n/n)^{-1}$ term to unity order.

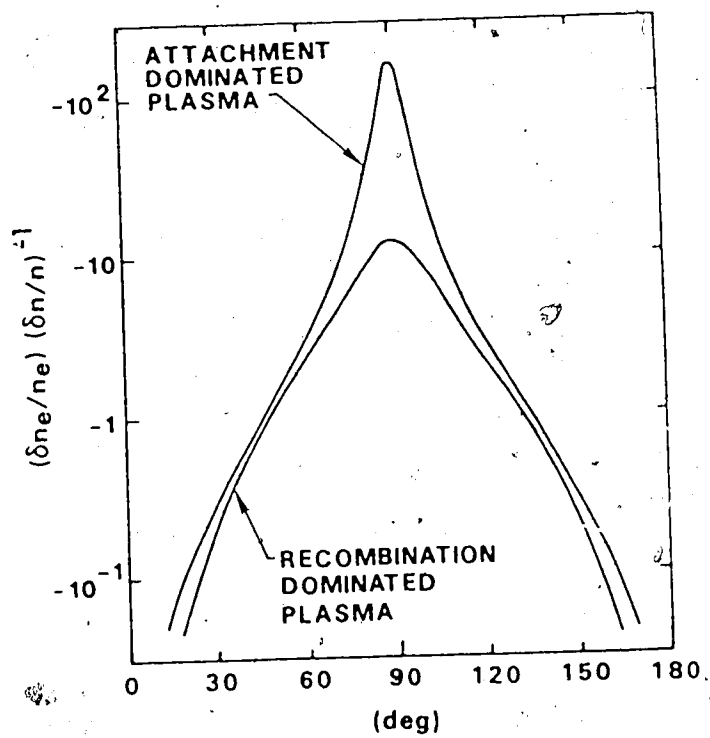


Fig. 2.3: Fractional response of the electron density to a perturbation in gas density computed for a 20 Torr $\text{CO}_2\text{-N}_2\text{-He}$ (1:7:12) mixture. From Nighan and Wigand [27].

Finally, there is the term $JEF_V(2 + \tau_{VT}^2)$ in the expression for b in (2.18). This term can be negative for cases where the V-T relaxation times are strongly decreasing functions of the gas temperature and can thereby lead to thermal instabilities. The instability in this case is caused by local thermal heating due to vibrational relaxation. As the gas temperature increases the V-T relaxation time τ_{VT} decreases, thereby increasing the energy release within the gas due to vibrational relaxation. If thermal conduction is unable to transport this energy away, the gas temperature will continue to increase giving rise to instability. The characteristic time for the evolution of this instability is generally 10^{-3} to 10^{-2} sec. Since pressure remains relatively constant in these time ranges, the gas density decreases and the local electrical conductivity rises sharply, producing local concentrations in the current flow. Vibrational modes of instability are unaffected by external sources of ionization (unlike the thermal modes) and can therefore be the limiting factor in E-beam sustained molecular lasers.

Nighan and Wiegand [27] have evaluated the instability conditions (2.17) for various scale lengths and pressures typical of medium pressure CO_2 laser gas discharges. These results are reproduced in Figure 2.4 which shows the reciprocal of the thermal instability growth rate (i.e. $\tau_g \equiv \omega^{-1}$) as a function of discharge power density. The data shows that the computed growth times are comparable to the gas residence time in the discharge for typical CO_2 convection laser discharges. However, one can avoid plasma constriction by convecting the unstable plasma from the discharge region in a time less than that required for the collapse of the glow to occur.

2.4 CONCLUSION

In the preceding pages it has been shown that there are two major manifestations of instabilities in convection cooled CO_2 laser discharges, *namely* striations (also known as charged particle production and loss instability) and plasma constriction (also known as thermal instability). Striations result from two major instability modes, i.e. ionization instability and negative-ion or attachment instability. Plasma constriction (often termed as

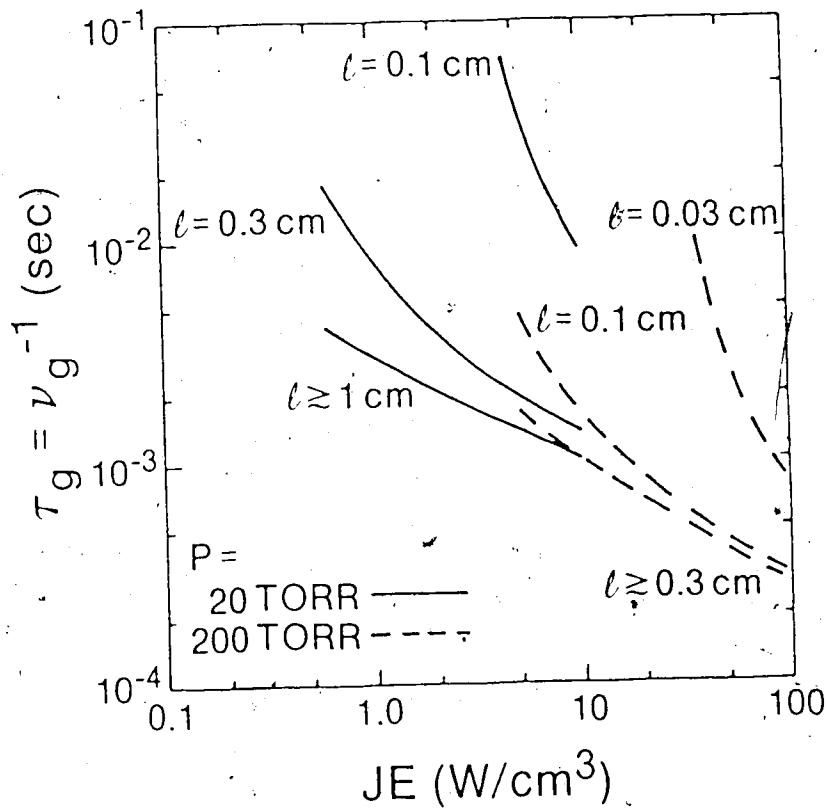


Fig. 2.4: Computed thermal instability growth time in the direction normal to the direction of J and E ($\phi = 90^\circ$) for a self sustained $\text{CO}_2\text{-N}_2\text{-He}$ (1:7:12) laser discharge at a gas temperature of 300°K (From Nighan and Wiegand [27]).

thermal instability) also arises from two major instability modes, *i.e.* thermal translational instability and vibrational instability. Whereas striations can be avoided by the use of external ionization sources or by adding detaching species (such as CO) to the gas mixture, thermal instabilities are always present in CO₂ laser discharges. If left unattended, these thermal instabilities can result in glow-to-arc collapse thereby seriously degrading laser action.

A number of techniques have evolved over the years to overcome thermal instabilities. All these techniques have relied upon the brute-force method of physically transporting the gas away from the unstable region. The reasoning behind this is that, if the residence time of the gas in the unstable region is less than the typical growth time of the instability, the instability will eventually die out. Methods that have been considered are: the use of convective gas flow and the introduction of turbulence in the discharge. While these techniques do improve the discharge stability, they entail the use of heavy blower systems; which increases the size, complexity and cost of the whole laser system.

A technique, that has recently received attention, is magnetic stabilization. Unlike previous techniques, magnetic stabilization involves the motion of charged particles rather than the bulk neutral gas. Thermal instability modes, as summarized in (2.16), arise due to a local rise in gas temperature which results in a local increase in current density that causes the gas to heat even further. The magnetic stabilization technique, however, does not allow this local increase in current density; thereby circumventing the positive feedback mechanism by which thermal instabilities grow. It does so by using magnetic fields to create large $\vec{E} \times \vec{B}$ drifts of the primary electrons emitted from the cathode, which then results in secondary emissions far from the unstable region. In order to move these charged particles by a distance greater than the instability scale lengths, one requires only modest magnetic fields (of the order of a few hundred Gauss for a 10 Torr CO₂ laser discharge). Such magnetic fields are relatively simple and inexpensive to produce, even using permanent magnets. Thus, the magnetic stabilization method appears highly attractive.

CHAPTER III

MONTE CARLO SIMULATION OF MAGNETIC FIELD EFFECT ON GROWTH OF INSTABILITIES IN LASER GASES

3.1 INTRODUCTION

In Chapter 2 it was shown that there are two major modes of instability in CO₂ convection lasers: *i.e.* striations and thermal instability. Of the two, the striation modes of instability are less serious since a laser glow discharge can be maintained despite their presence. Additionally, the striation modes of instability can be avoided altogether by the addition of detaching species (such as CO) to the laser mixture. Thermal instabilities, on the other hand, are much more serious because they can result in the discharge degenerating into an arc. For CO₂ laser conditions of interest, thermal instabilities have been shown to actually grow as a function of time. The thermal instability exponential growth rates, were shown in Fig. 2.4. These data show that the computed growth times are comparable to the inter-electrode gas residence time, for typical CO₂ convection laser conditions (*i.e.*, 10⁻³ to 10⁻² s). Thus, the main role of flow in convection cooled lasers is to move the unstable plasma from the discharge region in a time less than that required for a glow-to-arc transition to occur.

Other methods, such as external ionization and pre-ionization, have been used in conjunction with convective flow to help reduce instability growth. A technique which has recently received attention is the use of magnetic fields to reduce instability growth rates [40-42]. The advantages are quite obvious; one can build an inexpensive magnetic field source, external to the discharge region, without directly disturbing the discharge characteristics.

Initially it was conjectured that with the coupling between the charged and neutral particles, the Lorentz force would drive a strong convective gas flow within the discharge region. However, more recent and detailed computer simulations [41] reveal that because of the secondary flows that are generated, the maximum flow velocities are limited to relatively

modest values (typically 30 m/s). Consequently, this magnetically driven, bulk gas transport is insufficient to explain the observed stabilization of high power discharges. A complementary mechanism that has been proposed is the dispersion of the localized charged particle perturbations in the sheath region as a result of the transverse drifts induced by the Lorentz force. Such a dispersion must occur in a time interval less than that required for the instability to fully develop. To test this theory a Monte Carlo simulation of electron and ion motion within the cathode fall region of CO_2 laser gas discharges has been used.

3.2 MODELLING CONSIDERATIONS

Gas lasers normally employ a glow discharge for realizing the required molecular excitations. As described in Chapter 1, these glow discharges can be considered as comprising of the following regions: the cathode glow, the cathode dark space (or cathode fall region), the negative glow, the Faraday dark space, the positive column and finally the anode glow. Of these, the Cathode fall region has been found to be the most important, with respect to glow-to-arc transitions, because the electric field is strongest here. The behaviour of electrons and ions in this region must be clearly understood if any significant progress with these magnetically stabilized discharges is to be made.

Electron motion is typically described by swarm parameters, such as the ionization coefficients, attachment coefficients, drift velocity and diffusion coefficients. Traditionally, there have been two approaches to modelling electron swarms; the Boltzmann equation analysis and the Monte Carlo simulation technique. The Boltzmann equation method gives approximate solutions and is practicable only for low E/n values [44] where elastic collisions dominate and the scattering after a collision is almost isotropic. The Monte-Carlo technique, on the other hand, can be used for a large range of E/n values and can simulate problems where effects such as electron excitation and ionization are also important. The Monte Carlo simulation technique involves a detailed following of the electron trajectory in three dimensions; taking into account anisotropic scattering of these electrons due to collisions.

Accurate electron-gas collision cross sections are required in order for the Monte Carlo simulation to effectively model the gas discharge. Fortunately, these parameters have been extensively measured and tabulated over the past fifty years.

The only major problem encountered in utilizing the Monte Carlo technique is the excessive computation time that is required to properly model a gas discharge. This problem has been reduced somewhat with the advent of fast computers. A further improvement has been made in the present computational technique in order to increase speed. Conventional techniques [44-48] involve the division of the region to be modelled into a large number of grid points at which the phase-space parameters (i.e. positions and velocities) are calculated. Additionally, a large number of time steps are used in order to calculate these parameters. The use of these techniques for modelling a region with a magnetic field results in both excessive computational cost and round-off errors. The method used in this study for calculating particle trajectories involves a hybrid analytical-computational technique whereby the phase space points are only calculated at the points of collision. This not only reduces the number of computations required but is inherently more accurate since round-off errors are reduced.

3.3 THE SIMULATION ALGORITHM

The Monte Carlo technique involves following each one of a large number of particles from its source through its life history to its 'death'; using relevant probabilities at each stage of its career in determining its subsequent fate. It is important, in order for the Monte Carlo technique to be accurate, that the relevant probabilities for each of the elementary events in the 'life history' of the particle be well known. The Monte Carlo technique has been applied by a number of workers [44-46] to simulate electron swarm motion in gas discharges having a uniform electric field and undergoing both elastic and inelastic collisions. Such interactions involve random processes whose probabilistic and statistical nature is very well understood. This work was extended to a non-uniform electric field by Tran Ngoc An *et. al.* [47-48]. In

this present work a further extension has been made, which accomodates the presence of a uniform magnetic field perpendicular to the electric field.

3.3.1 Tracking Electron Motion

In this formulation, the test electron is assumed to start from a single point at the cathode with a velocity component in the $-E$ direction and with an energy value uniformly distributed between 0 and 10 electron-volts. The electron is assumed to move freely under the action of a non-uniform electric field and a uniform magnetic field, until it collides with a gas molecule. Whenever a collision occurs, the type of encounter (i.e. elastic, excitation or ionization) is determined together with the associated energy loss. The new direction of the scattered electron is determined by using scattering probability distribution functions. The electron is then allowed to continue its free motion in the electric and magnetic field until it again collides with a gas molecule. In this way, the electron is continuously tracked until it exits the cathode fall region. The final position, velocity, energy, total time of flight and the number of collisions that occurred are all stored in histograms. The secondary electrons produced by ionization are also traced in a similar fashion. When all the primary and secondary electrons have been thus traced, the swarm parameters are determined by the average state of all of these electrons. The larger the number of primary electrons the smaller the sampling error. If N_e is the number of primary electrons, the standard deviation on the mean can be shown to be $1/\sqrt{N_e}$ [49].

Figure 3.1 shows the phase-space co-ordinate system used in the present computation. The electron phase-space is specified by its x , y and z positions, the angle θ which the velocity vector makes with the v_z -axis and the angle ϕ which its projection on the v_x - v_y plane makes with the v_x -axis. At the point of collision, C , the electron path is deflected by angles θ_d and ϕ_d from its original path.

The conditions assumed in the present analysis are: (i) a non-uniform E field in the $-z$ direction, (ii) a uniform magnetic field B_0 in the $+x$ direction, (iii) no interaction between

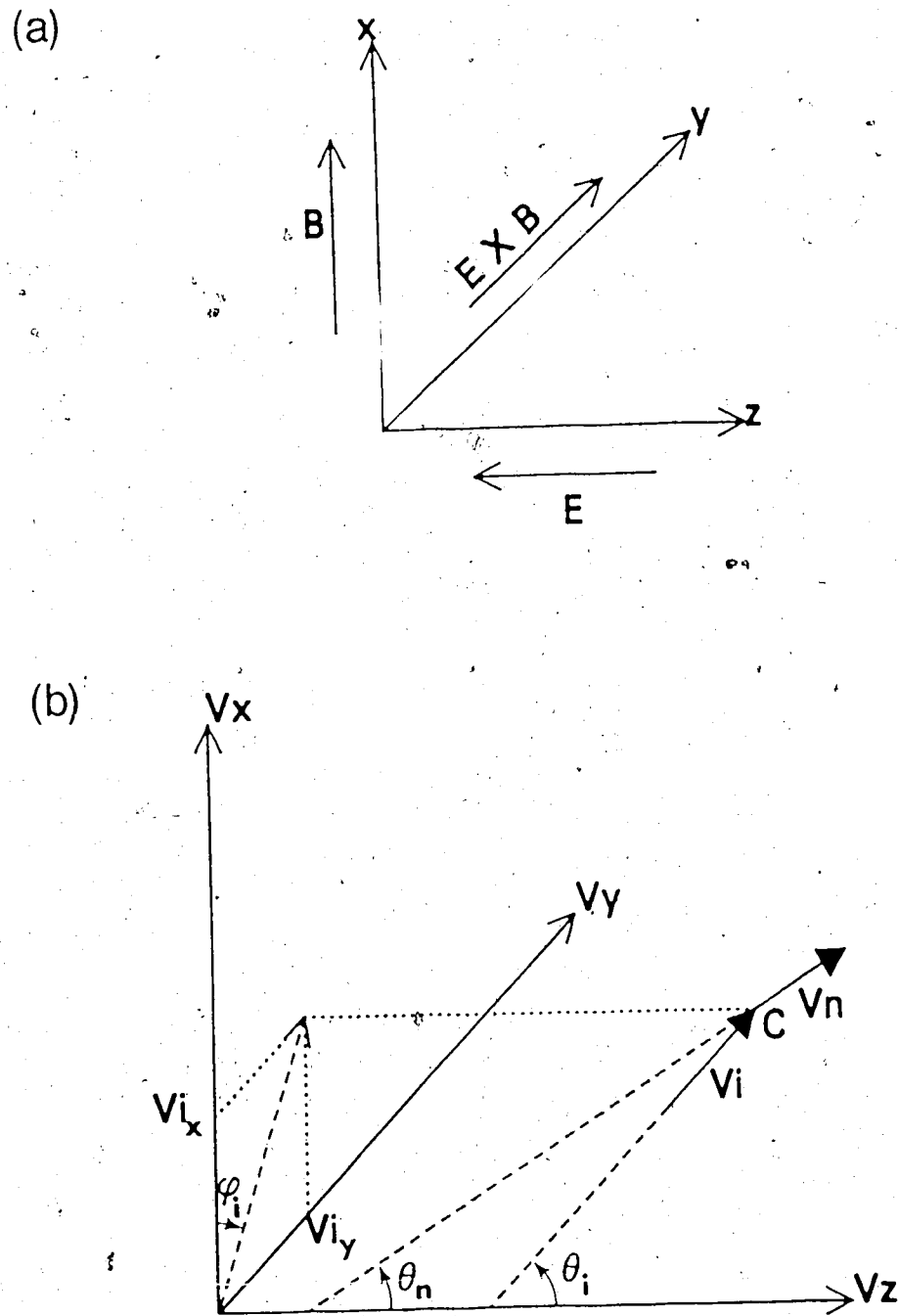


Fig. 3.1: Electron phase-space co-ordinate system. The magnetic field is assumed to have only an x-component.

(a) Space co-ordinates.

(b) Velocity co-ordinates.

charged particles (because of the low fractional ionization $\approx 10^{-7}$), (iv) stationary gas atoms and (v) no collisions of the second kind (i.e. excited atoms being further excited).

3.3.2 Determination of electron path length

At the start of each computation the path length traversed by the electron before it collides with a molecule is required. The path length, S , is known to be exponentially distributed about the mean free path, λ , of the electron so that [49]:

$$S = -\lambda \ln(R_1) \quad (3.1)$$

where R_1 is a random number uniformly distributed between 0 and 1. When a mixture of He, N_2 and CO_2 is considered, the mean free path λ is given by:

$$\lambda^{-1} = \lambda_{He}^{-1} + \lambda_{N_2}^{-1} + \lambda_{CO_2}^{-1} \quad (3.2)$$

where λ_{He} , λ_{N_2} and λ_{CO_2} are the mean free paths of an electron in He, N_2 and CO_2 respectively.

3.3.3 Determination of electron motion between collisions

In-between collisions the electron is assumed to move freely under the influence of the electric and magnetic fields. The electric field in the cathode fall region can be approximated by a linearly decreasing function [47]:

$$E(z) = \left(\frac{2V_0}{d_c}\right) \left[1 - \left(\frac{z}{d_c}\right)\right] \quad (3.3)$$

where: V_0 and d_c are the Cathode fall voltage and cathode fall distance respectively.

The basic momentum balance equation for an electron in a uniform magnetic field B_0 and an electric field $E(z)$ is given by:

$$m\left(\frac{dv}{dt}\right) = q(E + v \times B) \quad (3.4)$$

where v , q and m are the electron velocity vector, charge and mass respectively.

By assuming initial velocities $v_x(0)$, $v_y(0)$, $v_z(0)$ and initial positions $x(0)$, $y(0)$ and $z(0)$, the solution to (3.4) is:

$$\begin{aligned} v_x(t) &= v_x(0) \\ v_y(t) &= -\left[\frac{\omega_c v_z(0)}{A}\right] \sin(At) + \left[\frac{\omega_c B}{A}\right] (\cos(At) - 1) + v_y(0) \\ v_z(t) &= v_z(0) \cos(At) + B \sin(At) \end{aligned} \quad (3.5)$$

where $\omega_c = qB_0/m$,

$$A = \sqrt{\omega_c^2 - 2qV_0/(md_c^2)} \quad \text{and}$$

$$B = -\left[\frac{2qV_0}{md_c A}\right] \cdot \left[1 - \frac{z(0)}{d_c}\right] + \frac{\omega_c v_y(0)}{A}$$

The position vectors $x(t)$, $y(t)$ and $z(t)$ are obtained as integrals of $v_x(t)$, $v_y(t)$ and $v_z(t)$.

The distance ' S ' travelled by the electron within a time ' t ' is given by the path integral:

$$S = \int_0^t \sqrt{v_x^2 + v_y^2 + v_z^2} dt \quad (3.6)$$

This integral is a relatively complicated elliptic integral which is solved numerically rather than analytically in the program.

It should be noted that the subscript '0' in (3.5) and (3.6) identifies velocity and position values at the last collision point, which are regarded as the initial conditions.

The algorithm described thus far consists of generating a random number R_1 , determining a path length S from equation (3.1) and solving for t from equation (3.6). Equation (3.6) is solved for t by using an iterative technique. The integral for each guess t , is evaluated numerically using Simpson's rule.

3.3.4 Determination of collision type

Knowing the value of t , one can determine the x , y and z coordinates at the onset of the next collision. Whenever a collision between the test electron and a gas molecule occurs, the following must be determined: (i) which gas species was involved in the collision, (ii) the type of collision, *i.e.* whether elastic or inelastic, and if inelastic to determine to what level the molecule is excited and (iii) the new direction of the electron after collision. All these require the use of various cross-sections (total, elastic, excitation, ionization and differential) for the individual gases. Additionally, all these cross-sections are highly electron energy dependent. Consequently, it is necessary to have accurate cross-sectional data if the simulation is to give accurate results. After a thorough literature survey, the most recent and accurate cross-sectional data was compiled. The references that have been used are given in Table 3.1. The cross-sectional data is reproduced here graphically for Helium (Figure 3.2), Nitrogen (Figure 3.3) and Carbon Dioxide (Figure 3.4). The differential cross-sections are tabulated for Helium, Nitrogen and Carbon Dioxide in Tables 3.2, 3.3 and 3.4. The energy range considered in these cross sections is from 0 to 100 eV. This range is more than sufficient for the type of laser gas discharges being modelled.

With the use of this array of cross-sectional data one can now proceed with the simulation. The simulation code uses random numbers at each collision point to determine:

1. **The gas species involved in a collision.** This is obtained by using a random number R_2 (uniformly distributed between 0 and 1) in conjunction with the total cross-section and partial pressure of each species. This step is only required when a multi-species gas is considered. A collision with a helium molecule is assumed if:

$$R_2 < \frac{P_{\text{He}} \sigma_{t\text{He}}}{(P_{\text{He}} \sigma_{t\text{He}} + P_{\text{N}_2} \sigma_{t\text{N}_2} + P_{\text{CO}_2} \sigma_{t\text{CO}_2})} \quad (3.7)$$

whereas a collision with a N_2 molecule is assumed if:

Table 3.1: References used for the Various Cross Sections of Helium, Nitrogen and Carbon-Dioxide.

(a) HELIUM

TYPE OF CROSS-SECTION	ONSET ENERGY (eV)	REFERENCE	RANGE (eV)
Total Scattering	0	Andrick & Bitsch [50] de Heer & Jansen [51]	1.0 - 20 20 - 500
Excitation ($2^3s + 2^1s$)	19.805	Fleming & Higginson [52] de Heer & Jansen [51]	19 - 30 30 - 1000
Excitation (2^1p)	21.203	de Heer & Jansen [51]	30 - 500
Ionization	24.586	Rapp & E. Golden [53]	24 - 500
Differential	-----	Shyn <i>et. al.</i> [54]	2 - 100

(b) NITROGEN

Total Scattering	0	Golden [55] Shyn <i>et. al.</i> [56]	0.36 - 4.4 5.0 - 90
Vibrational Exc. (Level 1)	0.291, 0.582, 0.873, 1.46, 1.75, 2.04, 2.33	Engelhardt <i>et. al.</i> [57]	0 - 3
Excitation (Levels 2-5)	6.22, 7.39 8.59, 11.05	Engelhardt <i>et. al.</i> [57]	6.22 - 100
Ionization	15.7	Rapp & E. Golden [53]	15.7 - 100
Diss. Ionization	25.5	Rapp & E. Golden [53]	25.5 - 100
Differential	-----	Shyn <i>et. al.</i> [54]	1.5 - 100

(c) CARBON-DIOXIDE

TYPE OF CROSS-SECTION	ONSET ENERGY (eV)	REFERENCE	RANGE (eV)
Total Scattering	0	Ramsauer & Kollath [58] Bruche [59]	0.14 - 2.7 2.9 - 100
Vibrational Exc. (Level 1)	0.0827, 0.291, 0.580, 0.870	Hake & Phelps [60]	0 - 100
Excitation (Levels 2,4,5)	3.1, 7.0 10.0	Hake & Phelps [60]	3 - 100
Dissociation (Levels 3,6)	6.1 11.5	Corvin & Corrigan [61] Ajello [62]	6 - 100 11 - 100
Ionization	13.3	Rapp & E. Golden [53]	13 - 100
Diss. Ionization	25.0	Rapp & E. Golden [53]	25 - 100
Differential	----	Shyn <i>et. al.</i> [63]	3 - 90

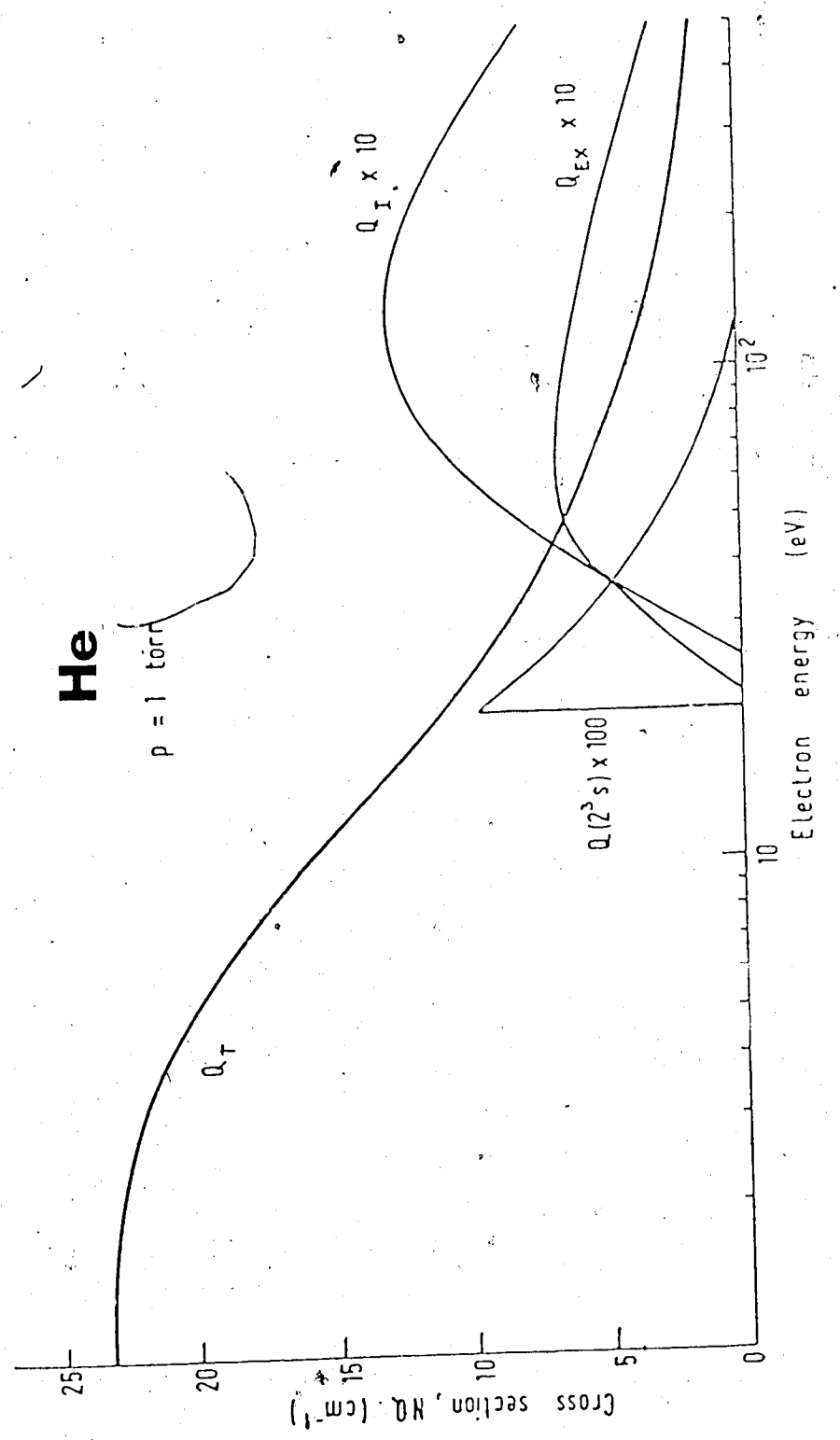


Fig. 3.2: Various collisional cross-sections for Helium [64].

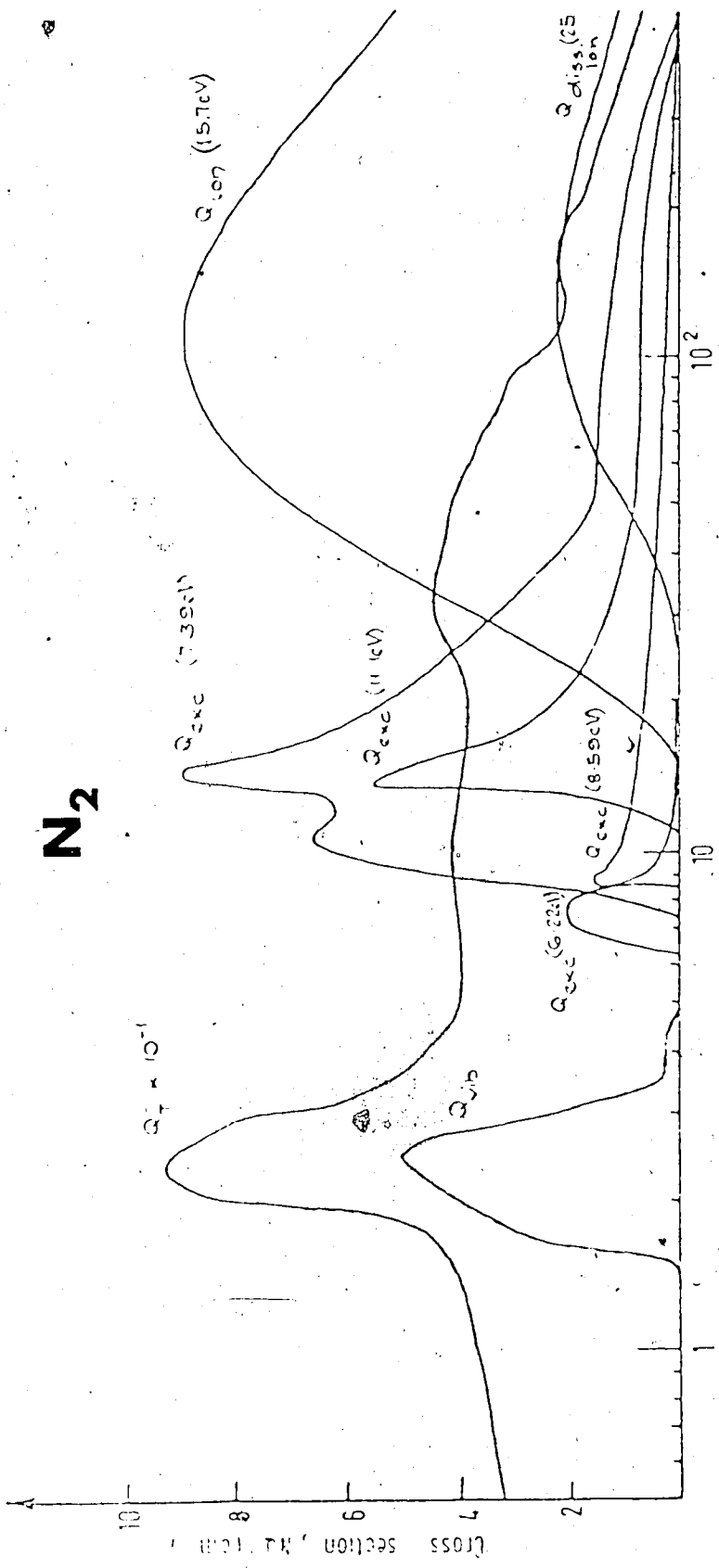


Fig. 3.3: Various collisional cross-sections for Nitrogen [46].

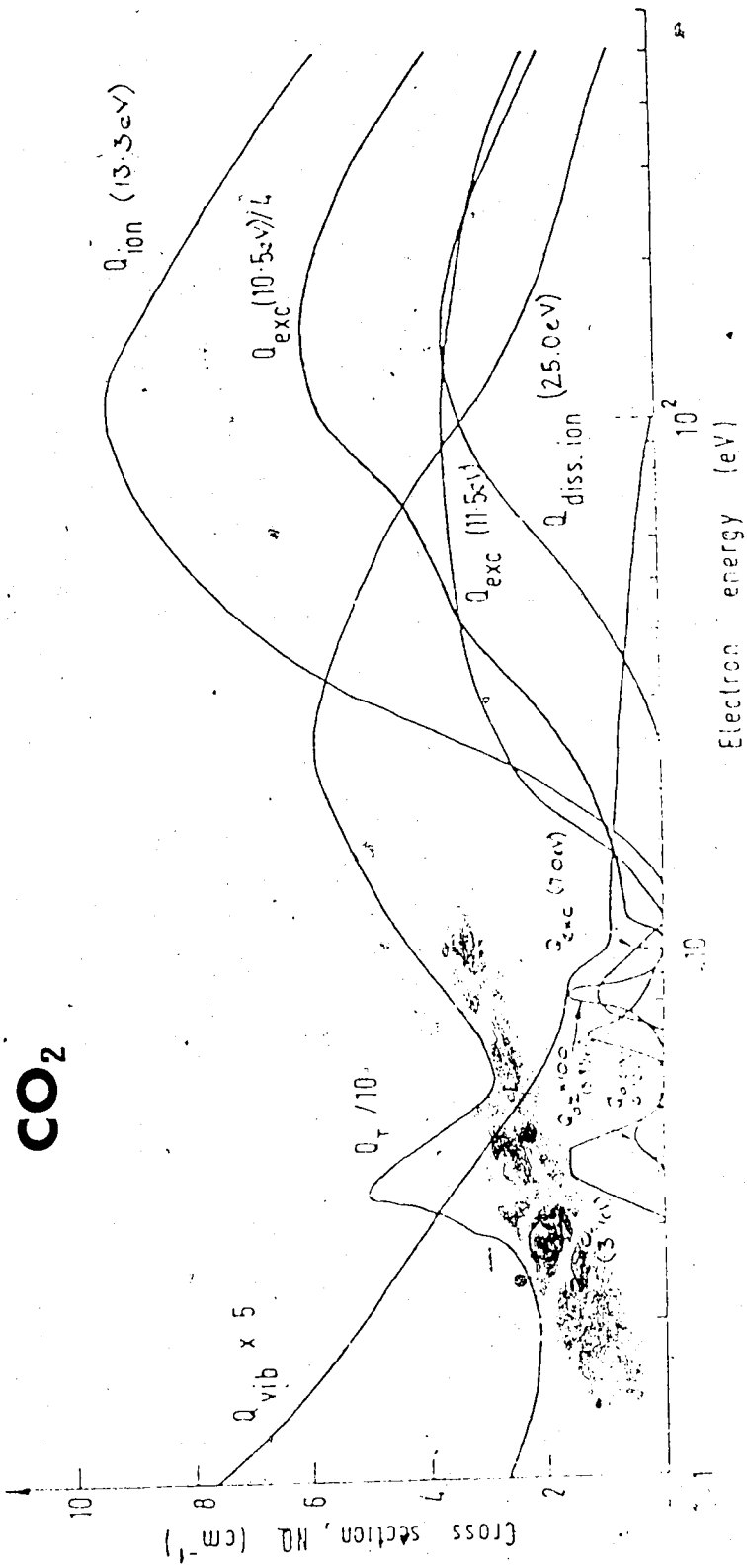


Fig. 3.4: Various collisional cross-sections for Carbon Dioxide [46].

Table 3.2: Differential cross-sections ($d\sigma/d\Omega$), for elastic electron-helium scattering. The units of ($d\sigma/d\Omega$) are 10^{-18} cm²/s [54].

θ (deg)	E (eV)									
	5.0	10.0	15.0	20.0	30.0	50.0	70.0	100.0		
6								92.1	68.3	
12	22.4	23.0	29.2	38.9	54.6	68.8	79.1	75.1	72.6	47.1
18						59.0	68.4	58.5	53.3	35.1
24	26.2	25.6	28.3	33.6	45.4	53.6	57.5	46.6	41.2	27.2
30						41.0	47.3	35.6	31.0	18.6
36	30.1	28.5	27.8	30.8	36.7	40.3	39.4	28.3	23.1	14.0
48	32.7	30.7	28.4	27.6	29.3	30.4	26.7	17.6	13.6	7.8
60	35.6	32.2	29.8	26.6	23.3	23.8	18.8	11.5	8.6	4.8
72	38.0	37.0	32.4	26.4	21.3	19.6	13.9	8.3	5.9	3.0
84	41.8	41.3	35.5	27.1	21.8	17.7	11.8	6.4	4.4	2.1
96	45.1	45.8	40.3	29.5	22.0	17.1	10.8	5.4	3.5	1.7
108	50.3	52.2	45.0	33.8	24.5	17.5	10.8	4.9	3.0	1.4
120	56.2	57.7	51.6	38.4	27.8	19.0	11.1	4.9	2.8	1.3
132	63.5	62.1	57.2	43.7	31.0	20.2	12.2	4.9	2.7	1.1
144	66.1	66.5	59.5	48.8	34.8	21.5	12.9	5.3	2.8	1.2
156	69.7	68.4	68.8	53.9	38.5	22.8	13.9	5.6	2.9	1.2
168	74.9	73.5	73.0	58.1	43.5	24.5	15.4	6.1	3.0	1.2

Table 3.3: Differential cross-sections ($d\sigma/d\Omega$), for elastic electron-nitrogen scattering. The units of ($d\sigma/d\Omega$) are 10^{-18} cm²/s [56].

θ (deg)	E (eV)										
	3.0	4.0	5.0	7.0	10.0	20.0	30.0	40.0	50.0	70.0	100.0
6										1655.4	1592.6
12	298.8	184.2	158.7	210.9	255.2	674.8	875.8	991.0	1047.5	1102.2	934.3
18										552.2	429.5
24	262.0	162.0	161.7	202.8	240.1	421.1	408.5	403.1	360.1	297.9	212.7
30										139.2	90.3
36	212.2	159.4	159.9	191.3	199.1	216.2	182.6	144.0	105.4	77.8	48.4
48	155.9	125.7	134.8	169.7	153.5	117.7	75.6	53.0	38.0	26.7	19.5
60	108.3	95.1	103.0	129.9	103.2	63.3	35.1	23.7	17.7	13.3	10.9
72	77.9	71.4	77.9	88.1	62.7	33.3	19.1	13.5	10.2	7.4	7.5
84	66.0	56.1	62.9	67.5	46.9	19.6	13.3	8.5	6.6	6.3	7.3
96	61.7	50.2	57.5	55.9	36.1	22.1	12.4	7.9	6.6	7.5	7.4
108	68.2	52.5	56.9	59.9	45.0	34.8	18.4	12.3	11.0	10.8	8.2
120	79.0	59.6	61.1	71.5	60.3	52.5	30.8	24.2	21.4	17.6	10.5
132	115.8	73.8	70.7	82.6	76.4	70.0	50.6	42.8	35.8	24.5	13.6
144	174.3	92.1	87.5	101.7	93.7	93.5	77.6	65.1	51.6	31.7	18.0
156	237.1	116.9	100.6	110.8	108.0	121.2	104.2	90.4	67.7	39.2	22.6
168	300.0	141.7	113.8	120.5	121.9	148.8	130.9	115.8	83.7	46.6	28.1

Table 3.4: Differential cross-sections ($d\sigma/d\Omega$), for elastic electron-carbon dioxide scattering. $(d\sigma/d\Omega)$ are in arbitrary units [63].

θ (deg)	E (eV)										
	3.0	4.0	5.0	7.0	10.0	20.0	30.0	40.0	50.0	70.0	90.0
6	148	686	389	278	1094	6327	6834	9560	7400	6545	8482
12	144	595	356	269	855	4401	4160	4945	3682	3109	2677
18	143	503	333	259	684	2726	2600	2500	1844	1530	972
24	142	435	317	248	547	1734	1560	1185	849	649	375
30	141	378	294	234	408	1109	847	529	462	306	165
36	141	301	274	223	335	751	520	313	255	170	91
42	140	262	259	208	276	494	312	191	144	105	54
48	135	233	242	198	221	336	208	119	90	65	34
54	125	212	231	194	174	237	146	84	60	41	24
60	133	196	210	181	147	184	104	64	46	30	19
66	133	177	192	164	122	127	79	49	35	26	18
72	142	168	173	148	106	98	61	35	31	23	14
78	139	158	154	136	96	82	52	32	27	19	12
84	138	146	140	123	90	65	46	29	24	17	11
90	144	140	123	116	86	64	49	27	20	15	11
96	147	134	109	103	80	67	56	29	20	15	11
102	159	135	98	96	79	73	65	31	21	20	13
108	162	133	81	92	86	91	76	37	32	23	16
114	176	143	82	93	101	109	88	52	46	35	20
120	187	148	87	98	127	126	101	138	67	44	25
126	196	162	93	108	148	160	119	107	97	55	29
132	210	179	112	128	194	199	152	145	132	68	36
138	212	201	139	157	242	244	193	216	171	88	41
144	213	237	187	196	302	309	267	249	212	106	51
150	215	294	254	251	362	373	297	314	255	127	65
156	220	361	329	310	408	414	357	370	297	150	76
162	220	408	389	363	501	527	438	431	339	175	88
168	226	526	467	414	593	645	535	486	375	207	102
174	228	625	589	476	718	782	669	542	412	240	114

$$\frac{P_{\text{He}} \sigma_{\text{He}}}{(P_{\text{He}} \sigma_{\text{He}} + P_{\text{N}_2} \sigma_{\text{N}_2} + P_{\text{CO}_2} \sigma_{\text{CO}_2})} < R_2 < \frac{(P_{\text{He}} \sigma_{\text{He}} + P_{\text{N}_2} \sigma_{\text{N}_2})}{(P_{\text{He}} \sigma_{\text{He}} + P_{\text{N}_2} \sigma_{\text{N}_2} + P_{\text{CO}_2} \sigma_{\text{CO}_2})} \quad (3.8)$$

If neither of these inequalities hold, then a collision with a CO_2 molecule is assumed. Here P_{He} , P_{N_2} and P_{CO_2} denote the partial pressures and σ_{He} , σ_{N_2} and σ_{CO_2} denote the total cross-sections of helium, nitrogen and carbon-dioxide.

2. The type of collision - elastic or inelastic. To determine which collision type occurs another random number R_3 , which is uniformly distributed between 0 and 1, is used. If:

$$\begin{aligned} R_3 > \Sigma \sigma_j / \sigma_t &\Rightarrow (\text{elastic collision occurred}), \\ R_3 < \Sigma \sigma_j / \sigma_t &\Rightarrow (\text{inelastic collision occurred}) \end{aligned} \quad (3.9)$$

Here σ_j is the cross-section for the j 'th excitation level and σ_t is the total collisional cross-section (including both elastic and inelastic collisions).

To determine which level was excited, inelastic cross-sections are scanned from 1 to J .

R_3 can once again be used to determine the occurrence of the j 'th inelastic collision if:

$$\left(\frac{\sigma_j}{\sigma_t}\right) > R_3 > \left(\frac{\sigma_{j-1}}{\sigma_t}\right) \quad (3.10)$$

where $\sigma_0 = 0$. When $j = J$, an ionization collision can be assumed to have occurred.

Subsequently, the electron energy E_n after a collision occurs is determined as follows:

$$\begin{aligned} E_n &= E_i [1 - 2(m/M)(1 - \cos\theta_d)] \dots\dots (\text{elastic collision}) \\ E_n &= E_i - E_j \dots\dots\dots (\text{excitation collision}) \\ E_n &= (E_i - E_{\text{ion}})/2 \dots\dots\dots (\text{ionization collision}) \end{aligned} \quad (3.11)$$

where E_i is the energy of the electron before collision, E_j the excitation energy onset of the j 'th level, E_{ion} the ionization energy, m the electron mass, M the mass of the molecule and θ_d is the angle by which the electron is deflected in the plane of incidence.

The energy of the electron after collision can be used as the starting condition for the free motion of the electron till its next collision. There still remains, however, to determine the direction of motion of the electron after collision.

3.3.5 Determining Scattering Parameters

As has already been shown in Fig. 3.1, only two angles θ and ϕ are necessary to specify the direction of motion of the electron. If we assume that θ_i and ϕ_i are directional angles of the electron just before collision and if θ_d and ϕ_d are the angles by which the electron is deflected, the new directional angles θ_n and ϕ_n can be given by, (see Appendix I):

$$\begin{aligned}\theta_n &= \cos^{-1} [\cos\theta_d \cos\theta_i - \sin\theta_d \cos\phi_d \sin\theta_i] \\ \phi_n &= \cos^{-1} \left[\frac{1}{\sin\theta_n} \{ \sin\theta_d \cos\phi_d \cos\theta_i \cos\phi_i - \sin\theta_d \sin\phi_d \sin\phi_i \right. \\ &\quad \left. + \cos\theta_d \sin\theta_i \cos\phi_i \} \right]\end{aligned}\quad (3.12)$$

To determine the deflection angles θ_d and ϕ_d one can use two more uniformly distributed random numbers R_4 and R_5 . Since ϕ_d represents the scattering about the plane of incidence it is symmetrically distributed from 0 to 2π radians, and can be given by:

$$\phi_d = 2\pi R_4 \quad (3.13)$$

The determination of θ_d is somewhat more complicated since the scattering in that direction is anisotropic. One can, however, make use of scattering probability density data, given in Tables 3.2, 3.3 and 3.4, to determine the values of θ_d . Figure 3.5 is a family of plots, of the scattering probability density $p(\omega)$ as a function of the solid angle ω , for electrons in Helium. Electron energies range from 0 to 100 eV. As can be seen from this figure, high energy electrons suffer very little scattering as compared to low energy electrons. The scattering probabilities are, however, nonlinear functions of electron energy. This is specially true at the low electron energy range. These results are as one would expect. At low electron energies, the

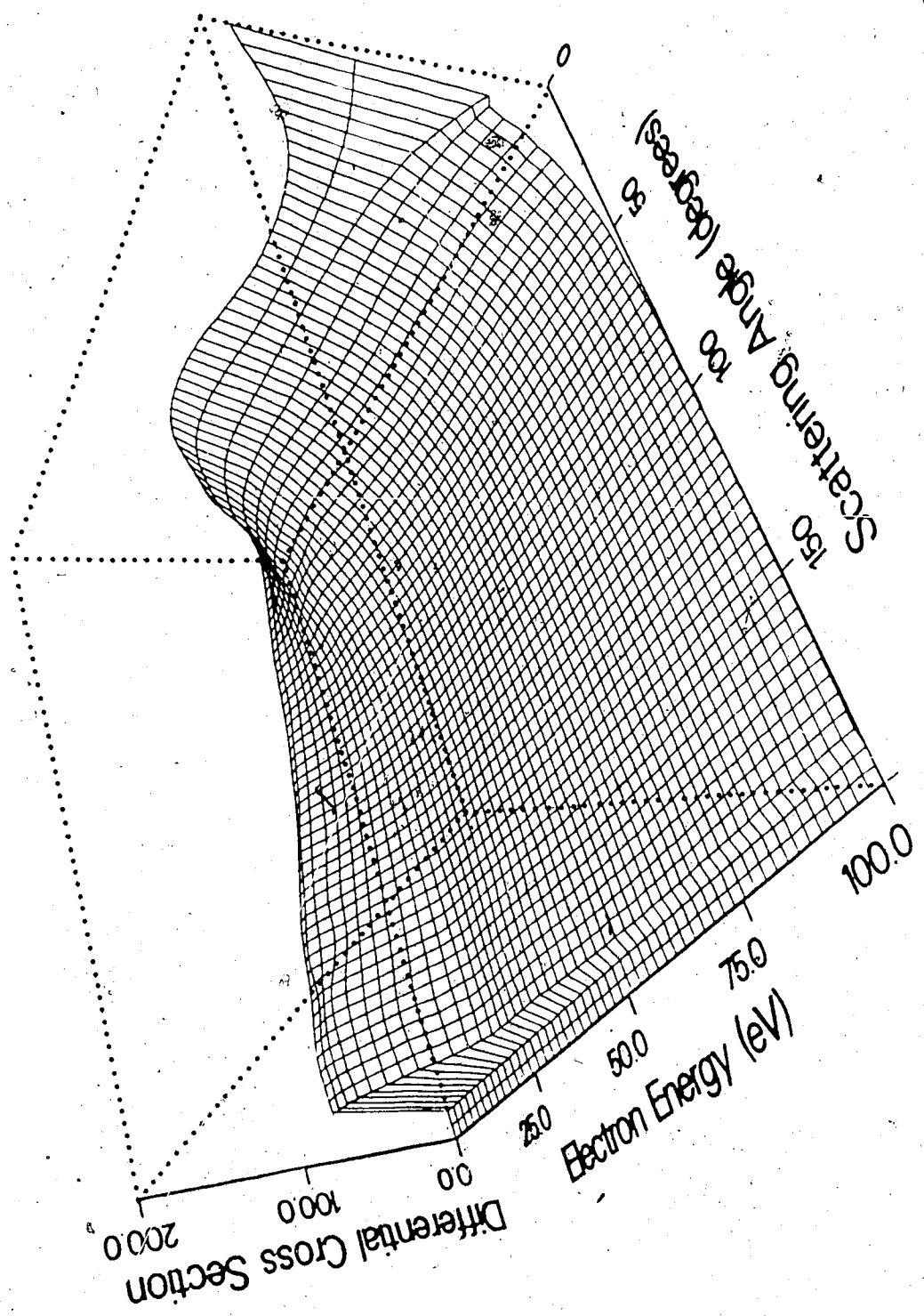


Fig. 3.5: Scattering probability densities for electrons in Helium, for energies ranging from 0 eV to 100 eV. The cross sections are in units of 10^{-18} cm²/s.

electron can easily interact with the contacting gas molecules, thereby suffering anisotropic scattering. Similar results can be seen for N_2 and CO_2 .

It should be added that the scattering density plot was obtained without considering magnetic field effects. This is because the presence of a small magnetic field should have little affect on the scattering probability. Scattering is primarily an atomic phenomena occurring over very short distances of the order of angstroms, whereas magnetic fields influence the electron motion over the Larmor radius distance, which is orders of magnitude longer.

In order to generate random numbers distributed according to the probability density function of Fig. 3.5 (and Tables 3.2-3.4), one can use uniformly distributed random numbers and transform them according to the inverse of the cumulative distribution function [64]. In other words, one can determine the value of ω_d distributed with probability density $p(\omega)$ by using a uniformly distributed random number R_s , which satisfies the following relation:

$$R_s = \left[\int_0^{\omega_d} p(\omega) \cdot d\omega \right] / \left[\oint p(\omega) \cdot d\omega \right] \quad (3.14)$$

where \oint represents integration over the whole sphere.

Equation (3.14) gives us the solid angle ω_d which is distributed according to $p(\omega)$. However, we are more interested in finding the scattering angle θ_d . Thus using the relation $d\omega = 2\pi \sin\theta \cdot d\theta$ one can transform (3.14) into:

$$R_s = \left[\int_0^{\theta_d} p(\theta) \cdot \sin\theta \cdot d\theta \right] / \left[\int_0^{\pi} p(\theta) \cdot \sin\theta \cdot d\theta \right] \quad (3.15)$$

The integral $\int_0^{\theta} p(\theta) \cdot \sin\theta \cdot d\theta$ for θ varying from 0 to π radians and normalised by the factor $\int_0^{\pi} p(\theta) \cdot \sin\theta \cdot d\theta$ is shown in Fig. 3.6 for a range of energy values from 0 to 100 eV. Thus, one must first generate a uniformly distributed random number R_s , and based on the energy of the electron before collision one must use Fig. 3.6 to determine the deflection angle θ_d . Since $p(\omega)$ has been tabulated for only a few energy values it is necessary to interpolate for energy values other than those given.

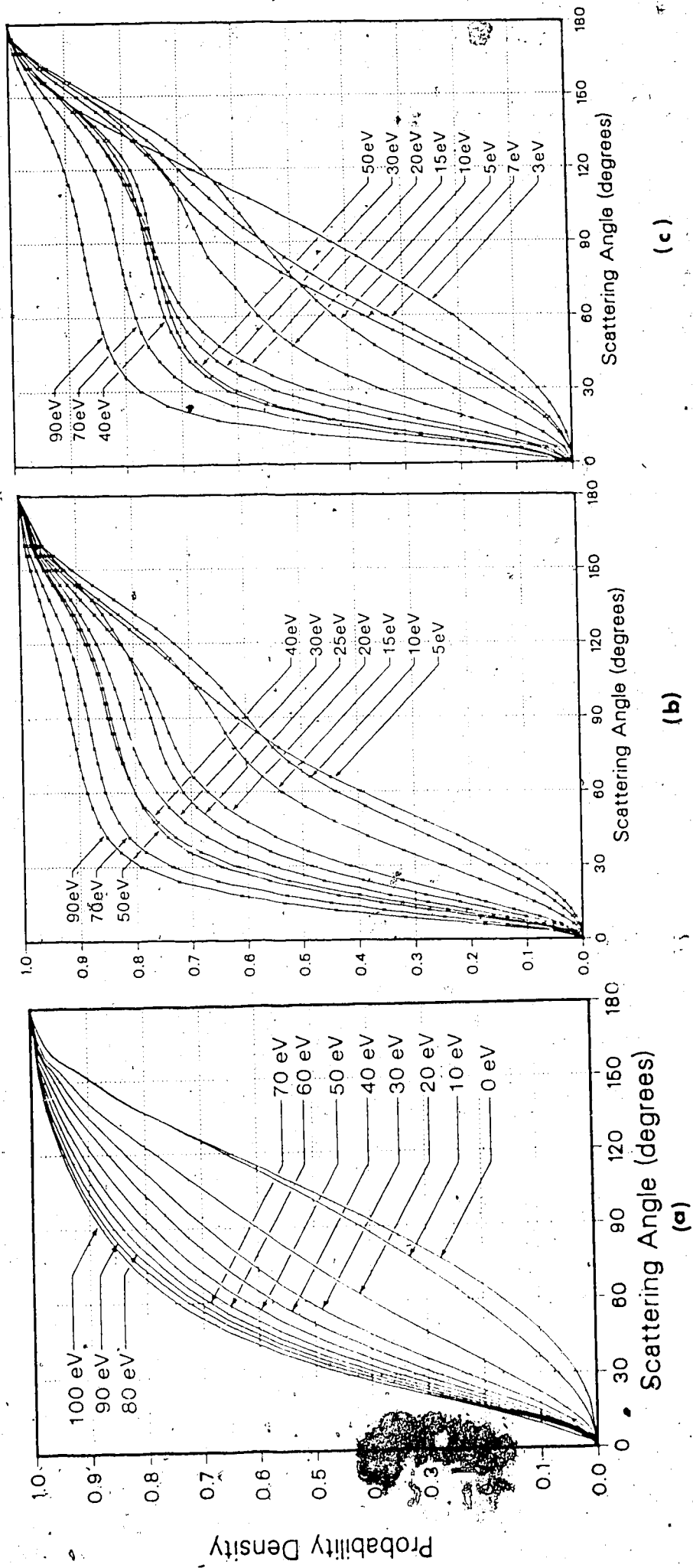


Fig. 3.6: Cumulative distribution function for scattering of electrons in different gas species for energies between 0 and 100 eV:

- (a) Helium gas
- (b) Nitrogen gas
- (c) Carbon-Dioxide gas

3.3.6 Termination Parameters

The electron path is followed from its source at the cathode, through its life history of collisions, until it crosses the cathode fall region. The moment this happens, the final state of the electron is stored; along with other data such as the time of flight of the electron, the number of collisions that occurred on the way and the resolution of these collisions into the number of collisions with each individual gas species. The collisions with each gas species is further subdivided into the number of elastic, excitation and ionization collisions.

The secondary electrons that are created by each individual primary electron are traced in a similar manner and their final states also stored. The whole sequence of events is repeated for a large number of primary electrons and the final swarm parameters are calculated as an average of all the electrons. The swarm parameters considered in the present simulation are: the drift velocities in the electric field direction (i.e. z) and in the $\vec{E} \times \vec{B}$ direction (i.e. y) and the Hall parameter. The drift velocity is calculated by dividing the total distance travelled (in the z or y direction) by the time of flight of the test electron. The Hall parameter, β , provides a measure of the number of closed orbits that an electron makes between collisions and is given by:

$$\beta = \frac{\omega_e}{\nu_e} \quad (3.16)$$

where: ω_e = cyclotron frequency = $[|q|B_0/m]$ and

ν_e = mean collisional frequency = \bar{v}/λ

The complete sequence of events described so far has been summarized in the form of a flowchart given in Fig. 3.7.

3.3.7 Motion of Ions

It is important not only to follow the motion of the electrons but also to follow that of the ions. Ion bombardment onto the cathode surface gives rise to a new generation of

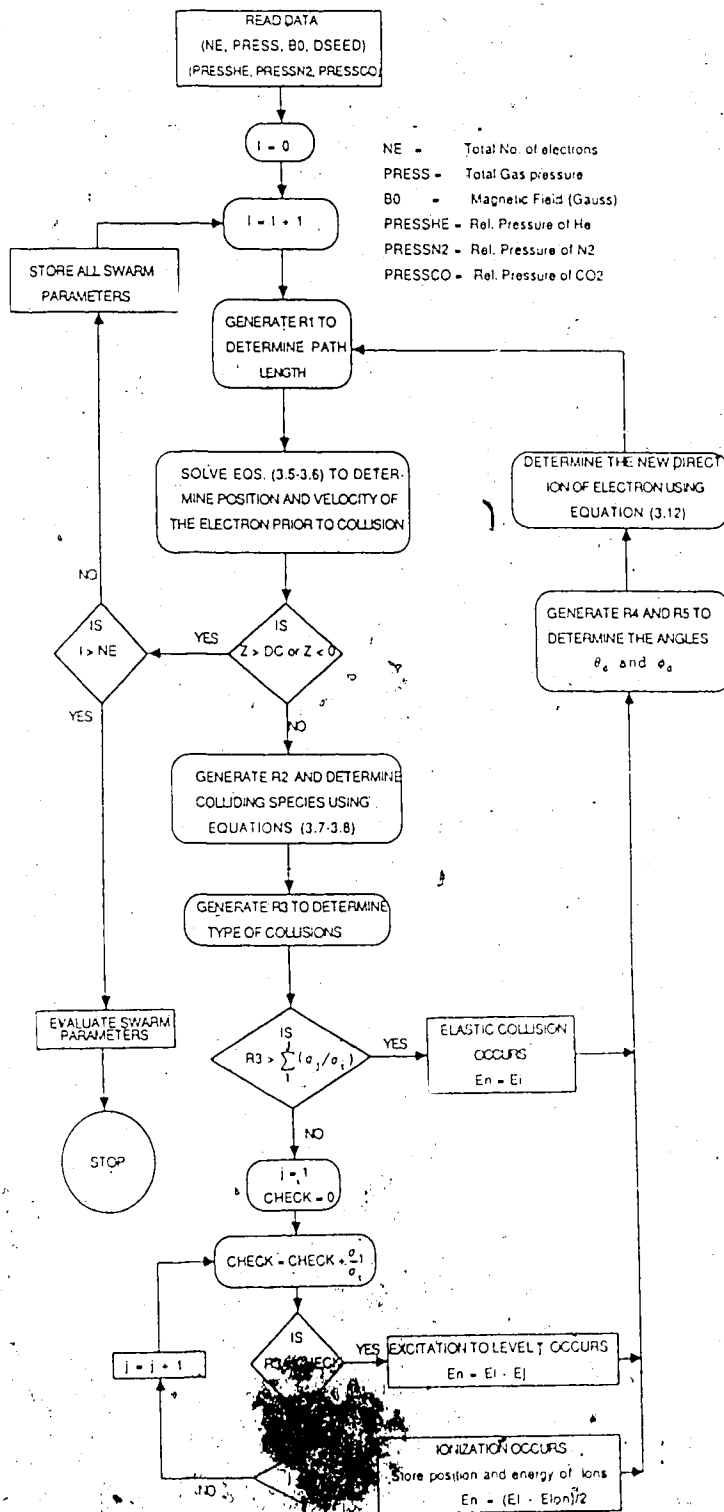


Fig. 3.7: Flowchart of the Monte-Carlo simulation program

electrons; thereby maintaining the discharge. Since the ions move much more slowly than the electrons and since their motion is characterised by random motion dominated by elastic collisions, mobility theory can be applied to describe their motion. Using the mobility values of the individual gas ion species, the time taken by the ions to return to the cathode is estimated. This drift time, when added to the time taken for the test electron to create that particular ion (i.e. the elapsed time from the moment the primary electron left the cathode till the ionization event), gives the total time before the discharge can be regenerated. This value can be used to estimate the drift velocity of the discharge in the $\vec{E} \times \vec{B}$ direction; which has been termed as 'transverse discharge velocity' in this paper. The transverse discharge velocity can be used to determine the lateral spread of the discharge within typical instability growth times.

3.4 RESULTS

A computer program, based on the algorithm described in the previous section, has been used to simulate various gas discharges at different pressures and magnetic fields. The computations have been accomplished using the high speed and precision offered by the CYBER-205 system. Specific swarm parameters have been calculated for pressures of 5, 10 and 30 torr. This range of pressure is typical of many operating CO₂ lasers. Magnetic fields ranging from 1 Gauss to 1000 Gauss have been considered. The cathode fall voltage, assuming stainless steel electrodes, is set to be 150 Volts for He, 215 Volts for N₂ and 450 Volts for CO₂ [65]. In addition, the pressure-cathode fall distance product is assumed to be 13 mm-Torr for He, 42 mm-Torr for N₂ and 40 mm-Torr for CO₂ [65]. These values are known to remain constant over a wide range of pressures. For a mixture of these gases, as is the case in CO₂ lasers, the value of the cathode fall voltage and the pressure-cathode fall distance product are assumed to be the pressure weighted averages of the individual gases. The mobility value of helium ions in helium gas varies between 0.85 to 0.16 m²/V-sec [66], depending on the value of the electric field. Similarly, the mobility of nitrogen ions in

nitrogen gas is $0.2 \text{ m}^2/\text{V}\cdot\text{sec}$, and for carbon-dioxide ions in carbon-dioxide gas is $0.073 \text{ m}^2/\text{V}\cdot\text{sec}$ [67]. The mean free path (m.f.p.) of an electron in Helium, is assumed to be $8 \times 10^{-4} \text{ m}$. at 1 Torr pressure; while the corresponding values of m.f.p. in N_2 and CO_2 are $2.7 \times 10^{-4} \text{ m}$. and $1.8 \times 10^{-4} \text{ m}$. respectively [17].

Table 3.5 gives a summary of the results of the simulation for each of the three gases; He, N_2 and CO_2 ; as well as for a laser gas mixture. The number of test electrons used to calculate the swarm parameters for the 5 torr case was 500. It was found that a much larger number of test electrons were needed for the 10 torr and 30 torr cases, in order to properly determine these parameters. Consequently 2000 electrons were used in these simulations. This implies an accuracy of approximately 2.2% for the swarm parameters. It should be noted here that the swarm parameters have been calculated as the average over not just the test electrons, but over the total number of test electrons plus the primary ionization electrons.

A number of interesting patterns emerge out from the results in Table 3.5.

1. For all the three gases; He, N_2 and CO_2 ; it is seen that the larger the value of the magnetic field the greater the number of collisions. For He at 5 torr, the number of collisions increases dramatically from 53 at 1 Gauss to 120 at 1000 Gauss. The corresponding increases for N_2 and CO_2 , for the same increase in magnetic field, are from 888 to 1390, and from 1275 to 1609, respectively. For the 10 torr case, which is much more collision dominated, the increase in the number of collisions with increased magnetic field is much less; 55 to 69 for He, 689 to 959 for N_2 and from 1373 to 1469 for CO_2 . For the 30 torr case, which is predominantly collision dominated, the increase is almost unnoticeable.
2. The average transit time of flight of the test electrons also shows an increase with respect to the magnetic field for all the 3 gases; with the increase more noticeable for the lower pressures.
3. Similarly, the average distance, y , travelled by the electron in the $\vec{E} \times \vec{B}$ direction increases with higher B values. As one would expect, the final x -position remains

Table 3.5: Swarm parameters for Helium, Nitrogen, Carbon-Dioxide and CO₂ laser mixture gas discharges at various magnetic fields and pressures.

Table 3.5(a): Swarm parameters for a Helium gas discharge at various pressures and magnetic fields.

(i) 5 Torr ($d_c = 2.6$ mm.)

Mag. Field (Gauss)	Total No. of Colls.	Hall Parameter	Distribution of collision types (Percentage)		Avg. Dist. Y (x d)	Final Energy (eV)	Avg. transit time (ns)	Discharge Velocity (m/s)
			Elastic : Level 1	Level 2 : Ionisation				
1	53.50	0.00108	95.665	0.176 : 1.923 : 2.236	0.005	19.19	8.736	0.0
500	69.57	0.55998	96.517	0.189 : 1.564 : 1.729	0.562	17.965	12.03	14150
1000	119.65	1.17400	97.780	0.174 : 1.047 : 0.998	1.178	15.53	23.539	27860

(ii) 10 Torr ($d_c = 1.3$ mm.)

1	55.12	0.00054	95.679	0.189 : 1.946 : 2.186	0.008	19.74	4.740	0.0
500	58.42	0.26987	95.889	0.195 : 1.891 : 2.026	0.295	19.35	4.875	13010
1000	69.57	0.55998	96.517	0.189 : 1.564 : 1.729	0.562	17.97	6.015	26200

(iii) 30 Torr ($d_c = 0.43$ mm.)

1	55.12	0.00018	95.642	0.185 : 1.975 : 2.198	0.010	19.75	1.579	0.0
500	53.71	0.08986	95.603	0.187 : 1.956 : 2.254	0.08	19.38	1.467	9900
1000	56.64	0.18127	95.914	0.172 : 1.850 : 2.063	0.203	19.05	1.567	18400

Table 3.5(b): Swarm parameters for a Nitrogen gas discharge at various pressures and magnetic fields.

(i) 5 Torr ($d_c = 8.4$ mm.)

Mag. Field (Gauss)	Total No. of Collis.	Hall Parameter	Distribution of collision types (Percentage)						AVG. Dist. Y ($\times d_c$)	Final Energy (ev)	AVG. transit time (ns)	Dis-charge Vel. (m/s)		
			Elas- tic	1	2	3	4	5					6	Ionisa- tion
1	888.64	0.0013	96.62	1.005	0.539	1.334	0.233	0.233	0.0	0.040	-0.0135	1.526	67.64	0.0
500	958.97	0.5957	96.99	0.971	0.459	1.194	0.171	0.195	0.0	0.016	0.4089	1.806	79.53	2432
1000	1390.9	1.2381	97.87	0.843	0.302	0.756	0.115	0.113	0.0	0.006	0.8036	1.6722	140.41	5811

(ii) 10 Torr ($d_c = 4.2$ mm.)

1.0	689.83	0.0005	96.78	0.858	0.519	1.305	0.193	0.302	0.0	0.036	0.003	3.0550	25.12	0.0
500	814.68	0.2944	96.57	1.030	0.492	1.420	0.218	0.251	0.0	0.023	0.200	1.8483	31.06	1997
1000	958.97	0.5969	96.99	0.971	0.459	1.194	0.171	0.195	0.0	0.015	0.408	1.8059	39.77	4328

(iii) 30 Torr ($d_c = 1.4$ mm.)

1.0	689.83	0.00015	96.78	0.858	0.519	1.305	0.195	0.302	0.0	0.036	0.002	2.553	8.375	0.0
500	746.43	0.0920	96.48	1.044	0.514	1.455	0.211	0.271	0.0	0.0280	0.069	2.0761	9.371	1015
1000	784.70	0.19403	96.50	1.032	0.521	1.442	0.213	0.265	0.0	0.0230	0.124	1.8914	9.542	2630

Table 3.5(c): Swarm parameters for a Carbon-Dioxide gas discharge at various pressures and magnetic fields

(i) 5 Torr ($d_c = 8.0$ mm.)

Mag. Field (Gauss)	Total No. of Colls.	Hall Parameter	Distribution of collision types (LEVELS)							Final Energy (eV)	Avg. Dist. y ($\times d_c$)	Final Energy (eV)	Avg. transit time (ns)	Dis-charge Vel. (m/s)
			Elas-: 1	2	3	4	5	6	7					
1	1275	0.0007	92.35	2.24	0.456	0.215	0.323	0.999	0.252	0.0	0.164	2.210	162.9	0.0
500	1469	0.3513	95.45	2.434	0.382	0.185	0.291	0.862	0.218	0.0	0.182	2.311	206.4	887.6
1000	1609	0.6911	95.49	2.572	0.388	0.169	0.267	0.758	0.191	0.0	0.157	2.387	232.3	1740

(ii) 10 Torr ($d_c = 4.0$ mm.)

1.0	1373	0.0003	95.53	2.185	0.385	0.187	0.291	0.994	0.220	0.0	0.203	2.813	83.76	0.0
500	1367	0.1751	95.45	2.336	0.398	0.188	0.292	0.915	0.221	0.0	0.199	2.327	94.96	639.1
1000	1469	0.3513	95.45	2.434	0.382	0.185	0.291	0.862	0.218	0.0	0.182	2.311	103.18	1571

(iii) 30 Torr ($d_c = 1.33$ mm.)

1.0	1264	0.0001	95.49	2.351	0.396	0.170	0.276	0.925	0.205	0.0	0.192	2.373	31.82	0.0
500	1337	0.0569	95.45	2.363	0.381	0.191	0.286	0.910	0.218	0.0	0.193	2.445	32.68	610
1000	1314	0.1144	95.36	2.381	0.397	0.188	0.308	0.922	0.238	0.0	0.205	2.423	31.02	1354

Table 3.5(d): Swarm parameters for a CO₂-LASER gas discharge at 30 Torr pressure and various magnetic fields.

Mag. Field (Gauss)	Total No. of Colls. types-		Hall Parameter	Distribution of collision types (Percentage)				AVG. Dist. y ($\times d_c$)	Final Energy (eV)	Avg. transit time (ns)	Dis-charge Vel. (m/s)					
	He	N ₂		HELIUM	NITROGEN	CARBON-DIOXIDE	Elas-: tot.: Ion-: tic : Exct.: sat.									
1	188	84	0.0002	99.63	0.222	0.152	89.60	9.464	0.933	90.72	7.619	1.661	0.0008	4.282	5.357	0
100	202	91	0.0218	99.71	0.167	0.121	89.62	9.340	1.042	91.04	7.318	1.642	0.0065	4.292	5.816	322
500	204	92	0.1093	99.70	0.176	0.124	89.63	9.367	1.008	91.00	7.326	1.670	0.0831	4.259	5.948	3343
1000	208	94	0.2219	99.71	0.169	0.122	89.78	9.208	1.013	91.10	7.326	1.574	0.1586	4.134	6.053	5130

uniformly distributed about zero for all cases. Clearly the positive y -shift is the result of this induced $\vec{E} \times \vec{B}$ electron drift.

4. The average energy of the electron, at the point of exit from the cathode fall region, shows a decrease with increasing magnetic fields. Once again this decrease is less noticeable for the high pressure cases.

These patterns suggest that as the magnetic field strength is increased, the electrons have an increased $\vec{E} \times \vec{B}$ drift in the ' y ' direction and correspondingly they have to travel a greater distance before emerging out of the cathode fall region. This increase in distance travelled would also result in an increased number of collisions with gas molecules, less energy build-up of the electron, and consequently a longer transit period.

Figure 3.8(a) is a plot of the positions of the ionization events along the cathode fall for all of the test electrons used. These results are for the case of a 5 Torr Helium discharge with an applied magnetic field of 1000 G. The corresponding transverse discharge velocity distribution is plotted in Fig. 3.8(b). As one would expect, the further the ionization event occurs from the cathode the larger is the value of its ' y ' position. However, because the drift of the ions is very high near the cathode, the net $\vec{E} \times \vec{B}$ discharge velocity tends to be fairly constant throughout the cathode fall region. Figure 3.9 gives the transverse discharge velocity distribution in the form of a histogram. Similar results are obtained with other discharge conditions.

Table 3.5 also provides an excellent means for comparing the results for the three gases. One finds, for instance, that of the three gases, helium has the least number of collisions (≈ 55), N_2 has a much larger number of collisions (≈ 900) and CO_2 has the maximum number of collisions (≈ 1350). These figures are not surprising, considering the fact that the total collision cross-section for He is very small compared to N_2 , and even smaller compared to CO_2 . A direct consequence of the fewer number of collisions in He is that the electrons have a chance, in-between collisions, to build up a higher energy from the electric field. Consequently, the average energy of the electrons in He ($\approx 19\text{eV}$) is much larger than

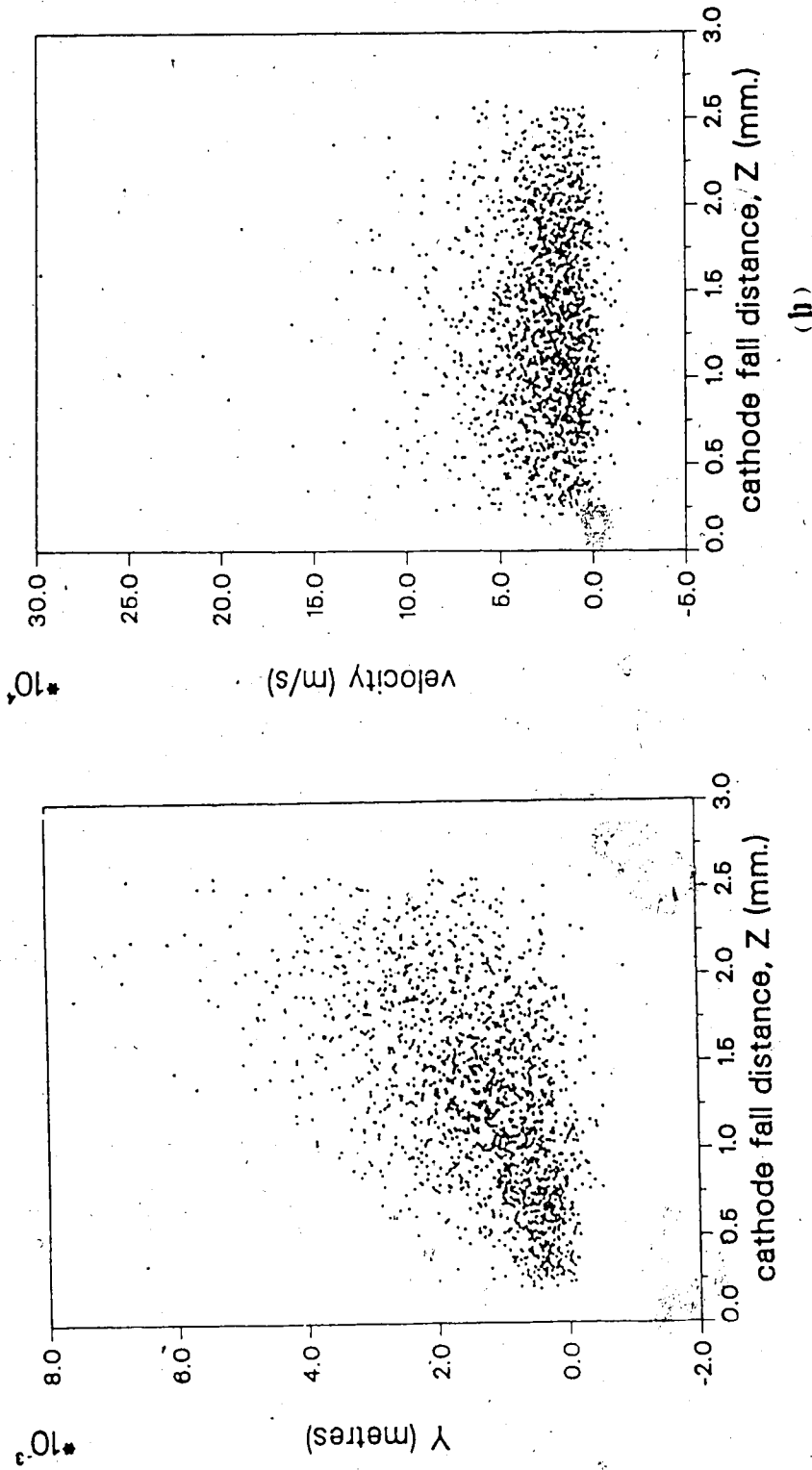


Fig. 3.8. Discharge parameters for a 5 Torr Helium discharge with a magnetic field of 1000 Gauss

(a) Position of ions formed as a result of ionization from primary and secondary electrons.

(b) Discharge velocity distribution in the $\vec{E} \times \vec{B}$ direction (i.e. y direction).

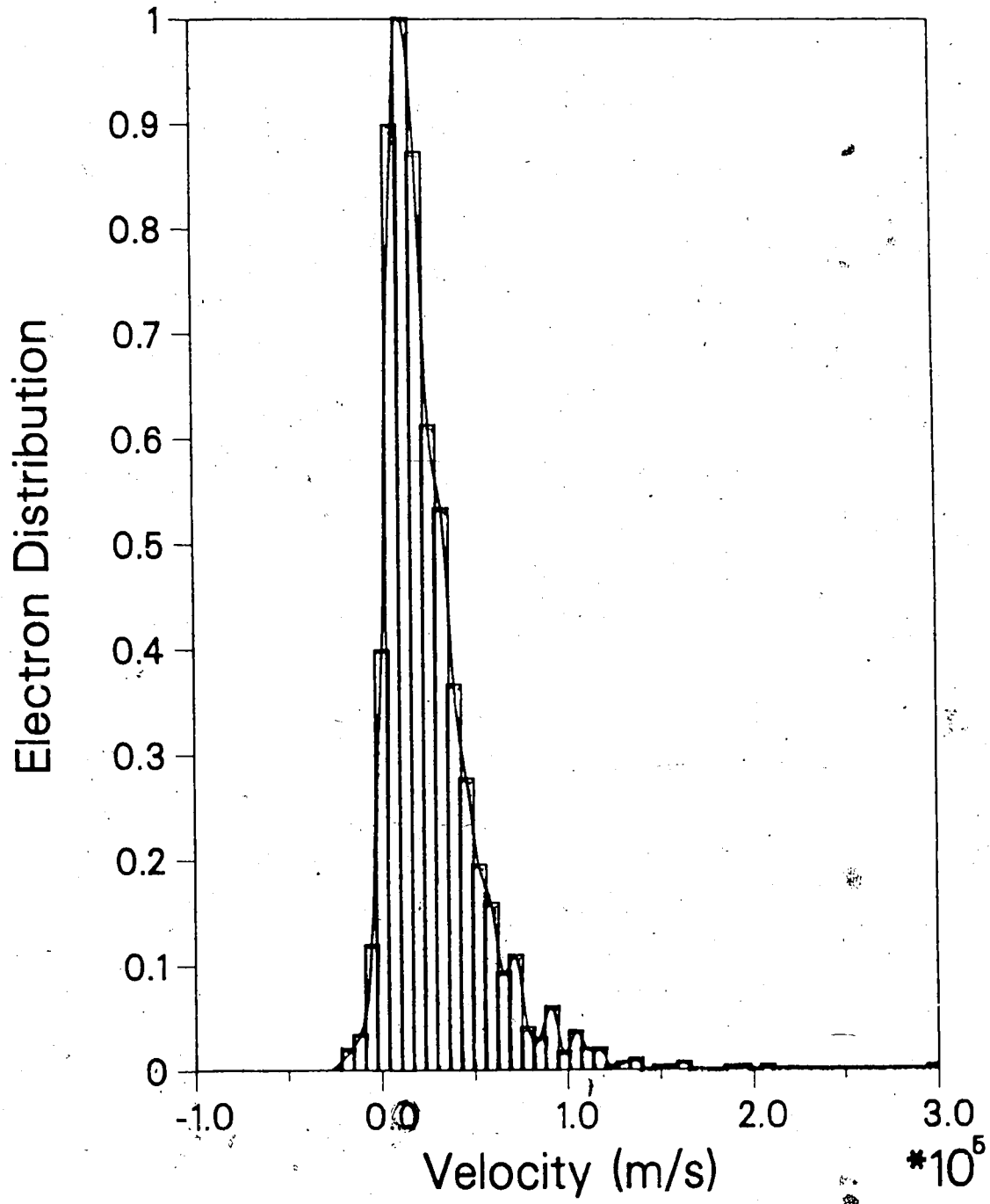


Fig. 3.9: Histogram of the transverse discharge velocity distribution.

that of N_2 ($\approx 2.1\text{eV}$) and CO_2 ($\approx 2.4\text{eV}$). Another consequence of the reduced number of collisions, is that the Hall parameter is larger and the transit time shorter for He, as compared to the other

For the three gases examined, elastic collisions are seen to dominate over inelastic collisions. In He, about 2% of the collisions result in ionizations; compared to about 0.02% for N_2 and about 0.2% for CO_2 . The reason for this is, once again, due to the fewer number of collisions in He. This feature results in a higher energy build-up of the test electrons in He, and consequently a greater chance of ionization collisions. Of the three gases, carbon-dioxide has the lowest ionization potential (13.3 eV; compared to 15.7 eV for nitrogen and 24.6 eV for helium). This accounts for the higher number of ionization collisions in carbon-dioxide.

The results for the laser gas discharge, consisting of 20 torr He, 8 torr N_2 and 2 torr CO_2 , indicates how useful the Monte Carlo technique is for simulating complicated systems. From the results that are obtained, one can clearly see that the system is highly collision dominated. The Hall parameter rises to a maximum of only 0.2, for the 1000 Gauss case. As was the case for individual gases, the number of collisions in the laser gas mixture also rises with increasing magnetic field. However, due to its highly collision dominated nature, this increase is barely perceptible. It is also seen that there are far more collisions with He and N_2 than with CO_2 molecules. Two factors influence the number of collisions with individual gas molecules; namely the gas pressure and the total collision cross-section.

The total number of collisions with each gas species has been categorized into elastic, excitation and ionization collisions. For the sake of simplicity, the excitation cross sections for each of the gases have been lumped together. It is interesting to note that for the laser gas mixture, the CO_2 component has the highest percentage of ionization collisions ($\approx 1.65\%$); as compared to the N_2 component ($\approx 1.0\%$) and the He component ($\approx 0.12\%$). This is because the average energy of the electron ($\approx 4.8\text{eV}$) is far below the ionization potential of He and is slightly below that of N_2 as well. This fact has been independently observed by Wiegand *et al.*

al. [68].

In addition to the above results, the details of the discharge velocity are very interesting. The dependence of the "transverse discharge velocity", as a function of the magnetic field, has been plotted in Figs. 3.10-3.13 for all three gases and for the laser gas mixture. The results confirm the linear dependence of the transverse discharge velocity upon magnetic field strength. It is seen that for each of the gases the discharge velocity decreases with increased pressure. This is due to the gases being more collision dominated at the higher gas pressures. The discharge velocity for helium ions is much higher than that of N_2 or CO_2 . This feature is to be expected due to the much higher mobility of the Helium ion. For a laser gas mixture the weighted average of the discharge velocity for the individual gases is calculated to determine the overall discharge velocity. As one would expect, the highly mobile He ions contribute the most to the overall discharge velocity.

Figure 3.14 shows the dependence of the transverse discharge velocity on total gas pressure. Although there is a significant decrease in the value of this parameter with pressure, the magnitude is still very large, even at the highest pressure thus far examined in the simulation. These results are also in general agreement with experiment in that the magnetic stabilization process has been found to be effective up to pressures of several hundred Torr [42]. An important consideration in pressure scaling of the magnetic stabilization process appears to be that the Hall parameter be close to unity.

The role that a magnetic field may play in preventing the growth of regenerative instabilities in the cathode and bulk regions may be estimated by comparing the ratio of transverse discharge drift, within a glow-to-arc transition time, to the typical spatial dimensions found for such an instability. If this ratio is much larger than 1, the magnetic field can be considered to be effective in spreading any localized perturbations in electron density or current over the discharge volume, in a time less than an instability time. Consequently, the discharge is immune to this type of instability. A typical thermal instability has been shown to have a time of formation of the order 10^{-3} seconds [27]. Within this time

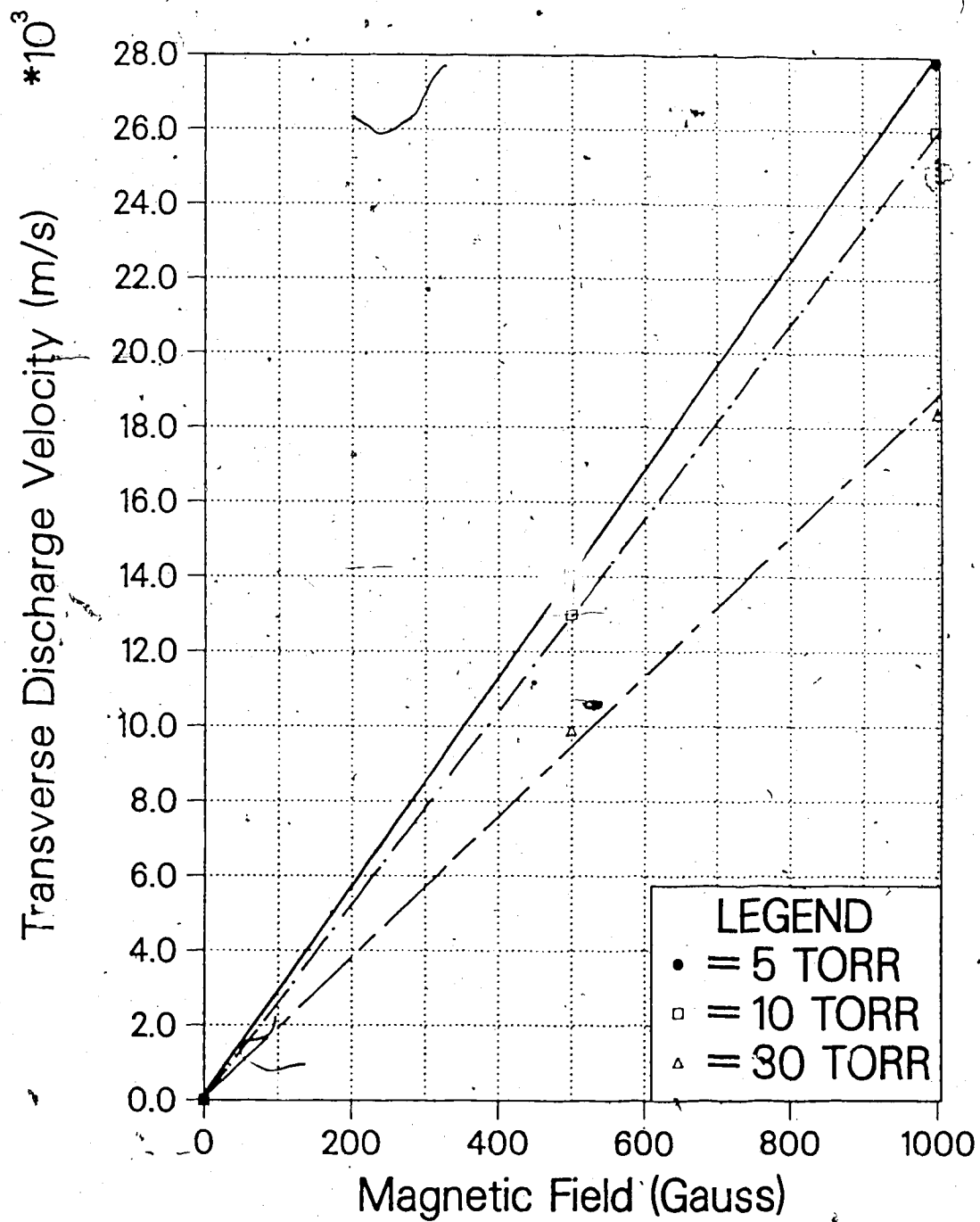


Fig. 3.10: Plot of transverse discharge velocity as a function of the applied magnetic field for a Helium gas discharge at 5, 10 and 30 Torr.

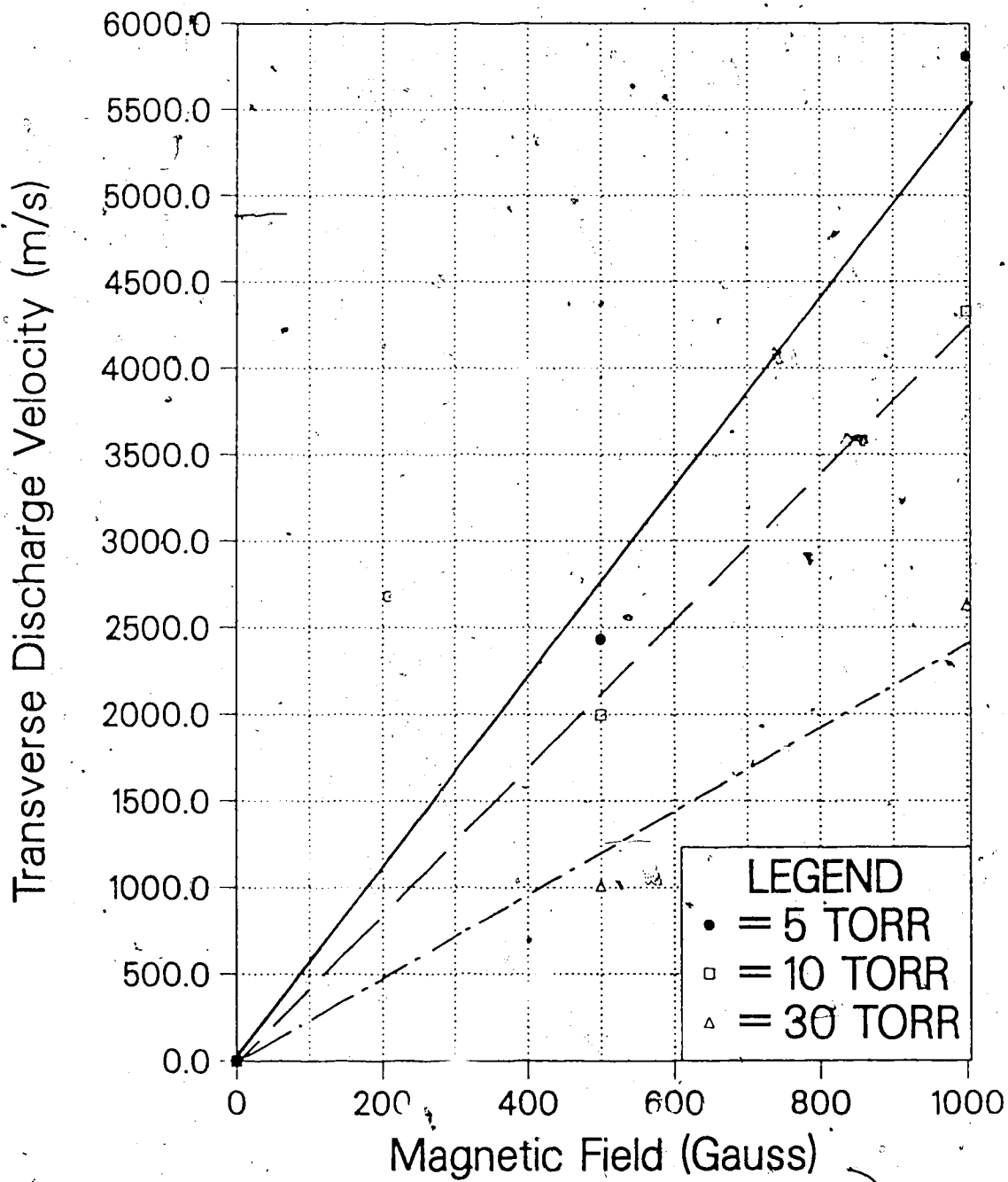


Fig. 3.11: Plot of transverse discharge velocity as a function of the applied magnetic field for a Nitrogen gas discharge at 5, 10 and 30 Torr.

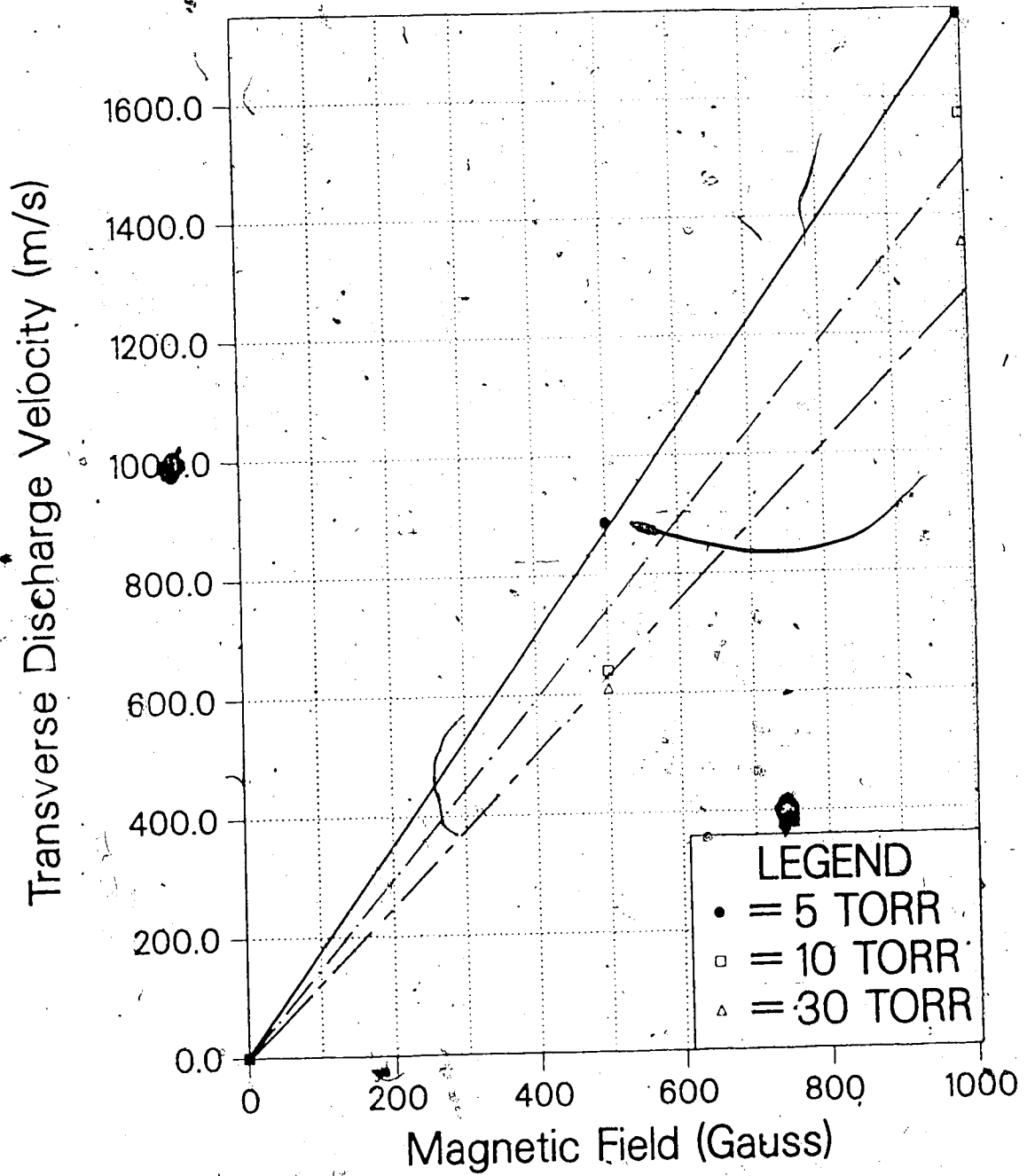


Fig. 3.12: Plot of transverse discharge velocity as a function of the applied magnetic field for a Carbon-Dioxide gas discharge at 5, 10 and 30 Torr.

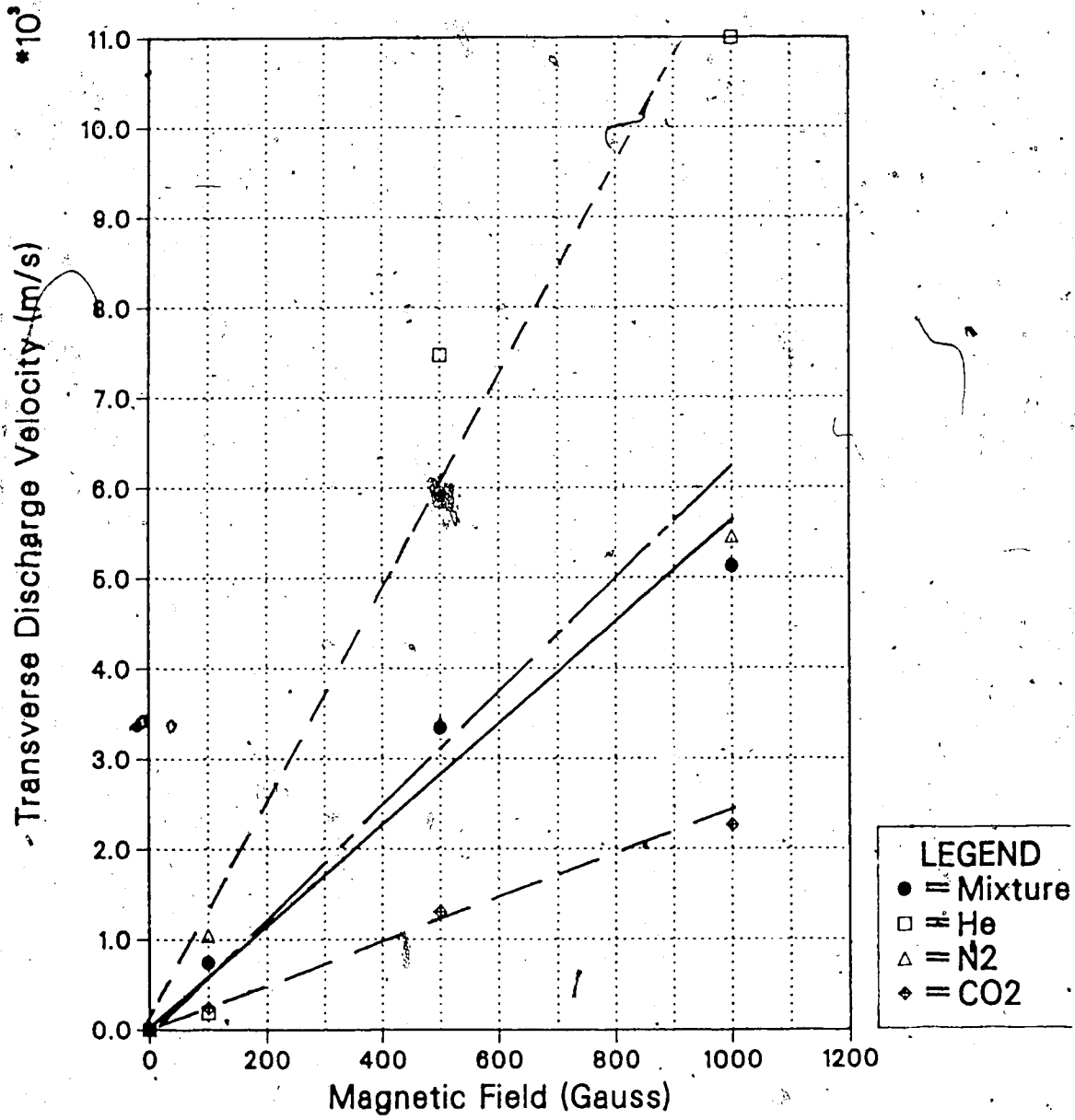


Fig. 3.13: Plot of transverse discharge velocity as a function of the applied magnetic field for a CO₂ Laser gas discharge at 30 Torr.

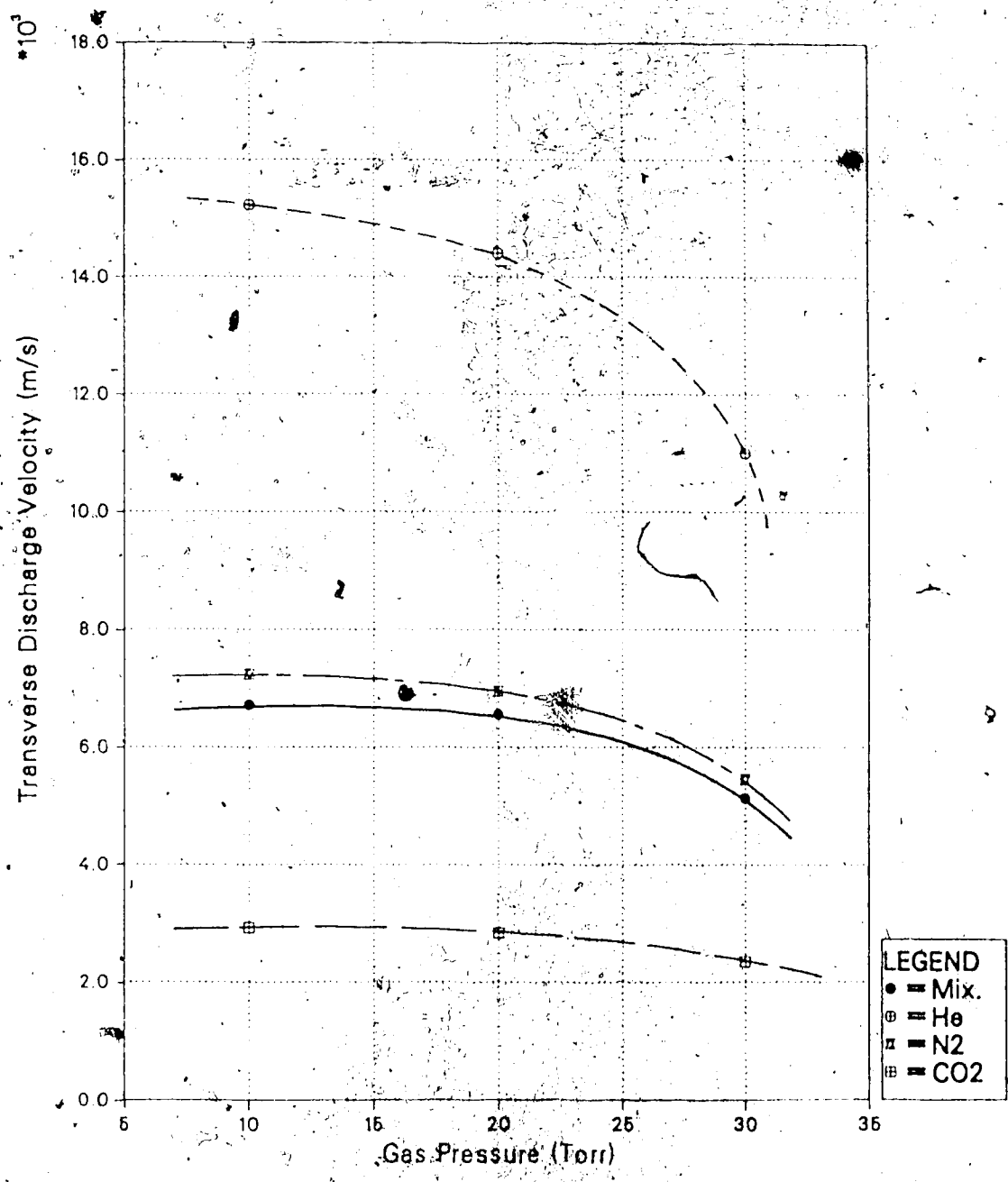


Fig. 3.14: Variation of transverse discharge velocity with total gas pressure for a typical medium pressure CO₂ laser mixture assuming a magnetic field strength of 500 Gauss

period the laser discharge would have been swept out by nearly 30 cm for a 100 Gauss field and by nearly 300 cm for a 500 Gauss field. These translations considerably exceed the typical spatial dimensions found for this kind of instability; (typically 1 cm). These results help to explain, in large measure, the excellent discharge stability observed by Capjack *et. al.* [40,41].

CHAPTER IV

SUMMARY AND CONCLUSIONS

4.1 Summary of thesis

The effective suppression of electrothermal instabilities in medium pressure gas discharges, through the interaction of appropriately profiled magnetic fields with the plasma itself, has been documented for a number of electrode configurations [40-42]. This phenomenon, initially believed to be a bulk plasma effect, has in more recent experiments and computer simulations become identified primarily with the cathode region of the discharge system.

Thus, in an attempt to more fully comprehend and fully exploit the features of this new discharge stabilization process, an indepth computer simulation of a "magnetized cathode glow" has been undertaken in this thesis. This simulation code, called MAGSIM, employs the Monte Carlo technique which is known to be suitable for analyzing a large number of particles. For the typical CO₂ laser mixture case of present interest, this involved a detailed three dimensional cataloging of electron and ion motion, under conditions of full anisotropic scattering. In order to get realistic results, the Monte Carlo technique employed here requires a precise knowledge of the collision cross-sections and scattering parameters of the interacting species. Because of extensive previous experimental work in plasma physics, such data is readily available.

Past workers have utilized the Monte Carlo approach to simulate electron motion in a plasma, under the influence of a weak and uniform electric field, but with no space charge. This present work has extended the basic Monte Carlo approach to describe both elastic and inelastic scattering within the space charge sheaths of a magnetized cathode fall region. Thus, the case considered here involves a highly nonuniform electric field of large strength, together with a superimposed transverse magnetic field of variable intensity.

The computational technique used in this present simulation is different from earlier techniques where the cathode fall region is broken up into various grids and the phase-space parameters determined at each grid point. Instead, the equations of motion of an electron in a non-uniform electric field and a transverse magnetic field have been solved analytically and the results used to determine the phase-space parameters only at the points of collision. Such a method, aside from saving computational time is also less subject to round off errors.

4.2 Results

The Monte Carlo procedure described above was performed on a fast parallel processor using a CYBER 205 computer, to simulate He, N₂ and CO₂ gases at various pressures and with different applied magnetic field strengths. Additional simulations were performed for a typical CO₂ laser mixture [69-71].

The simulations have provided some interesting results which correlate well with various experimental observations. In particular, these simulations have given insight into the stabilization mechanism in CO₂ lasers employing magnetic field stabilization. It is now believed that the primary stabilization mechanism involves a Lorentz driven transverse motion of charge carriers within the space charge sheaths at the cathode surface. The decrease in charge residence time resulting from this rapid mixing velocity is found to be adequate to compensate for electro-thermally induced perturbations in electron density. The process, thereby provides a significantly decreased susceptibility to glow-to-arc transitions.

The magnetic stabilization process has also been experimentally found to be effective up to pressures of several hundred Torr. An important consideration in pressure scaling of the process appears to be, that the Hall parameter be at least unity. For values of the Hall parameter less than unity, random collisions dominate the Lorentz induced drift of the electrons, thereby undermining the magnetic stabilization process.

4.3 Future Considerations

Whereas, the present Monte Carlo simulation code, MAGSIM, has been carefully designed; there still remains considerable scope for improvement. Some of the features that could be considered for future work are:

1. *The cathode fall region should be analyzed self-consistently.* The present code is not self-consistent; in that the effect of excitations and ionizations on the cathode fall distance and the resulting electric field have not been considered. The increased number of collisions due to the magnetic field is equivalent to a higher gas pressure, which implies that the cathode fall distance should actually decrease with higher magnetic field values. A self-consistent model, though desirable, is extremely difficult to solve and is not anticipated to change the conclusions of this work regarding the mechanisms and physical processes involved in magnetic discharge stabilization.
2. *Analysis of other regions of the discharge.* In this thesis, only the cathode fall region has been modelled. The rationale for this was that the cathode fall sheath, with its high electric field strength, is the region of primary importance with regard to magnetic stabilization processes. Nevertheless, it would be interesting to explore the effect of magnetic fields on other regions of the discharge, such as the positive column; which occupies the major portion of the discharge and where most of the laser excitation collisions occur. The code is well suited, with only a few minor modifications, for application to the positive column region. When a magnetic field is applied to the discharge it is expected that fundamental changes will occur in the positive column dynamics. Fluctuations in discharge properties will be coupled differently for the magnetized and non-magnetized cases, since the magnetic field will alter the joule heating fluctuations and consequently the relation between electron density or temperature and gas density fluctuations. Thus the dispersion relations, used to derive instability conditions, would have to be modified in order to include the effect of magnetic fields.
3. *Determine gas kinetic reactions.* Nighan *et. al.* [43] have shown that complex reactions

take place within a typical convectively cooled CO_2 laser gas discharge. Some of the species (e.g. CO or CO_3^-), thereby created, can significantly alter the laser gas discharge stability. It would, therefore, be worthwhile compiling all gas kinetic reactions and rates and then determining various species concentrations as a function of time. One could then add some of these more important species to the code.

4. *Measurements of cathode fall voltages and distances.* In the MAGSIM code, estimates had to be made of the cathode fall voltage and distance for a CO_2 laser mixture. These were obtained by using a pressure weighted average of cathode fall voltage and distance of the individual gases. However, it would be worthwhile to have accurate experimental values of these parameters.
5. *Evaluate cross-sectional data at fractions of electron-Volts instead of at every electron-Volt energy.* In this thesis, the cross-sectional data has been tabulated at one volt increment of electron energy over the range of 0 to 100 eV. Thus, whenever an electron-gas molecule collision is determined, the electron energy is calculated to the closest electron-volt and the various cross-sections of collision (and scattering) determined from the appropriate published tables. For some gases, such as CO_2 , these cross-sections might change considerably within fractions of an electron-volt of electron energy, thereby making the approximations too crude. An increased sub-division of cross-sectional data could result in more accurate approximations.
6. *Study of other laser systems.* It should be feasible to apply the present MAGSIM code to other laser systems with equal effectiveness provided accurate cross-sectional and scattering parameter data is available. A case in point is the excimer laser which is well known to be plagued by electro-thermal instabilities. Consequently, at the present state-of-the-art, such lasers can only operate in a very short pulse mode. It would be interesting, and possibly profitable, to examine the magnetic stabilization technique for these types of lasers.

In addition to making these improvements in the MAGSIM code, there is need for pursuing a

number of useful experiments:

1. *Design CO₂ laser systems with large magnetic fields.* Most of the CO₂ lasers employing magnetic stabilization have operated in the 10-30 Torr pressure range with magnetic fields of only a few 100 Gauss. The results provided by MAGSIM have revealed that these magnetic fields are too low to effectively sweep away instabilities, in all but lower pressure devices. Consequently, in order to effectively apply these techniques to higher pressure devices will necessitate the design of CO₂ laser structures capable of generating magnetic field strength of the order of 1000 Gauss. In fact, the magnetic field could be profiled such that a large field exists only close to the cathode. This would considerably reduce the cost of such magnetically stabilized structures.
2. *Design novel electrode structures to improve efficiency of the CO₂ lasers.* In order to achieve a truly significant increase in the efficiency of CO₂ lasers, it will be necessary to reduce the cathode fall potential drop, since this energy dissipation process does not contribute to lasing. Thus, in all probability, completely new concepts and types of electrode structures will need to be developed if this possibility is to be realized. Two new electrode designs, one using hollow cathode electrodes and the other using plasma electrodes, could conceivably reduce these cathode and anode fall potential drops by significant amounts.

The *hollow cathode* creates stagnant regions with high temperatures near the emitting surface, such that a low-density zone is created immediately adjacent to the secondary emission face. This results in the emitted electrons achieving higher energies, with fewer interfering collisions than in a conventional cathode. Thus, less energy is required by the cathode fall region to create a self-sustained discharge. Consequently, less cathode fall voltage is needed.

In the *plasma electrode* method, a plasma region is created close to the cathode surface in order that the primary electron does not need to create ions for self-sustenance. Computer simulations have suggested that very little energy is needed to

make these ions drift to the cathode to create regenerative secondary electrons. Thus, this method should also cause the cathode fall voltage to drop.

Both of these schemes could, therefore, reduce the voltage drop across the cathode region; thereby significantly increasing the efficiency of these laser systems. For high power laser systems, even a small percentage increase in efficiency could translate into very large increase in the optical power output of these devices.

It is the hope of this author that some, if not all, of these schemes will one day be used to create a new generation of higher efficiency and higher power laser systems.

REFERENCES

- [1] A. Javan, W.R. Bennett, Jr., and D.R. Herriott, "Population Inversion and continuous Optical Maser oscillation in a gas discharge containing a He-Ne mixture," *Phys. Rev. Lett.*, vol. 6, pg. 106, 1961.
- [2] C.K.N. Patel, "Continuous-wave laser action on vibrational-rotational transition of CO₂," *Phys. Rev.*, vol. 136, pp. A1187-A1193, Nov. 1964.
- [3] C.K.N. Patel, "Selective excitation through vibrational energy transfer and optical maser action in N₂-C₂," *Phys. Rev.*, vol. 13, pp. 617-618, Nov. 1964.
- [4] G. Moeller and J. Rigden, "High-power laser action in CO₂-He mixtures," *Appl. Phys. Lett.*, Vol. 7, pp. 274-279, Nov. 1965.
- [5] C.K.N. Patel, P.K. Tien and J.H. McFee, "CW high-power CO₂-N₂-He laser," *Appl. Phys. Lett.*, vol. 7, pp. 290-292, Dec. 1965.
- [6] T.F. Deutsch, F.A. Horrigan and R.I. Rudko, "CW operation of high-pressure flow CO₂ lasers," *Appl. Phys. Lett.*, vol. 15, pp. 88-97, Aug. 1969.
- [7] R. Dumanchin and J. Rocca-Serra, "Augmentation de l'energie et de la puissance fournie par unite de volume dans un laser a CO₂ en regime pulse," *C.R. Acad. Sci.*, vol. 269, pp. 916-917, Nov. 1969.
- [8] A.J. Beaulieu, "Transversely excited atmospheric pressure CO₂ lasers," *Appl. Phys. Lett.*, vol. 16, pp. 504-505, Jun. 1970.
- [9] H.M. Lamberton and Pearson, "Improved excitation techniques for atmospheric pressure CO₂ lasers," *Electron. Lett.*, Vol. 7, pg. 141, Jan. 1971.

- [10] R. Dumanchin, J.C. Farcy, M. Michon and J. Rocca-Serra, "High power density pulsed molecular laser," presented at the *VI th Int. Quantum Electronics Conf.*, Kyoto, Japan, Sept. 7-10, 1970.
- [11] A.K. Laffamme, "Double discharge excitation for atmospheric pressure CO₂ lasers," *Rev. Sci. Instru.*, Vol. 41, pp. 1881, Nov. 1970.
- [12] D.B. Nichols and W.M. Brandenburg, "Radio-frequency preionization in a supersonic transverse electrical discharge laser", *IEEE J. Quantum Electron. (Corresp.)*, Vol. QE-8, pp. 718-719, Aug. 1972.
- [13] R. Dumanchin, M. Michon, J.C. Farcy, G. Boudinet and J. Rocca-Serra, "Extension of CO₂ TEA laser capabilities," presented at the *Conf. on Laser Engineering and Applications*, Washington, D.C., June 2-4, 1971.
- [14] O.R. Wood, II, "High-pressure pulsed molecular lasers," *Proc. IEEE*, Vol. 62, No. 3, pp. 355-397, March 1974.
- [15] A.J. Demaria, "High-power CO₂ lasers," *Proc. IEEE*, Vol. 61, No. 6, pp. 731-748, June 1973.
- [16] D.C. Tye, "Advances in Quantum Electronics," (D.W. Goodwin, ed.), Vol. 1, *Academic Press*, New York 1970.
- [17] E. Nasser, "Fundamentals of gaseous ionization and plasma electronics," *Wiley-Interscience*, N.Y., pp. 397-423, 1971.
- [18] I.E. Kline, "Pulsed glow discharges in laser excitation and breakdown," *IEEE Trans. Elect. Insu.*, Vol. 17, No. 2, pp. 121-124, Apr. 1982.

- [19] L.J. Denes and J.J. Lowke, "V-I characteristics of pulsed CO₂ laser discharges," *Appl. Phys. Lett.*, Vol. 23, pp. 130-132, 1973.
- [20] E.A. Crawford and A.V. Phelps, "Formative time lags in CO₂ laser discharges," *Appl. Phys. Lett.*, Vol. 25, pp. 59-61, 1974.
- [21] T.V. George and L.J. Denes, "Electron density measurements in collision dominated plasmas," *Appl. Phys. Lett.*, Vol. 26, pp. 1-3, 1 Jan. 1975.
- [22] R. Turner, "The glow-to-arc transition in a pulsed high-pressure gas discharge," *J. Appl. Phys.*, Vol. 52, No. 2, pp. 681-692, Feb. 1981.
- [23] R.A. Haas, "Plasma stability of electric discharges in molecular gases," *Phys. Rev. A.*, Vol. 8, No. 2, pp. 1017-1043, Aug. 1973.
- [24] W.L. Nighan, W.J. Wiegand and R.A. Haas, "Ionization instability in CO₂ laser discharges," *Appl. Phys. Lett.*, Vol. 22, No. 11, pp. 579-582, June 1973.
- [25] D.H. Douglas-Hamilton and S.A. Mani, "An electron attachment plasma instability," *Appl. Phys. Lett.*, Vol. 23, No. 9, pp. 508-510, Nov. 1973.
- [26] D.H. Douglas-Hamilton and S.A. Mani, "Attachment instability in an externally ionized discharge," *J. Appl. Phys.*, Vol. 45, No. 10, pp. 4406-4415, Oct. 1974.
- [27] W.L. Nighan and W.J. Wiegand, "Causes of arcing in CW CO₂ convection laser discharges," *Appl. Phys. Lett.*, Vol. 25, No. 11, pp. 633-636, Dec. 1974.
- [28] J.H. Jacob and S.A. Mani, "Thermal instability in high-pressure laser discharges," *Appl. Phys. Lett.*, Vol. 26, No. 2, pp. 53-55, Jan. 1975.

- [29] C.A. Fenstermacher, Nutter, Leland and Bayer, "Electron beam controlled electrical discharge as a method of pumping large volumes of CO₂ laser media at high pressure," *Appl. Phys. Lett.*, Vol. 20, pp. 56-60, Jan. 1972.
- [30] J.D. Daugherty, E.R. Pugh and D.H. Douglas-Hamilton, "A stable, scalable, high pressure gas discharge as applied to the CO₂ laser," *Bull. Amer. Phys. Soc.*, Vol. 17, pg. 399, Mar. 1972.
- [31] N.G. Basov, E.M. Belenov, V.A. Danilychev and A.F. Suchkov, "Possibility of producing tunable infrared gas lasers," *JETP Lett.*, Vol. 14, pp. 375-376, Nov. 1971.
- [32] M. Richardson, A. Alcock, K. Leopold and P. Burtyn, "A 300-J multigigawatt CO₂ laser," *IEEE J. Quant. Elect.*, Vol. 9, No. 2, pp. 236-242, Feb. 1973.
- [33] H. Seguin and J. Tulip, "Photoinitiated and photosustained lasers," *J. Appl. Phys. Lett.*, Vol. 21, pp. 414-415, Nov. 1972.
- [34] L.E. Kline and L.J. Denes, "Investigations of glow discharge formation with volume preionization," *J. Appl. Phys.*, Vol. 46, pp. 1567-1574, 1975.
- [35] R.K. Garnsworthy, L.E.S. Mathias and C.H. Carmichael, "Atmospheric pressure pulsed CO₂ laser utilising preionization by high energy electrons", *Appl. Phys. Lett.*, Vol. 19, pp. 506-508, 1971.
- [36] L.W. Casperson and M.S. Shekhani, "Mode properties of annular gain lasers," *Appl. Optics*, Vol. 14, No. 11, pp. 2653-2661, Nov. 1975.
- [37] G.R. Oche and H.E. Sontag, "A compact cylindrical CO₂ TEA laser," *IEEE J. Quant. Elect.*, Vol. 12, No. 12, pp. 752-756, Dec. 1976.

- [38] K. Cheng and L.W. Casperson, "Properties of a coaxial cw laser," *Appl. Opt.*, Vol. 18, No. 13, July 1979.
- [39] C.J. Buczek, R.J. Fréiberg, P.P. Chenausky and R.J. Wayne, "Magnetic Stabilization of the Plasma Column in Flowing Molecular Lasers", *Proc. IEEE*, Vol. 59, No. 4, pg 659, 1971.
- [40] H.J.J. Seguin, C.E. Capjack, D. Antoniuk and V.A. Seguin, "A magnetically stabilized radial discharge for a high-power laser," *Appl. Phys. Lett.*, Vol. 39, No. 3, pp. 203-205, Aug. 1981.
- [41] C.E. Capjack, D.M. Antoniuk and H.J.J. Seguin, "Dynamics of magnetically stabilized laser discharge," *J. Appl. Phys.*, Vol. 52, No. 7, pp. 4517-4522, July 1981.
- [42] D.M. Antoniuk, H.J.J. Seguin and C.E. Capjack, "Electrode Design for a Magnetically Stabilized Glow Discharge," *Applied Physics B*, Vol. 35, pp. 155-162, 1984.
- [43] W.L. Nighan and W.J. Wiegand, "Influence of Negative-Ion Processes on Steady State Properties and Striations in Molecular Gas Discharges," *Physical Review A*, Vol. 10, No. 3, pp. 922-945, Sept. 1974.
- [44] T. Itoh and T. Musha, "Monte Carlo Calculations of Motion of Electrons in Helium," *J. of the Phys. Soc. of Japan*, Vol. 15, No. 9, pp. 1675-80, Sept. 1960.
- [45] R.W.L. Thomas and W.R.L. Thomas, "Monte Carlo Simulation of Electrical Discharges in Gases," *J. Phys. B*, Vol. 2, Ser. 2, pp. 562-70, 1969.
- [46] H.N. Kucukarpaci, H.T. Saelee and J. Lucas, "Electron Swarm Parameters in Helium and Neon," *J. Phys. D.: Appl. Phys.*, Vol. 14, No. 9, pp. 9-25, 1981.

- [47] T.N. An, E. Marode and P.C. Johnson, "Monte Carlo Simulation of Electrons Within the Cathode Fall Region of a Glow Discharge in Helium," *J. Phys. D.: Appl. Phys.*, Vol. 10, pp. 2317-28, 1977.
- [48] T.N. An, E. Marode, G. Fournier and P. Segur, *Journal de Physique C7*, supplément au no. 7, Tome 40, pp. 533-534, 1979.
- [49] E.D. Cashwell and C.J. Everett, *A Practical Manual on the Monte Carlo Method for random walk problems*, Pergamon Press, New York, pp. 27-28, 1959.
- [50] D. Andrick and A. Bitsch, "Experimental Investigation and Phase Shift Analysis of Low Energy Electron-Helium Scattering," *J. Phys. B8*, pp. 394-409, 1975.
- [51] F.J. de Heer and R.H.J. Jansen, "Total Cross Sections for Electron Scattering by Helium," *J. Phys. B.10*, pp. 3741-57, 1977.
- [52] R.J. Fleming and G.S. Higginson, "Remeasurement of 2'S Excitation Cross Section in Helium," *Proc. Phys. Soc. 84*, pg. 531, 1964.
- [53] D. Rapp and P. Englander-Golden, "Total Cross Sections for Ionisation and Attachment in Gases," *J. Chem. Phys. 43*, pp. 1464-79, 1965.
- [54] T.W. Shyn, "Angular Distribution of Electrons Elastically Scattered from Gases," *Phys. Rev. A22*, pp. 916-29, 1980.
- [55] D.E. Golden, "Low Energy Resonances in e⁻-N₂ Total Scattering Cross Sections: The Temporary Formation of N₂," *Phys. Rev. Lett. 17*, pp. 847-8, 1966.
- [56] T.W. Shyn, R.S. Stolarski, and G.R. Carignan, "Angular Distribution of Electrons Elastically Scattered from N₂," *Phys. Rev. A6*, pg. 1011, 1972.

- [57] A.G. Engelhardt, A.V. Phelps, and C.G. Risk, "Determination of Momentum Transferred and Inelastic Collision Cross Sections for Electrons in Nitrogen Using Transport Coefficients," *Phys. Rev.* **135**, pp. A1566-74, 1964.
- [58] C. Ramsauer and R. Kollath, "Die Winkelverteilung bei der Streuung Langsamer Elektronen an Gasmolekullen," *Ann. Physik* **12**, pp. 529-61, 1932.
- [59] E. Bruche, "Wirkungsquerschnitt und Molekulbau," *Ann. Physik.* **83**, pp. 1065-1128, 1927.
- [60] R.D. Hake Jr. and A.V. Phelps, "Momentum Transfer and Inelastic-Collision Cross Sections for Electrons in O₂, CO and CO₂," *Phys. Rev.* **158**, pp. 70-84, 1967.
- [61] K.K. Corwin and S.J.B. Corrigan, "Dissociation of Carbon-Dioxide in the Positive Column of a Glow Discharge," *J. Chem. Phys.* **50**, pp. 2570-4, 1969.
- [62] J.M. Ajello, "Emission Cross Sections of CO₂ by Electron Impact in the Interval 1260-4500 Å II," *J. Chem. Phys.* **55**, pp. 3169-77, 1971.
- [63] T.W. Shyn, W.E. Sharp, and G.R. Carignan, "Angular Distribution of Electrons Elastically Scattered from CO₂," *Phys. Rev. A* **22**, pp. 919,925, 1980.
- [64] H.T. Saelee, 'Monte-Carlo Simulation of Electron Swarms in Gases', Ph. D. Thesis, University of Liverpool, pg. 15, 1976.
- [65] A. Von Engel, *Ionized Gases*, Oxford Univ. Press, London, pp. 229-30, 1965.
- [66] L.S. Frost, "Effect of Variable Ionic Mobility and Ambipolar Diffusion", *Phys. Rev.* **105**, pp. 354-356, (1957).

- [67] A. Von Engel, *Electric Plasmas: Their nature and uses*, (Taylor and Francis, New York, 1983), p. 72.
- [68] W.J. Wiegand and W.L. Nighan, "Plasma Chemistry of CO₂-N₂-He Discharges," *Appl. Phys. Lett.* 22, p. 583, 1973.
- [69] R. Razdan, C.E. Capjack, and H.J.J. Seguin, "Influence of a Magnetic Field on the Growth of Instabilities in a Helium Glow Discharge Using Monte Carlo Simulation of the Cathode Fall Region," *J. Appl. Phys.* 57, pp. 4954-61, 1 June 1985.
- [70] R. Razdan, C.E. Capjack, and H.J.J. Seguin, "Charge Carrier Dynamics of a CO₂ Laser Plasma in a Magnetized Cathode Glow," *Appl. Phys. Lett.* 48, pp. 1513-15, 2 June 1986.
- [71] R. Razdan, C.E. Capjack, and H.J.J. Seguin, "Monte Carlo Simulation of the Cathode Fall Region of a CO₂ Laser Glow Discharge for Studying the Influence of Magnetic Fields on Instability Growth," *Appl. Opt.* 25, pp. 2915-25, 1 Sept. 1986.

APPENDIX I: DIRECTION OF AN ELECTRON AFTER SCATTERING

In order to determine the direction of an electron after it collides with a gas molecule, it is necessary to do a number of rotational transformation of co-ordinates. If we denote X-Y-Z as the initial rectangular co-ordinate system and specify the direction of the velocity vector by θ_1 and ϕ_1 (see Fig. 3.1); then we must rotate this co-ordinate system first by angle ϕ_1 and then by θ_1 to get the final local co-ordinate system. Let us denote X'-Y'-Z' as the co-ordinate system formed by rotating the X-Y-Z co-ordinates clockwise about the Z-axis through an angle ϕ_1 . Thus, a point (x,y,z) on the original X-Y-Z co-ordinate system is transformed to (x',y',z') on the new X'-Y'-Z' co-ordinate system, where:

$$\begin{aligned} x &= x' \cos \phi_1 - y' \sin \phi_1 \\ y &= x' \sin \phi_1 + y' \cos \phi_1 \\ z &= z' \end{aligned} \tag{A1.1}$$

Now, if we rotate the X'-Y'-Z' co-ordinate system counter-clockwise by an angle θ_1 about the Y'-axis, we end up with the local co-ordinate system at the point of collision, i.e. the X''-Y''-Z'' co-ordinate system. Once again, a point (x',y',z') on the X'-Y'-Z' co-ordinate system is transformed to a point (x'',y'',z'') on the X''-Y''-Z'' co-ordinate system, where:

$$\begin{aligned} x' &= x'' \cos \theta_1 + z'' \sin \theta_1 \\ y' &= y'' \\ z' &= -x'' \sin \theta_1 + z'' \cos \theta_1 \end{aligned} \tag{A1.2}$$

Solving (A1.1) and (A1.2), we can get x, y and z in terms of x'', y'' and z'':

$$\begin{aligned} x &= x'' \cos \theta_1 \cos \phi_1 - y'' \sin \phi_1 + z'' \sin \theta_1 \cos \phi_1 \\ y &= x'' \cos \theta_1 \sin \phi_1 + y'' \cos \phi_1 + z'' \sin \theta_1 \sin \phi_1 \\ z &= -x'' \sin \theta_1 + z'' \cos \theta_1 \end{aligned} \tag{A1.3}$$

At the point of collision, the electron is deflected through an angle θ_d and rotated through an angle ϕ_d . The direction of the electron after collision, assuming a local co-ordinate system,

$$\begin{aligned}x'' &= \sin\theta_d \cos\phi_d \\y'' &= \sin\theta_d \sin\phi_d \\z'' &= \cos\theta_d\end{aligned}\quad (A1.4)$$

Combining (A1.3) and (A1.4) we get x , y and z in terms of θ_i , θ_c , ϕ_i and ϕ_c . we

$$\begin{aligned}x &= \cos\theta_i \cos\phi_i \sin\theta_d \cos\phi_d - \sin\phi_i \sin\theta_d \sin\phi_d + \sin\theta_i \cos\phi_i \cos\theta_d \\y &= \cos\theta_i \sin\phi_i \sin\theta_d \cos\phi_d + \cos\phi_i \sin\theta_d \sin\phi_d + \sin\theta_i \sin\phi_i \cos\theta_d \\z &= -\sin\theta_i \sin\theta_d \cos\phi_d + \cos\theta_i \cos\theta_d\end{aligned}\quad (A1.5)$$

If the new direction of the electron's velocity vector after collision is denoted by θ_n and ϕ_n with respect to the X-Y-Z co-ordinate system, we have:

$$\begin{aligned}x &= \sin\theta_n \cos\phi_n \\y &= \sin\theta_n \sin\phi_n \\z &= \cos\theta_n\end{aligned}\quad (A1.6)$$

Relating (A1.5) and (A1.6) gives us the directional angles θ_n and ϕ_n in terms of θ_i , θ_d , ϕ_i and ϕ_d :

$$\begin{aligned}\theta_n &= \cos^{-1}[-\sin\theta_i \sin\theta_d \cos\phi_d + \cos\theta_i \cos\theta_d] \\ \phi_n &= \cos^{-1}\left[\frac{1}{\sin\theta_n} \{\cos\theta_i \cos\phi_i \sin\theta_d \cos\phi_d - \sin\phi_i \sin\theta_d \sin\phi_d + \sin\theta_i \cos\phi_i \cos\theta_d\}\right]\end{aligned}\quad (A1.7)$$

APPENDIX II: LISTING OF THE PROGRAM MAGSIM

• MAGSIM •

MONTE-CARLO SIMULATION OF MAGNETICALLY
STABILIZED CO₂-LASERS

RAJENDER RAZDAN, APRIL 1975

Program written to determine various swarm parameters in a magnetically stabilized CO₂ laser discharge.

SUMMARY OF PROGRAM

Unit 1 reads the following data: the number of test electrons (NE), the total gas pressure (PRESS), the applied magnetic field (BO) and a random number seed, DSEED. Unit 2 reads the relative pressures of He, N₂ and CO₂. Units 3, 4 and 5 read the cross-section and scattering angle data.

A call to subroutine INIT is made to determine the initial position and velocity of the test electron. A call to subroutine RANDOM is made to determine the path length, 'S', of the electron before collision occurs.

A call to subroutine ACCEL determines the acceleration of the electron over this distance 'S' and also the new position and velocity of the electrons. To do this it is necessary to determine the time, 'T', taken by the electron to travel length 'S'. Subroutine TIMER does this. Knowing 'T' one can determine the velocity and position of the electron at the end of distance 'S'.

The main program determines which species the test electron collides with and then calls one of the subroutines COLHE, COLN2 or COLCO2 to determine the type of collision (elastic or inelastic). In the inelastic case, the excitation level is determined. In case of an ionization collision Subroutine NEWVEL is invoked to calculate and store the velocity components of the secondary electrons.

Subroutines NEWSTA determines the direction and velocity of the electron after collision. A new path length, S, is then computed and the whole sequence of steps listed above is repeated. While accelerating through each step, S, a check is made to determine if the electron is within the cathode fall region. If the electron is outside this region its final state is stored. The same sequence of operations is repeated for all the 'NE' electrons in the swarm.

Subroutines VELHE, VELN2 and VELCO2 calculates the Lorentz discharge velocity of the He, N₂ and CO₂ components of the laser gas mixture. The net Lorentz discharge velocity is calculated as a weighted average of these three components.

 PROGRAMS AND SUBROUTINES USED:

MAIN Program

Subroutine *INIT* (X, Y, Z, VX, VY, VZ, PRESHE, PRESN2, PRESCO, L)
 Subroutine *RANDOM* (RAND)
 Subroutine *ENERGY* (VX, VY, VZ, VEL2, EN)
 Subroutine *ACCEL* (X, Y, Z, VX, VY, VZ, S, T, TIME, EN, *)
 Subroutine *COLHE* (X, Y, Z, VX, VY, VZ, EN, TIME, *)
 Subroutine *COLN2* (X, Y, Z, VX, VY, VZ, EN, TIME, *)
 Subroutine *COLCO2* (X, Y, Z, VX, VY, VZ, EN, TIME, *)
 Subroutine *NEWVEL* (KI, VXI, VYI, VZI, XI, YI, ZI, ENI, X, Y, Z, EN)
 Subroutine *NEWSTA* (EN, X, Y, Z, VX, VY, VZ, IFLAG, *)
 Subroutine *TIMER* (X, Y, Z, VX, VY, VZ, S, T)
 Subroutine *UNSIMP* (F, A, B, ACC, USUM, ERROR, AREA, DXMAX, IFLAG)
 Subroutine *VELHE* (I1, I2, INEGHE, YIHE, ZIHE, TIHE, TOTVHE)
 Subroutine *VELN2* (I1, I2, INEGN2, YIN2, ZIN2, TIN2, TOTVN2)
 Subroutine *VELCO2* (I1, I2, INEGCO, YICO2, ZICO2, TICO2, TOTVCO)

 VARIABLES USED:

NE Total number of test-electrons considered for the simulation.
BB Magnetic field in the Y direction.
DO Cathode fall distance at 1 Torr pressure.
 = 13 mm. for Helium.
 = 42 mm. for Nitrogen.
 = 40 mm. for Carbon-Dioxide.
VC Cathode fall voltage drop for iron electrodes.
 = 150 Volts for Helium.
 = 215 Volts for Nitrogen.
 = 450 Volts for Carbon-Dioxide.
EM Electron mass = $9.1 \text{ E-}31 \text{ kg}$.
QE Electron charge = $1.6 \text{ E-}19 \text{ coul}$.
L M.f.p. of electron at $T=288 \text{ K}$ and $P=760 \text{ torr}$,
 = $105.33 \text{ E-}8 \text{ m}$. in Helium.
 = $35.525 \text{ E-}8 \text{ m}$. in Nitrogen.
 = $23.7 \text{ E-}8 \text{ m}$. in Carbon-dioxide
S Distance travelled by electron before colliding with a gas molecule.
SPHE(1,J), SPN2(1,J), SPCO2(1,J)... Scattering angles read by Fortran units 3, 4
 and 5. 'I' corresponds to energy levels from 0 to 100 eV.
 'J' corresponds to the values of random numbers from 0 to 1
 in steps of .0125. Thus, given the value of EN and a random
 no. R5, one can determine the scattering angle using
 SPHE(EN,R5), *SPN2(EN,R5)* or *SPCO2(EN,R5)*.
QHE(1,J), QN2(1,J), QCO2(1,J).... Cross-sectional data read into Fortran units
 3, 4 and 5. I corresponds to the energy level of the electron (varying
 from 1 eV to 100 eV in steps of 1 eV) and J corresponds to the
 various excitation levels (total, level J, ... and ionization).
THETA .. Angle which the velocity vector makes with the Z-axis
 (note: E field is in the -Z direction).
PHI Angle which the projection of the velocity vector on the X-Y plane
 makes with the X-axis.
R1 Random no. used to determine the distance travelled by the test

- electron before collision.
- * R2 Random no. used to determine which gas species collides with
the test electron.
 - * R3 Random no. used to determine what type of collision (elastic or inelastic)
occurred.
 - * R4 Random no. used to determine the scattering angle, THETA, from
SPHE(I,J), SPN2(I,J) or SPCO2(I,J).
 - * R5 Random no. used to determine the scattering angle, PHI.
($PHI = 2 * 3.1415927 * R4$)
 - * KIHE,K2HE,KIHE Number of excitations to the first, second and
ionization level of Helium.
 - * KIN2,K2N2..KIN2 Number of excitations to the first, second... and
ionization level of Nitrogen.
 - * KICO2,K2CO2..KICO2 .. Number of excitations to the first, second... and
ionization level of Carbon-Dioxide..
 - * (X,Y,Z,VX,VY,VZ,EN)..... Position, velocity and energy of test electron.
 - * (XIHF,YIHE,ZIHE,VXIHE,VYIHE,VZIHE,ENIHE)... Position, velocity and energy
of Helium ions.
 - * (XIN2,YIN2,ZIN2,VXIN2,VYIN2,VZIN2,ENIN2)... Position, velocity and energy
of N2 ions.
 - * (XICO2,YICO2,ZICO2,VXICO2,VYICO2,VZICO2,ENICO2).. Position, velocity and
energy of CO2 ions.
 - * (TIHE,TIN2,TICO2)..... Time of formation of He, N2 and CO2 ions.
 - * (XNWHE,YNWHE,ZNWHE,VXNWHE,VYNWHE,VZNWHE)... Position & velocity
of secondary electrons created by ionizing collisions with He.
 - * (XNWN2,YNWN2,ZNWN2,VXNWN2,VYNWN2,VZNWN2)... Position & velocity
of secondary electrons created by ionizing collisions with N2.
 - * (XNWCO2,YNWCO2,ZNWCO2,VXNWCO,VYNWCO,VZNWCO).. Position & vel.
of secondary electrons created by ionizing collisions with CO2.
 - * TOTNC..... Total number of collisions for all primary and secondary electrons.
 - * TOTNHE..... Total number of collisions with Helium species.
 - * TOTN2..... Total number of collisions with Nitrogen species.
 - * TOTNCO..... Total number of collisions with Carbon-Dioxide species.
 - * TNIHE,TN2HE,TNIHE.... Total number of excitation collisions
(level 1, 2 and ionization) with Helium species.
 - * TNIN2,TN2N2..TNIHE.... Total number of excitation collisions
(level 1, 2,... ionization) with Nitrogen.
 - * TNICO2,TN2CO2,..TNICO2..... Total number of excitation collisions
(level 1, 2,... ionization) with Carbon-Dioxide.
 - * NIPRI,KHEPRI,KN2PRI,KCOPRI.... Total number of primary ionizations
subdivided into those with He, N₂ and CO₂.
 - * FINALT..... Total time of flight of the test electron before it reaches the end
of the cathode fall region.
 - * AVGEN..... Average value of energy of the 'NE' electrons after they have reached
they have reached the cathode.
 - * AVGT:..... Average value of the time taken by the electrons to cross the
cathode fall region.
 - * AVGX..... Average value of distance covered in the X-direction.
 - * AVGY..... Average value of the y distance covered by the electrons when they
reach the end of the cathode fall.
 - * AVGV..... Average velocity of the electrons after crossing the cathode fall region.
 - * AVGNU..... Mean collisional frequency (avg. vel./ mean free path).
 - * HALL..... Hall parameter, (ie. cyclotron freq./ collisional freq.).
 - * DRIFTE..... Average drift velocity in the electric field direction.
 - * DRIFTX..... Average drift velocity in the magnetic field direction.
 - * DRIFTB..... Average drift velocity in the Lorentz (EXB) direction.

* AVGNQ..... Average number of collisions for each test electron. *
 * AVGNHE..... Average number of collisions with Helium molecules. *
 * AVGN2..... Average number of collisions with N2 molecules. *
 * AVGNCO..... Average number of collisions with CO2 molecules. *
 * AVN1HE,AVN2HE,AVNIHE... Average number of excitation collisions *
 * (Level 1,2 and ionization) with Helium. *
 * AVN1N2,AVN2N2,...AVNIHE... Average number of excitation collisions *
 * (Level 1,2,... ionization) with Nitrogen. *
 * AVN1CO,AVN2CO,...AVNICO... Average number of excitation collisions *
 * (Level 1,2,... ionization) with Carbon-Dioxide. *

C C
 C MAIN PROGRAM C
 C C

C Define all the variables as double precision and dimension the various arrays.

C
 C IMPLICIT REAL(A - H,O - Z)
 C REAL L, L1, MU(19)
 C INTEGER TOTNC, TOTNHE, TOTNN2, TOTNCO, TNIHE, TN2HE, TNIHE, TN1N2,
 1 TN2N2, TN3N2, TN4N2, TN5N2, TN6N2, TNIN2, TNICO2, TN2CO2,
 2 TN3CO2, TN4CO2, TN5CO2, TN6CO2, TN7CO2, TNICO2, TNI, TNACO2
 C DIMENSION SPHE(101,81), SPN2(101,81), SPCO2(101,81), QHE(100,4),
 1 QN2(100,8), QCO2(100,10), XIHE(100), YIHE(100),
 2 ZIHE(100), VXIHE(100), VYIHE(100), VZIHE(100),
 3 ENIHE(100), XIN2(100), YIN2(100), ZIN2(100), VXIN2(100),
 4 VYIN2(100), VZIN2(100), ENIN2(100), XICO2(100),
 5 YICO2(100), ZICO2(100), VXICO2(100), VYICO2(100),
 6 VZICO2(100), ENICO2(100), TIHE(100), TIN2(100),
 7 X6N2(100), Y6N2(100), Z6N2(100), VX6N2(100), VY6N2(100),
 8 VZ6N2(100), EN6N2(100), X7CO2(100), Y7CO2(100),
 9 Z7CO2(100), VX7CO2(100), VY7CO2(100), VZ7CO2(100),
 EN7CO2(100), TICO2(100), XNWHE(100), YNWHE(100),
 1 ZNWHE(100), VXNWHE(100), VYNWHE(100), VZNWHE(100)
 C DIMENSION XNWN2(100), YNWN2(100), ZNWN2(100), VXNWN2(100),
 1 VYNWN2(100), VZNWN2(100), XNWCO2(100), YNWCO2(100),
 2 ZNWCO2(100), VXNWCO(100), VYNWCO(100), VZNWCO(100),
 3 TENBAR(45), INBAR(45), AENBAR(45)

C Define all the COMMON blocks.

C
 C COMMON /EDATA/ DC, VC, B0, MU, PRESS
 C COMMON /ARRAND/ DSEED
 C COMMON /XSEC/ SPHE, QHE, SPN2, QN2, SPCO2, QCO2
 C COMMON /CHE/ XIHE, YIHE, ZIHE, VXIHE, VYIHE, VZIHE, ENIHE, TIHE,
 1 KIHE, K2HE, KIHE
 C COMMON /CN2/ XIN2, YIN2, ZIN2, VXIN2, VYIN2, VZIN2, ENIN2, TIN2,
 1 X6N2, Y6N2, Z6N2, VX6N2, VY6N2, VZ6N2, EN6N2,
 2 K1N2, K2N2, K3N2, K4N2, K5N2, K6N2, K1N2
 C COMMON /CCO2/ XICO2, YICO2, ZICO2, VXICO2, VYICO2, VZICO2, ENICO2,
 1 X7CO2, Y7CO2, Z7CO2, VX7CO2, VY7CO2, VZ7CO2, EN7CO2,
 2 TICO2, K1CO2, K2CO2, K3CO2, K4CO2, K5CO2, K6CO2, K7CO2,

3 KICO2, KACO2

C

C Define the data values.

C

DATA EM /9.1D-31/, QE /-1.6D-19/

C

C Read the data values for NE = No. of electrons

C

PRESS = Gas pressure in Torr

C

B0 = Mag. field in Tesla

C

DSEED = Random no. seed.

C

READ (1,*) NE, PRESS, B0, DSEED

C

C Read in the partial pressures of He:N2:CO2.

C

READ (2,*) PRESHE, PRESN2, PRESCO

C

C Define the cathode fall distance and voltage (DC and VC)

C

TOTPRE = PRESHE + PRESN2 + PRESCO

PRESHE = PRESHE / TOTPRE

PRESN2 = PRESN2 / TOTPRE

PRESCO = PRESCO / TOTPRE

C

DCHE = 13D-03

DCN2 = 42D-03

DCCO2 = 40D-03

DC = (PRESHE*DCHE + PRESN2*DCN2 + PRESCO*DCCO2) / PRESS

C

VCHE = 150.0

VCN2 = 215.0

VCCO2 = 450.0

VC = PRESHE * VCHE + PRESN2 * VCN2 + PRESCO * VCCO2

C

C Now determine the actual pressures of the constituent gases.

C

PRESHE = PRESS * PRESHE

PRESN2 = PRESS * PRESN2

PRESCO = PRESS * PRESCO

C

C Write the heading for the output file.

C

IB0 = B0 * 1.000001D4

IPRESS = PRESS

IDSEED = DSEED

WRITE (6,10) IB0, IPRESS, IDSEED

10 FORMAT (7X, 'MONTE-CARLO SIMULATION OF ELECTRON SWARM FLOW IN',

1 'THE CATHODE FALL REGION', /, 15X, 'OF A LASER GAS',

2 'DISCHARGE UNDER THE INFLUENCE OF', /, 25X, 'ELECTRIC',

3 'AND MAGNETIC FIELDS', //, 9X, 'ELECTRIC FIELD IS',

4 'LINEARLY VARYING ACROSS THE CATHODE FALL REGION', /, 12X,

5 'AND IS IN THE -Z, ' DIRECTION.', /, 9X,

6 'MAGNETIC FIELD IS EQUAL TO', 13, ' GAUSS IN THE +X',

7 'DIRECTION.', /, 9X, 'PRESSURE IS', 13, ' TORR.', //,

8 9X, 'DSEED IS', 19, //, 12X, 'X', 4(/, 12X, ' '), /, 8X,

9 'B', 4(3X, '-', /, 8X, ' '), 3X, ' ', /, 12X, ' ', /, 12X, ' '

22('', 'Z', /, 20X, 'E', 10(''))

C
 C Read in the cross-sectional data from units 3, 4 and 5 (files X-HE+X-HE1, XN2+XN21
 C and XCO2+XCO21). Note that the cross-sections for He, N2 and CO2 are given actually
 C as NQ product (with units of m-inverse). N = no. of gas molecules p.u. volume and
 C Q = actual cross-section at pressure = 1 torr and temp. = 273 degrees C.

C
 C QHE(1,1) -----> Total cross-section
 C QHE(1,2) -----> Excitation onset 19.8 eV
 C QHE(1,3) -----> Excitation onset 21.5 eV
 C QHE(1,4) -----> Ionization onset 24.5 eV

C
 C Read in the cross-sectional data from unit 4 (files X-N2+X-N21)

C QN2(1,1) -----> Total cross-section
 C QN2(1,2) -----> Vibration excitation
 C QN2(1,3) -----> Excitation onset 6.22 eV
 C QN2(1,4) -----> Excitation onset 7.39 eV
 C QN2(1,5) -----> Excitation onset 8.59 eV
 C QN2(1,6) -----> Excitation onset 11.1 eV
 C QN2(1,7) -----> Excitation onset 15.7 eV
 C QN2(1,8) -----> Ionization onset 25.5 eV

C
 C Read in the cross-sectional data from unit 5 (files X-CO2+X-CO21)

C QCO2(1,1) -----> Total cross-section
 C QCO2(1,2) -----> Vibration excitation
 C QCO2(1,3) -----> Excitation onset 3.1 eV
 C QCO2(1,4) -----> Excitation onset 6.1 eV
 C QCO2(1,5) -----> Excitation onset 7.0 eV
 C QCO2(1,6) -----> Excitation onset 10.5 eV
 C QCO2(1,7) -----> Excitation onset 11.5 eV
 C QCO2(1,8) -----> Ionization onset 13.3 eV
 C QCO2(1,9) -----> Diss. ion. onset 25.0 eV

DO 20 I = 1, 100

READ (3,*) QHE(1,1), QHE(1,2), QHE(1,3), QHE(1,4)

20 CONTINUE

C
 C Read in the scattering angle data from unit 1 (file X-HE1).

DO 30 I = 1, 101

READ (3,*) (SPHE(I,J),J=1,81)

30 CONTINUE

DO 40 I = 1, 100

READ (4,*) QN2(1,1), QN2(1,2), QN2(1,3), QN2(1,4), QN2(1,5),
 1 QN2(1,6), QN2(1,7), QN2(1,8)

40 CONTINUE

C
 C Read in the scattering angle data from unit 2 (file X-N21).

DO 50 I = 1, 101

READ (4,*) (SPN2(I,J),J=1,81)

50 CONTINUE

DO 60 I = 1, 100

READ (5,*) (QCO2(1,1), QCO2(1,2), QCO2(1,3), QCO2(1,4),
1 QCO2(1,5), QCO2(1,6), QCO2(1,7), QCO2(1,8), QCO2(1,9), QCO2(1,10))
60 CONTINUE

C

C Read in the scattering angle data from unit 5 (file X-CO21).

C

DO 70 I = 1, 101

READ (5,*) (SPCO2(I,J), J=1,81)
70 CONTINUE

C

C The terms MU(1) to MU(19) give the mobility of helium ions as a
C function of (E/p) ratio. See reference 66 (Frost).

C

MU(1) = 0.83
MU(2) = 0.78
MU(3) = 0.71
MU(4) = 0.67
MU(5) = 0.62
MU(6) = 0.595
MU(7) = 0.555
MU(8) = 0.525
MU(9) = 0.5
MU(10) = 0.48
MU(11) = 0.35
MU(12) = 0.28
MU(13) = 0.25
MU(14) = 0.22
MU(15) = 0.2
MU(16) = 0.18
MU(17) = 0.17
MU(18) = 0.165
MU(19) = 0.16

C

C Initialize the values of total energy, radius, no. of collisions,
C no. of ionisations, time and y.

C

TOTEN = 0.0
TOTX = 0.0
TOTNC = 0.0
TOTNHE = 0.0
TOTN2 = 0.0
TOTNCO = 0.0
TOTT = 0.0
TOTY = 0.0

C

TN1HE = 0.0
TN2HE = 0.0
TN1HE = 0.0

C

TN1N2 = 0.0
TN2N2 = 0.0
TN3N2 = 0.0
TN4N2 = 0.0
TN5N2 = 0.0
TN6N2 = 0.0

TNIN2 = 0.0

C

TN1CO2 = 0.0

TN2CO2 = 0.0

TN3CO2 = 0.0

TN4CO2 = 0.0

TN5CO2 = 0.0

TN6CO2 = 0.0

TN7CO2 = 0.0

TNICO2 = 0.0

TNACO2 = 0.0

C

TOTVHE = 0.0

TOTVN2 = 0.0

TOTVCO = 0.0

C

INEGHE = 0

INEGN2 = 0

INEGCO = 0

KHEPRI = 0

KN2PRI = 0

KCOPRI = 0

C

C Initialise the histograms for energy at various regions of the cathode fall region.

C INBAR gives the total number of samples from which the energy histograms are created

C and TENBAR gives the total sum of energy at that particular point. The average

C energy at each of these points is obtained by dividing TENBAR by IENBAR.

C

DO 80 IB = 1, 45

TENBAR(IB) = 0.0

INBAR(IB) = 0

80 CONTINUE

C

DO 960 I = 1, NE2

C

C Initialise the various variables (i.e. number of collisions,

C time, excitations to various levels) to zero.

C

IBAR = 1

NCOLN1 = 0

NCOLHE = 0

NCOLN2 = 0

NCOLCO = 0

UNALT = 0.0

TIME = 0.0

C

K1HE = 0

K2HE = 0

KIHE = 0

C

K1N2 = 0

K2N2 = 0

K3N2 = 0

K4N2 = 0

K5N2 = 0

K6N2 = 0

KIN2 = 0

C

K1CO2 = 0

K2CO2 = 0

K3CO2 = 0

K4CO2 = 0

K5CO2 = 0

K6CO2 = 0

K7CO2 = 0

KICO2 = 0

KACO2 = 0

C

C Initialise the position and velocity of the electron.

C

CALL INIT(X, Y, Z, VX, VY, VZ, PRESHE, PRESN2, PRESCO, L)

C

C Store the the energy of the electron in ENBAR whenever z is an integer

C multiple of 1 mm. For values inbetween, (skipped by z) set ENBAR = 999.

C These values will be neglected when computing energy histograms.

C

90 ICHECK = Z * 1000. * PRESS

IF (ICHECK .LT. IBAR) GO TO 100

TENBAR(ICHECK) = TENBAR(ICHECK) + EN

INBAR(ICHECK) = INBAR(ICHECK) + 1

IBAR = ICHECK + 1

C

C Generate random no. R1 to decide path length of electron before collision.

C

100 CALL RANDOM(R1)

S = -L * ALOG(R1)

CALL ACCEL(X, Y, Z, VX, VY, VZ, S, T, TIME, EN, &130)

FINALT = FINALT + T

C

C It is necessary to determine which atom the electron collided with. This

C requires a knowledge of the total cross-sections of the various component gases.

C

IEN = EN

ZZ = (EN - IEN) * 10.

IF (ZZ .GE. 5.) IEN = IEN + 1

IF (EN .GE. 100.) IEN = 100

IF (IEN .LE. 1) IEN = 1

PQHE = PRESHE * QHE(IEN,1)

PQN2 = PRESN2 * QN2(IEN,1)

PQCO2 = PRESCO * QCO2(IEN,1)

SUMQ = PQHE + PQN2 + PQCO2

C

C Determine type of collision and compute the new state of the electron.

C Use another random number, R2, to determine the new state.

C

NCOLL = NCOLL + 1

P1 = PQHE / SUMQ

P2 = (PQHE + PQN2) / SUMQ

CALL RANDOM(R2)

IF (R2 .LT. P1) GO TO 110

IF (R2 .GE. P1 .AND. R2 .LT. P2) GO TO 120

NCOLCO = NCOLCO + 1

```

CALL COLCO2(X, Y, Z, VX, VY, VZ, EN, TIME, &90, &130)
110 NCOLHE = NCOLHE + 1
CALL COLHE(X, Y, Z, VX, VY, VZ, EN, TIME, &90)
120 NCOLN2 = NCOLN2 + 1
CALL COLN2(X, Y, Z, VX, VY, VZ, EN, TIME, &90)

```

C
C Store the total sum of the various terms. These will be useful in determining the
C average value of energy, radius, no. of coll., no. of ionisations, x and y values.

```

130 TOTEN = TOTEN + EN
TOTX = TOTX + X
TOTNC = TOTNC + NCOLL
TOTNHE = TOTNHE + NCOLHE
TOTNN2 = TOTNN2 + NCOLN2
TOTNCO = TOTNCO + NCOLCO
TOTT = TOTT + FINALT
TOTY = TOTY + Y

```

C
TN1HE = TN1HE + K1HE
TN2HE = TN2HE + K2HE
TN1HE = TN1HE + KIHE

C
TN1N2 = TN1N2 + K1N2
TN2N2 = TN2N2 + K2N2
TN3N2 = TN3N2 + K3N2
TN4N2 = TN4N2 + K4N2
TN5N2 = TN5N2 + K5N2
TN6N2 = TN6N2 + K6N2
TNIN2 = TNIN2 + KIN2

C
TN1CO2 = TN1CO2 + K1CO2
TN2CO2 = TN2CO2 + K2CO2
TN3CO2 = TN3CO2 + K3CO2
TN4CO2 = TN4CO2 + K4CO2
TN5CO2 = TN5CO2 + K5CO2
TN6CO2 = TN6CO2 + K6CO2
TN7CO2 = TN7CO2 + K7CO2
TNICO2 = TNICO2 + KICO2
TNACO2 = TNACO2 + KACO2

C
C The following write statements are used to store the positions and time of
C ion formation for use later in calculating the Hall drift velocity.

C
IF (KIHE .LT. 1) GO TO 140
CALL VELHE(1, KIHE, INEGHE, YIHE, ZIHE, TIHE, TOTVHE)

C
140 IF (KIN2 .LT. 1) GO TO 150
CALL VELN2(1, KIN2, INEGN2, YIN2, ZIN2, TIN2, TOTVN2)

C
150 IF (KICO2 .LT. 1) GO TO 160
CALL VELCO2(1, KICO2, INEGCO, YICO2, ZICO2, TICO2, TOTVCO)

C
160 IF (KIHE .EQ. 0) GO TO 180
DO 170 J1 = 1, KIHE
XNWHE(J1) = XIHE(J1)
YNWHE(J1) = YIHE(J1)

```

ZNWHE(J1) = ZIHE(J1)
VXNWHE(J1) = VXIHE(J1)
VYNWHE(J1) = VYIHE(J1)
VZNWHE(J1) = VZIHE(J1)
170 CONTINUE
C
180 IF (KIN2 .EQ. 0) GO TO 200
DO 190 J1 = 1, KIN2
  XNWN2(J1) = XIN2(J1)
  YNWN2(J1) = YIN2(J1)
  ZNWN2(J1) = ZIN2(J1)
  VXNWN2(J1) = VXIN2(J1)
  VYNWN2(J1) = VYIN2(J1)
  VZNWN2(J1) = VZIN2(J1)
190 CONTINUE
C
200 IF (K6N2 .EQ. 0) GO TO 220
I1 = KIN2
DO 210 J1 = 1, K6N2
  I1 = I1 + 1
  XNWN2(I1) = X6N2(J1)
  YNWN2(I1) = Y6N2(J1)
  ZNWN2(I1) = Z6N2(J1)
  VXNWN2(I1) = VX6N2(J1)
  VYNWN2(I1) = VY6N2(J1)
  VZNWN2(I1) = VZ6N2(J1)
210 CONTINUE
C
220 IF (KICO2 .EQ. 0) GO TO 240
DO 230 J1 = 1, KICO2
  XNWCO2(J1) = XICO2(J1)
  YNWCO2(J1) = YICO2(J1)
  ZNWCO2(J1) = ZICO2(J1)
  VXNWCO2(J1) = VXICO2(J1)
  VYNWCO2(J1) = VYICO2(J1)
  VZNWCO2(J1) = VZICO2(J1)
230 CONTINUE
C
240 IF (K7CO2 .EQ. 0) GO TO 245
I1 = KICO2
DO 235 J1 = 1, K7CO2
  I1 = I1 + 1
  XNWCO2(I1) = X7CO2(J1)
  YNWCO2(I1) = Y7CO2(J1)
  ZNWCO2(I1) = Z7CO2(J1)
  VXNWCO2(I1) = VX7CO2(J1)
  VYNWCO2(I1) = VY7CO2(J1)
  VZNWCO2(I1) = VZ7CO2(J1)
235 CONTINUE
C
245 KII2HE = KIHE
  KII2N2 = KIN2 + K6N2
  KII2CO = KICO2 + K7CO2
  IF (KII2HE .LE. 0) GO TO 320
C-----C
C NOW FOLLOW THE PATH OF THE IONISED ELECTRONS FROM HELIUM ATOMS. C

```

```

C-----C
C
C Initialise the following variables to keep tag of the no. of
C electrons excited to higher levels by the newly ionised electron.
C     K11HE = Initial no. of ionised atoms.
C     K1HE = Total no. of ionised atoms.
C     K11HE = Initial no. of atoms excited to level 1.
C     K1HE = Total no. of atoms excited to level 1.
C     K21HE = Initial no. of atoms excited to level 2.
C     K2HE = Total no. of atoms excited to level 2.
C
C     Do similar initialisation for N2 and CO2.
C
C DO 310 J1 = 1, K112HE
C
C     K11HE = K1HE
C     K21HE = K2HE
C     K11HE = K1HE
C
C     K11N2 = K1N2
C     K21N2 = K2N2
C     K31N2 = K3N2
C     K41N2 = K4N2
C     K51N2 = K5N2
C     K61N2 = K6N2
C     K11N2 = K1N2
C
C     K11CO2 = K1CO2
C     K21CO2 = K2CO2
C     K31CO2 = K3CO2
C     K41CO2 = K4CO2
C     K51CO2 = K5CO2
C     K61CO2 = K6CO2
C     K71CO2 = K7CO2
C     K11CO2 = K1CO2
C     K11CO2 = K1CO2
C
C     K111HE = K11HE + 1
C     K211HE = K21HE + 1
C     K111HE = K11HE + 1
C
C     K111N2 = K11N2 + 1
C     K211N2 = K21N2 + 1
C     K311N2 = K31N2 + 1
C     K411N2 = K41N2 + 1
C     K511N2 = K51N2 + 1
C     K611N2 = K61N2 + 1
C     K111N2 = K11N2 + 1
C
C     K111CO = K11CO2 + 1
C     K211CO = K21CO2 + 1
C     K311CO = K31CO2 + 1
C     K411CO = K41CO2 + 1
C     K511CO = K51CO2 + 1
C     K611CO = K61CO2 + 1

```

```

K7IICO = K7ICO2 + 1
K8IICO = K8ICO2 + 1
K9IICO = K9ICO2 + 1

```

C

```

NCOLL = 0
NCOLHE = 0
NCOLN2 = 0
NCOLCO = 0

```

C

```

C Initialise the values of X, Y, Z, VX, VY and VZ
C to the values at the point of ionisation.

```

C

```

X = XNWHE(J1)
Y = YNWHE(J1)
Z = ZNWHE(J1)
VX = VXNWHE(J1)
VY = VYNWHE(J1)
VZ = VZNWHE(J1)

```

C

```

250 CALL RANDOM(R1)
S = -L * ALOG(R1)
CALL ACCEL(X, Y, Z, VX, VY, VZ, S, T, TIME, EN, &280)
FINALT = FINALT + T

```

C

```

IEN = EN
ZZ = (EN - IEN) * 10.
IF (ZZ .GE. 5.) IEN = IEN + 1
IF (EN .GE. 100.) IEN = 100
IF (IEN .LE. 1) IEN = 1
PQHE = PRESHE * QHE(IEN,1)
PQN2 = PRESN2 * QN2(IEN,1)
PQCO2 = PRESCO * QCO2(IEN,1)
SUMQ = PQHE + PQN2 + PQCO2

```

C

```

NCOLL = NCOLL + 1
P1 = PQHE / SUMQ
P2 = (PQHE + PQN2) / SUMQ
CALL RANDOM(R2)
IF (R2 .LT. P1) GO TO 260
IF (R2 .GE. P1 .AND. R2 .LT. P2) GO TO 270
NCOLCO = NCOLCO + 1
CALL COLCO2(X, Y, Z, VX, VY, VZ, EN, TIME, &250, &280)

```

260

```

NCOLHE = NCOLHE + 1
CALL COLHE(X, Y, Z, VX, VY, VZ, EN, TIME, &250)

```

270

```

NCOLN2 = NCOLN2 + 1
CALL COLN2(X, Y, Z, VX, VY, VZ, EN, TIME, &250)

```

C

280

```

TOTEN = TOTEN + EN
TOTX = TOTX + X
TOTNC = TOTNC + NCOLL
TOTNHE = TOTNHE + NCOLHE
TOTN2 = TOTN2 + NCOLN2
TOTNCO = TOTNCO + NCOLCO
TOTT = TOTT + FINALT
TOTY = TOTY + Y

```

C

$TN1HE = TN1HE + K1HE \cdot K11HE$
 $TN2HE = TN2HE + K2HE \cdot K21HE$
 $TN1HE = TN1HE + K1HE \cdot K11HE$

C

$TN1N2 = TN1N2 + K1N2 \cdot K11N2$
 $TN2N2 = TN2N2 + K2N2 \cdot K21N2$
 $TN3N2 = TN3N2 + K3N2 \cdot K31N2$
 $TN4N2 = TN4N2 + K4N2 \cdot K41N2$
 $TN5N2 = TN5N2 + K5N2 \cdot K51N2$
 $TN6N2 = TN6N2 + K6N2 \cdot K61N2$
 $TN1N2 = TN1N2 + K1N2 \cdot K11N2$

C

$TN1CO2 = TN1CO2 + K1CO2 \cdot K11CO2$
 $TN2CO2 = TN2CO2 + K2CO2 \cdot K21CO2$
 $TN3CO2 = TN3CO2 + K3CO2 \cdot K31CO2$
 $TN4CO2 = TN4CO2 + K4CO2 \cdot K41CO2$
 $TN5CO2 = TN5CO2 + K5CO2 \cdot K51CO2$
 $TN6CO2 = TN6CO2 + K6CO2 \cdot K61CO2$
 $TN7CO2 = TN7CO2 + K7CO2 \cdot K71CO2$
 $TN1CO2 = TN1CO2 + K1CO2 \cdot K11CO2$
 $TNACO2 = TNACO2 + KACO2 \cdot KA1CO2$

C

IF (K1HE .LT. K11HE) GO TO 290
 CALL VELHE(K11HE, K1HE, INEGHE, Y1HE, Z1HE, T1HE, TOTVHE)

C

290 IF (K1N2 .LT. K11N2) GO TO 300
 CALL VELN2(K11N2, K1N2, INEGN2, Y1N2, Z1N2, T1N2, TOTVN2)

C

300 IF (K1CO2 .LT. K11CO2) GO TO 310
 CALL VELCO2(K11CO2, K1CO2, INEGCO, Y1CO2, Z1CO2, T1CO2,
 1 TOTVCO)

C

310 CONTINUE

C

320 IF (K112N2 .LE. 0) GO TO 400

C

.....C

C NOW FOLLOW THE PATH OF THE IONISED ELECTRONS FROM NITROGEN ATOMS.C

.....C

C

C Initialise the following variables to keep tag of the no. of
 C electrons excited to higher levels by the newly ionised electron.

C

K11 = Initial no. of ionised atoms.

C

K1 = total no. of ionised atoms.

C

K11 = Initial no. of atoms excited to level 1.

C

K1 = total no. of atoms excited to level 1.

C

C

C

C

K61 = Initial no. of atoms excited to level 6.

C

K6 = total no. of atoms excited to level 6.

C

C

DO 390 J1 = 1, K112N2

C

K11HE = K1HE

K21HE = K2HE

K11HE = K1HE

C

$K1IN2 = K1N2$
 $K2IN2 = K2N2$
 $K3IN2 = K3N2$
 $K4IN2 = K4N2$
 $K5IN2 = K5N2$
 $K6IN2 = K6N2$
 $KIIN2 = KIN2$

C

$K1ICO2 = K1CO2$
 $K2ICO2 = K2CO2$
 $K3ICO2 = K3CO2$
 $K4ICO2 = K4CO2$
 $K5ICO2 = K5CO2$
 $K6ICO2 = K6CO2$
 $K7ICO2 = K7CO2$
 $KIICO2 = KICO2$
 $KAICO2 = KACO2$

C

$K1IHE = K1HE + 1$
 $K2IHE = K2HE + 1$
 $KIHE = KIHE + 1$

C

$K1IIN2 = K1IN2 + 1$
 $K2IIN2 = K2IN2 + 1$
 $K3IIN2 = K3IN2 + 1$
 $K4IIN2 = K4IN2 + 1$
 $K5IIN2 = K5IN2 + 1$
 $K6IIN2 = K6IN2 + 1$
 $KIIN2 = KIIN2 + 1$

C

$K1ICO = K1ICO2 + 1$
 $K2ICO = K2ICO2 + 1$
 $K3ICO = K3ICO2 + 1$
 $K4ICO = K4ICO2 + 1$
 $K5ICO = K5ICO2 + 1$
 $K6ICO = K6ICO2 + 1$
 $K7ICO = K7ICO2 + 1$
 $KIICO = KIICO2 + 1$
 $KAIICO = KAIICO2 + 1$

C

$NCOLL = 0$
 $NCOLHE = 0$
 $NCOLN2 = 0$
 $NCOLCO = 0$

C

C Initialise the values of X, Y, Z, VX, VY and VZ
 C to the values at the point of ionisation.

C

$X = XNWN2(J1)$
 $Y = YNWN2(J1)$
 $Z = ZNWN2(J1)$
 $VX = VXNWN2(J1)$
 $VY = VYNWN2(J1)$
 $VZ = VZNWN2(J1)$

C

```

330  CALL RANDOM(R1)
      S = -L * ALOG(R1)
      CALL ACCEL(X, Y, Z, VX, VY, VZ, S, T, TIME, EN, &360)
      FINALT = FINALT + T
C
      IEN = EN
      ZZ = (EN - IEN) * 10.
      IF (ZZ .GE. 5) IEN = IEN + 1
      IF (EN .GE. 100) IEN = 100
      IF (IEN .LE. 1) IEN = 1
      PQHE = PRESHE * QHE(IEN,1)
      PQN2 = PRESN2 * QN2(IEN,1)
      PQCO2 = PRESCO * QCO2(IEN,1)
      SUMQ = PQHE + PQN2 + PQCO2
C
      NCOLL = NCOLL + 1
      P1 = PQHE / SUMQ
      P2 = (PQHE + PQN2) / SUMQ
      CALL RANDOM(R2)
      IF (R2 .LT. P1) GO TO 340
      IF (R2 .GE. P1 .AND. R2 .LT. P2) GO TO 350
      NCOLCO = NCOLCO + 1
      CALL COLCO2(X, Y, Z, VX, VY, VZ, EN, TIME, &330, &360)
340  NCOLHE = NCOLHE + 1
      CALL COLHE(X, Y, Z, VX, VY, VZ, EN, TIME, &330)
350  NCOLN2 = NCOLN2 + 1
      CALL COLN2(X, Y, Z, VX, VY, VZ, EN, TIME, &330)
C
360  TOTEN = TOTEN + EN
      TOTX = TOTX + X
      TOTNC = TOTNC + NCOLL
      TOTNHE = TOTNHE + NCOLHE
      TOTNN2 = TOTNN2 + NCOLN2
      TOTNCO = TOTNCO + NCOLCO
      TOTT = TOTT + FINALT
      TOTY = TOTY + Y
C
      TN1HE = TN1HE + K1HE - K11HE
      TN2HE = TN2HE + K2HE - K21HE
      TN1HE = TN1HE + K1HE - K11HE
C
      TN1N2 = TN1N2 + K1N2 - K11N2
      TN2N2 = TN2N2 + K2N2 - K21N2
      TN3N2 = TN3N2 + K3N2 - K31N2
      TN4N2 = TN4N2 + K4N2 - K41N2
      TN5N2 = TN5N2 + K5N2 - K51N2
      TN6N2 = TN6N2 + K6N2 - K61N2
      TN1N2 = TN1N2 + K1N2 - K11N2
C
      TN1CO2 = TN1CO2 + K1CO2 - K11CO2
      TN2CO2 = TN2CO2 + K2CO2 - K21CO2
      TN3CO2 = TN3CO2 + K3CO2 - K31CO2
      TN4CO2 = TN4CO2 + K4CO2 - K41CO2
      TN5CO2 = TN5CO2 + K5CO2 - K51CO2
      TN6CO2 = TN6CO2 + K6CO2 - K61CO2
      TN7CO2 = TN7CO2 + K7CO2 - K71CO2

```

TNICO2 = TNICO2 + KICO2 - KIICO2
 TNACO2 = TNACO2 + KACO2 - KAICO2

C

IF (KIHE .LT. KIIIHE) GO TO 370
 CALL VELHE(KIIIHE, KIHE, INEGHE, YIHE, ZIHE, TIHE, TOTVHE)

C

370 IF (KIN2 .LT. KIIIN2) GO TO 380
 CALL VELN2(KIIIN2, KIN2, INEGN2, YIN2, ZIN2, TIN2, TOTVN2)

C

380 IF (KICO2 .LT. KIIICO) GO TO 390
 CALL VELCO2(KIIICO, KICO2, INEGCO, YICO2, ZICO2, TICO2,
 1 TOTVCO)

C

390 CONTINUE

C

400 IF (KII2CO .LE. 0) GO TO 520

C

C

C

C

C

C

C

C

C

C

C

C

C

C

C

C

C

C

C

C

C

C

C

C

C

C

C

C

C

C

C

C

C

C

C

C

C

C

C

C

C

C

C

C

C

C

C

C

C

..... C
 C NOW FOLLOW THE PATH OF THE IONISED ELECTRONS FROM CO2 ATOMS. C
 C C
 C

C Initialise the following variables to keep tag of the no. of
 C electrons excited to higher levels by the newly ionised electron.

C KII = Initial no. of ionised atoms.

C KI = Total no. of ionised atoms.

C KII1 = Initial no. of atoms excited to level 1.

C KI1 = Total no. of atoms excited to level 1.

C

C

C

C

C

C

C

C

C

C

C

C

C

C

C

C

C

C

C

C

C

C

C

C

C

C

C

C

C

C

C

C

C

C

C

C

C

DO 470 J1 = 1, KII2CO

KIIHE = KIHE

KIIHE = KIIHE

KIIHE = KIHE

C

KIIIN2 = KIIIN2

KIIIN2 = KIIIN2

KIIIN2 = KIIIN2

KIIIN2 = KIIIN2

KIIIN2 = KIIIN2

KIIIN2 = KIIIN2

KIIIN2 = KIIIN2

C

KIIICO2 = KIIICO2

KIIICO2 = KIIICO2

KIIICO2 = KIIICO2

KIIICO2 = KIIICO2

KIIICO2 = KIIICO2

KIIICO2 = KIIICO2

KIIICO2 = KIIICO2

KIIICO2 = KIIICO2

KIIICO2 = KIIICO2

KIIICO2 = KIIICO2

C

K111HE = K11HE + 1
 K211HE = K21HE + 1
 K311HE = K31HE + 1

C

K111N2 = K11N2 + 1
 K211N2 = K21N2 + 1
 K311N2 = K31N2 + 1
 K411N2 = K41N2 + 1
 K511N2 = K51N2 + 1
 K611N2 = K61N2 + 1
 K711N2 = K71N2 + 1

C

K111CO = K11CO2 + 1
 K211CO = K21CO2 + 1
 K311CO = K31CO2 + 1
 K411CO = K41CO2 + 1
 K511CO = K51CO2 + 1
 K611CO = K61CO2 + 1
 K711CO = K71CO2 + 1
 K111CO = K11CO2 + 1
 K111CO = K11CO2 + 1

C

NCOLL = 0
 NCOLHE = 0
 NCOLN2 = 0
 NCOLCO = 0

C

C Initialise the values of X, Y, Z, VX, VY and VZ
 C to the values at the point of ionisation.

C

X = XNWCO2(J1)
 Y = YNWCO2(J1)
 Z = ZNWCO2(J1)
 VX = VXNWCO(J1)
 VY = VYNWCO(J1)
 VZ = VZNWCO(J1)

C

410 CALL RANDOM(R1)
 S = -L * ALOG(R1)
 CALL ACCEL(X, Y, Z, VX, VY, VZ, S, T, TIME, EN, &440)
 FINALT = FINALT + T

C

IEN = EN
 ZZ = (EN - IEN) * 10.
 IF (ZZ .GE. 5.) IEN = IEN + 1
 IF (EN .GE. 100.) IEN = 100
 IF (IEN .LE. 1) IEN = 1
 PQHE = PRESHE * QHE(IEN,1)
 PQN2 = PRESN2 * QN2(IEN,1)
 PQCO2 = PRESCO * QCO2(IEN,1)
 SUMQ = PQHE + PQN2 + PQCO2

C

NCOLL = NCOLL + 1
 P1 = PQHE / SUMQ
 P2 = (PQHE + PQN2) / SUMQ
 CALL RANDOM(R2)

```

IF (R2 .LT. P1) GO TO 420
IF (R2 .GE. P1 .AND. R2 .LT. P2) GO TO 430
NCOLCO = NCOLCO + 1
CALL COLCO2(X, Y, Z, VX, VY, VZ, EN, TIME, &410, &440)
420  NCOLHE = NCOLHE + 1
CALL COLHE(X, Y, Z, VX, VY, VZ, EN, TIME, &410)
430  NCOLN2 = NCOLN2 + 1
CALL COLN2(X, Y, Z, VX, VY, VZ, EN, TIME, &410)
C
440  TOTEN = TOTEN + EN
TOTX = TOTX + X
TOTNC = TOTNC + NCOLL
TOTNHE = TOTNHE + NCOLHE
TOTNN2 = TOTNN2 + NCOLN2
TOTNCO = TOTNCO + NCOLCO
TOTT = TOTT + FINALT
TOTY = TOTY + Y
C
TN1HE = TN1HE + K1HE - K1IHE
TN2HE = TN2HE + K2HE - K2IHE
TNIHE = TNIHE + KIHE - KIHE
C
TN1N2 = TN1N2 + K1N2 - K1IN2
TN2N2 = TN2N2 + K2N2 - K2IN2
TN3N2 = TN3N2 + K3N2 - K3IN2
TN4N2 = TN4N2 + K4N2 - K4IN2
TN5N2 = TN5N2 + K5N2 - K5IN2
TN6N2 = TN6N2 + K6N2 - K6IN2
TNIN2 = TNIN2 + KIN2 - KIIN2
C
TN1CO2 = TN1CO2 + K1CO2 - K1ICO2
TN2CO2 = TN2CO2 + K2CO2 - K2ICO2
TN3CO2 = TN3CO2 + K3CO2 - K3ICO2
TN4CO2 = TN4CO2 + K4CO2 - K4ICO2
TN5CO2 = TN5CO2 + K5CO2 - K5ICO2
TN6CO2 = TN6CO2 + K6CO2 - K6ICO2
TN7CO2 = TN7CO2 + K7CO2 - K7ICO2
TNICO2 = TNICO2 + KICO2 - KIICO2
TNACO2 = TNACO2 + KACO2 - KAICO2
C
IF (KIHE .LT. KIIHE) GO TO 450
CALL VELHE(KIIHE, KIHE, INEGHE, YIHE, ZIHE, TIHE, TOTVHE)
C
450  IF (KIN2 .LT. KIIIN2) GO TO 460
CALL VELN2(KIIIN2, KIN2, INEGN2, YIN2, ZIN2, TIN2, TOTVN2)
C
460  IF (KICO2 .LT. KIIICO) GO TO 470
CALL VELCO2(KIIICO, KICO2, INEGCO, YICO2, ZICO2, TICO2,
1     TOTVCO)
C
470  CONTINUE
C
WRITE (6,480) DC, VC
480  FORMAT (2X, '..... CATHODE FALL DISTANCE = DC = ', E12.4, /
1     , 2X, '..... CATHODE FALL VOLTAGE = VC = ', E12.4)
C

```

$KHEPRI = KHEPRI + KII2HE$
 $KN2PRI = KN2PRI + KII2N2$
 $KCOPRI = KCOPRI + KII2CO$
 $NIPRI = KHEPRI + KN2PRI + KCOPRI$

C

C

C The final positions and velocities are tabulated after every
 C 100 primary electrons.

C

520 ICHECK = 1 / 500
 ICHECK = ICHECK * 500
 IF (1.NE. ICHECK .AND. 1.NE. NE) GO TO 960

C

C Compute the average values of energy, radius, no. of collisions,
 C no. of ionisations, time taken to cross the cathode fall and the
 C E X B drift.

C

$TOTN = 1 + NIPRI$
 $AVGEN = TOTEN / TOTN$
 $AVGNC = TOTNC / TOTN$
 $AVGNHE = TOTNHE / TOTN$
 $AVGNN2 = TOTNN2 / TOTN$
 $AVGNCO = TOTNCO / TOTN$

C

$AVNIHE = TNIHE / TOTN$
 $AVN1HE = TN1HE / TOTN$
 $AVN2HE = TN2HE / TOTN$

C

$AVNIN2 = TNIN2 / TOTN$
 $AVN1N2 = TN1N2 / TOTN$
 $AVN2N2 = TN2N2 / TOTN$
 $AVN3N2 = TN3N2 / TOTN$
 $AVN4N2 = TN4N2 / TOTN$
 $AVN5N2 = TN5N2 / TOTN$
 $AVN6N2 = TN6N2 / TOTN$

C

$AVNICO = TNICO2 / TOTN$
 $AVN1CO = TN1CO2 / TOTN$
 $AVN2CO = TN2CO2 / TOTN$
 $AVN3CO = TN3CO2 / TOTN$
 $AVN4CO = TN4CO2 / TOTN$
 $AVN5CO = TN5CO2 / TOTN$
 $AVN6CO = TN6CO2 / TOTN$
 $AVN7CO = TN7CO2 / TOTN$
 $AVNACO = TNACO2 / TOTN$

C

$AVGT = TOTT / TOTN$
 $AVGY = TOTY / TOTN$
 $AVGV = \text{SQRT}(2 * AVGEN * 1.6D-19 / EM)$
 $AVGNU = AVGV / L$
 $HALL = 1.6D-19 * B0 / (EM * AVGNU)$
 $DRIFTE = DC / AVGT$
 $DRIFTR = AVGR / AVGT$
 $DRIFTB = AVGY / AVGT$
 $ALPHE = (ALOG((AVNIHE + 1.))) / DC$
 $ALPN2 = (ALOG((AVNIN2 + 1.))) / DC$

```

ALPCO2 = (ALOG((AVNICO + 1.))) / DC
C
DO 530 IB = 1, 45
  IF (INBAR(IB) .GE. 1) GO TO 525
  AENBAR(IB) = 999.0
  GO TO 530
525  AENBAR(IB) = TENBAR(IB) / INBAR(IB)
530  CONTINUE
9
  WRITE (6,540)
540  FORMAT (//, 19X, 'RESULTS OF MONTE-CARLO SIMULATION', /,
1      19X, 33(' '), //, 2X, 91(' '))
C
  WRITE (6,550)
550  FORMAT (//, 8X, '# OF ELECT.', 8X, 'BO (GAUSS)', 8X,
1      'PRESS (TORR)', 8X, 'PARTIAL PRESS HE.N2 (O2)')
  WRITE (6,560) I, IB0, PRESS, PRESHE, PRESN2, PRESCO
560  FORMAT (T11, 14, T30, 14, T50, F4.1, T70, F4.1, T90, F4.1,
1      F4.1)
  WRITE (6,570)
570  FORMAT (//, 8X, 'TOT# COL', 10X, 'TOT# HE', 10X, 'TOT#
1      11X, 'TOT# CO2')
  WRITE (6,580) TOTNC, TOTNHE, TOTNN2, TOTNCO
580  FORMAT (T10, 16, T29, 16, T47, 16, T65, 16)
  WRITE (6,590)
590  FORMAT (//, 10X, 'AVG# COL', 11X, 'AVG# HE', 9X, 'AVG# N2',
1      11X, 'AVG# CO2')
  WRITE (6,600) AVGNCO, AVGNHE, AVGN2, AVGNCO
600  FORMAT (T10, 1PE11.4, T29, E11.4, T47, E11.4, T65, E11.4)
  WRITE (6,610)
610  FORMAT (//, 4X, 'COLLISION DISTRIBUTION FOR HELIUM', /,
1      4X, 33(' '))
  WRITE (6,620)
620  FORMAT (//, 10X, 'TOT# 1', 12X, 'TOT# 2', 11X, 'TOT# ION')
  WRITE (6,630) TN1HE, TN2HE, TN1HE
630  FORMAT (T10, 15, T29, 15, T47, 15)
  WRITE (6,640)
640  FORMAT (//, 10X, 'AVG# 1', 13X, 'AVG# 2', 12X, 'AVG# ION')
  WRITE (6,650) AVN1HE, AVN2HE, AVN1HE
650  FORMAT (T10, 1PE11.4, T29, E11.4, T47, E11.4)
  WRITE (6,660)
660  FORMAT (//, 4X, 'COLLISION DISTRIBUTION FOR NITROGEN', /,
1      4X, 35(' '))
  WRITE (6,670)
670  FORMAT (//, 9X, 'TOT# 1', 13X, 'TOT# 2', 12X, 'TOT# 3', 12X,
1      'TOT# 4')
  WRITE (6,680) TN1N2, TN2N2, TN3N2, TN4N2
  WRITE (6,680)
680  FORMAT (//, 9X, 'TOT# 5', 13X, 'TOT# 6', 12X, 'TOT# ION')
  WRITE (6,690) TN5N2, TN6N2, TN1N2
  WRITE (6,690)
690  FORMAT (//, 10X, 'AVG# 1', 13X, 'AVG# 2', 12X, 'AVG# 3', 12X,
1      'AVG# 4')
  WRITE (6,700) AVN1N2, AVN2N2, AVN3N2, AVN4N2
  WRITE (6,700)
700  FORMAT (//, 10X, 'AVG# 5', 13X, 'AVG# 6', 12X, 'AVG# ION')

```

```

WRITE (6,65C) AVN5N2, AVN6N2, AVNIN2
WRITE (6,710)
710  FORMAT (//, 4X, 'COLLISION DISTRIBUTION FOR CARBON-DIOXIDE', /,
1     4X, 41(' '))
WRITE (6,720)
720  FORMAT (//, 9X, 'TOT# 1', 13X, 'TOT# 2', 12X, 'TOT# 3', 12X,
1     'TOT# 4', 10X, 'TOT# 5')
WRITE (6,730) TN1CO2, TN2CO2, TN3CO2, TN4CO2, TN5CO2
730  FORMAT (T10, 15, T29, 15, T47, 15, T65, 15, T81, 15)
WRITE (6,740)
740  FORMAT (/, 9X, 'TOT# 6', 13X, 'TOT# 7', 11X, 'TOT# ION', 10X,
1     'TOT# ATCH')
WRITE (6,580) TN6CO2, TN7CO2, TN1CO2, TNACO2
WRITE (6,750)
750  FORMAT (//, 10X, 'AVG# 1', 13X, 'AVG# 2', 12X, 'AVG# 3', 12X,
1     'AVG# 4', 10X, 'AVG# 5')
WRITE (6,760) AVN1CO, AVN2CO, AVN3CO, AVN4CO, AVN5CO
760  FORMAT (T10, 1PE11.4, T29, E11.4, T47, E11.4, T65, E11.4, T81,
1     E11.4)
WRITE (6,770)
770  FORMAT (/, 10X, 'AVG# 6', 13X, 'AVG# 7', 12X, 'AVG# ION', 10X,
1     'AVG# ATCH')
WRITE (6,600) AVN6CO, AVN7CO, AVNICO, AVNACO
WRITE (6,780)
780  FORMAT (//, 27X, 'SWARM PARAMETERS (ALL AVERAGED)', /, 27X,
1     31(' '), //, 6X, 'TIME OF FLIGHT', 4X, 'FINAL ENERGY',
2     '(EV)', 6X, 'VELOCITY', 10X, 'XFINAL(M)', 7X, 'YFINAL(M)')
WRITE (6,760) AVGT, AVGEN, AVGV, AVGX, AVGY
WRITE (6,790)
790  FORMAT (/, 10X, 'ALPHA-PE', 11X, 'ALPHA-N2', 10X, 'ALPHA-CO2')
WRITE (6,650) ALPHE, ALPN2, ALPCO2
WRITE (6,800)
800  FORMAT (/, 10X, 'DRIFT-E', 12X, 'DRIFT-X', 11X, 'DRIFT-B')
WRITE (6,650) DRIFTE, DRIFTX, DRIFTB
WRITE (6,810)
810  FORMAT (//, 9X, 'COLL. FREQ', 10X, 'HALL PAR', 7X,
1     'MEAN FREE PATH')

```

C

```

WRITE (6,650) AVGNU, HALL, L
WRITE (6,820) KHEPRI, KN2PRI, KCOPRI, NIPRI
820  FORMAT (/, 2X, 91(' '), //, 8X, 'TOTAL NO. OF PRIMARY HE',
1     ' IONISATIONS = ', 15, /, 8X, 'TOTAL NO. OF PRIMARY',
2     ' N2 IONISATIONS = ', 15, /, 8X, 'TOTAL NO. OF',
3     ' PRIMARY CO2 IONISATIONS = ', 15, /, 8X, 44(' '), /,
4     'TOTAL NO. OF PRIMARY IONISATIONS', 5X, '= ', 15, /,
5     8X, 44(' '))

```

C

C WRITE DOWN THE AVERAGE TRANSVERSE DISCHARGE VELOCITY OF THE
C INDIVIDUAL GAS IONS AND THE OVERALL DISCHARGE VEL.

C

```

TNIHE = TNIHE - INEGHE
TNIN2 = TNIN2 - INEGN2
TNICO2 = TNICO2 - INEGCO
TNI = TNIHE + TNIN2 + TNICO2

```

C

```

WRITE (6,830) TNIHE, TNIN2, TNICO2, TNI

```



```

830  FORMAT (//, 8X, 'TOTAL NO. OF HE IONS = ', I5, /, 8X,
1      'TOTAL NO. OF N2 IONS = ', I5, /, 8X,
2      'TOTAL NO. OF CO2 IONS = ', I5, /, 8X, 30(' '), /, 8X,
3      'TOTAL NO. OF ALL IONS = ', I6, /, 8X, 30(' '))
      IF (TNIHE .GT. 0) GO TO 840
      AVGVHE = 0.0
      GO TO 850
840  AVGVHE = TOTVHE / TNIHE
850  IF (TNIN2 .GT. 0) GO TO 860
      AVGVN2 = 0.0
      GO TO 870
860  AVGVN2 = TOTVN2 / TNIN2
870  IF (TNICO2 .GT. 0) GO TO 880
      AVGVCO = 0.0
      GO TO 890
880  AVGVCO = TOTVCO / TNICO2
890  IF (TNI .GT. 0) GO TO 900
      AVGV = 0.0
      GO TO 910
900  AVGV = (TOTVHE + TOTVN2 + TOTVCO) / TNI
910  WRITE (6,920) AVGVHE, AVGVN2, AVGVCO, AVGV
920  FORMAT (//, 8X, 'AVERAGE VELOCITY OF HE IONS = ', E11.4, /,
1      8X, 'AVERAGE VELOCITY OF N2 IONS = ', E11.4, /, 8X,
2      'AVERAGE VELOCITY OF CO2 IONS = ', E11.4, /, 8X, 44(' '),
3      /, 8X, 'AVERAGE VELOCITY OF GAS MIXTURE = ', E11.4, /,
4      8X, 44(' '))
C
      WRITE (6,930)
930  FORMAT (//, 3X, 'THESE ARE THE ENERGY LEVELS AT VARIOUS ',
1      'POSITIONS IN THE CATHODE FALL REGION', /, 5X, 'E2', 6X,
2      'E4', 6X, 'E6', 6X, 'E8', 5X, 'E10', 5X, 'E12', 5X,
3      'E14', 5X, 'E16', 5X, 'E18', 5X, 'E20', 5X, 'E22')
C
      WRITE (6,940) (AENBAR(IB), IB=1,40)
940  FORMAT (4(10(2X,F6.2),/))
      WRITE (6,950) (INBAR(IB), IB=1,40)
950  FORMAT (/, 3X, 'THESE ARE THE NO. OF ELEMENTS OVER ',
1      'WHICH AVERAGING WAS DONE', 4(/, 10(2X,I6)))
C
      IF (AVGNHE .EQ. 0.0) GO TO 941
      AVN1HE = 100*AVN1HE/AVGNHE
      AVN2HE = 100*AVN2HE/AVGNHE
      AVN1HE = 100*AVN1HE/AVGNHE
C
941  IF (AVGNN2 .EQ. 0.0) GO TO 942
      AVN1N2 = 100*AVN1N2/AVGNN2
      AVN2N2 = 100*AVN2N2/AVGNN2
      AVN3N2 = 100*AVN3N2/AVGNN2
      AVN4N2 = 100*AVN4N2/AVGNN2
      AVN5N2 = 100*AVN5N2/AVGNN2
      AVN6N2 = 100*AVN6N2/AVGNN2
      AVN1N2 = 100*AVN1N2/AVGNN2
C
942  IF (AVGNCO .EQ. 0.0) GO TO 943
      AVN1CO = 100*AVN1CO/AVGNCO
      AVN2CO = 100*AVN2CO/AVGNCO

```

AVN3CO = 100*AVN3CO/AVGNCO
 AVN4CO = 100*AVN4CO/AVGNCO
 AVN5CO = 100*AVN5CO/AVGNCO
 AVN6CO = 100*AVN6CO/AVGNCO
 AVN7CO = 100*AVN7CO/AVGNCO
 AVNICO = 100*AVNICO/AVGNCO

C
 943 AVNEHE = 100.0 * (AVN1HE + AVN2HE + AVN3HE)
 AVNEN2 = 100.0 * (AVN1N2 + AVN2N2 + AVN3N2 + AVN4N2
 1 + AVN5N2 + AVN6N2 + AVN7N2)
 AVNECO = 100.0 * (AVN1CO + AVN2CO + AVN3CO + AVN4CO
 1 + AVN5CO + AVN6CO + AVN7CO + AVNICO)

C
 WRITE(6,951)AVNEHE,AVN1HE,AVN2HE,AVN3HE,AVNEN2,AVN1N2,
 1 AVN2N2,AVN3N2,AVN4N2,AVN5N2,AVN6N2,AVN7N2,
 2 AVNECO,AVNICO,AVN2CO,AVN3CO,AVN4CO,AVN5CO,
 3 AVN6CO,AVN7CO,AVNICO

951 FORMAT(1X, ' .91X, ' /, 10X, 'PERCENTAGE COLLISIONS WITH HELIUM',
 1 /, 5X, 4(F7.3,2X), /, 10X, 'PERCENTAGE COLLISIONS WITH N2',
 2 /, 5X, 8(F7.3,2X), /, 10X, 'PERCENTAGE COLLISIONS WITH CO2',
 3 /, 5X, 9(F7.3,2X))

960 CONTINUE

STOP
 END

C C
 SUBROUTINE INIT(X, Y, Z, VX, VY, VZ, PRESHE, PRESN2, PRESO, L)

C C

C

C This subroutine initialises the position and velocity of an electron as it leaves the cathode.

C

IMPLICIT REAL(A - H, O - Z)
 REAL LHEI, LN2I, LCO2I, L

C

C Initialise the position of electron to 0. Assume that the electron starts out with a z-component
 C of velocity with an energy distributed between 0 and 10 eV.

C

DATA EM /9.1D-31/
 CALL RANDOM(R1)
 X = 0.0
 Y = 0.0
 Z = 0.0
 VX = 0.0
 VY = 0.0
 VZ = SQRT(10.*1.6D-19*R1/EM)

C

C The mean free path of the electron is determined for any pressure.

C

LHEI = PRESHE / (105.33D-8 * 760.)
 LN2I = PRESN2 / (35.525D-8 * 760.)
 LCO2I = PRESO / (23.7D-8 * 760.)
 L = 1.0 / (LHEI + LN2I + LCO2I)
 RETURN
 END

C C

SUBROUTINE RANDOM(RAND)

C C

C
C This subroutine generates uniformly distributed random numbers between 0 and 1.

```

IMPLICIT REAL(A-H,O-Z)
REAL DSEED, R(1)
COMMON /ARRAND/ DSEED
SI = (7.**5) * DSEED
RI = 2.**31 - 1.
DSEED = AMOD(SI, RI)
RAND = DSEED / (2.**31)
RETURN
END

```

C C
SUBROUTINE ENERGY(VX, VY, VZ, VEL2, EN)
C C

C
C This subroutine calculates the electron energy in electron volts.

```

IMPLICIT REAL(A-H,O-Z)
DATA EM /9.1D-31/
VEL2 = VX * VX + VY * VY + VZ * VZ
EN = 0.5 * EM * VEL2
EN = EN / 1.6D-19
RETURN
END

```

C C
SUBROUTINE ACCEL(X, Y, Z, VX, VY, VZ, S, T, TIME, EN,*)
C C

C
C This subroutine calculates the acceleration of an electron due to the
C electric and magnetic field and also determines the new values of
C X, Y, Z positions and VX, VY, VZ velocities.

```

IMPLICIT REAL(A-H,O-Z)
REAL M, M2
COMMON /EDATA/ DC, VC, B0, MU, PRESS
DATA EM /9.1D-31/, QE /-1.6D-19/
W = QE * B0 / EM
M = SQRT((W*W) - ((2*QE*VC)/(EM*DC*DC)))
B = -((2*QE*VC)/(M*EM*DC)) * (1 - (Z/DC)) + (W*VY) / M
WB = W * B
M2 = M * M
CALL TIMER(X, Y, Z, VX, VY, VZ, S, T)
SINE = SIN(M*T)
COSINE = COS(M*T)
VXOLD = VX
VYOLD = VY
VZOLD = VZ
X = VX * T + X
Y = (W*VZOLD/M2) * (COSINE - 1.) + (WB/M2) * SINE + (VYOLD - (WB/
IM)) * T + Y
Z = (VZ/M) * SINE - (B/M) * (COSINE - 1.) + Z
VX = VXOLD
VY = -(W*VZOLD/M) * SINE + (WB/M) * (COSINE - 1.) + VYOLD
VZ = VZOLD * COSINE + B * SINE

```

C
TIME = TIME + T
CALL ENERGY(VX, VY, VZ, VEL2, EN)

C
 IF (Z .LT. 0.0 .OR. Z .GT. DC) GO TO 20
 10 RETURN
 20 RETURN 1
 END

C
 C C
 SUBROUTINE COLHE(X, Y, Z, VX, VY, VZ, EN, TIME,*)
 C C

C
 C The aim of this subroutine is to determine which of the following
 C types of collision is undergone by the electron.

- C (i) Elastic
 C (ii) Metastable triplet excitation) with excitation onset at 19.8 eV.
 C (iii) Excitation to 2nd level with onset at 21.5 eV.
 C (iv) Ionisation with onset at 24.5 eV.

C
 IMPLICIT REAL(A - H, O - Z)
 DIMENSION XIHE(100), YIHE(100), ZIHE(100), VXIHE(100), VYIHE(100),
 1 VZIHE(100), ENIHE(100), QHE(100,4), SPHE(101,81),
 2 EHE(3), TIHE(100)
 COMMON /XSECH/ QHE, SPHE, KIHE, K1HE, K2HE
 COMMON /ARRAND/ DSEED
 COMMON /CHEM/ XIHE, YIHE, ZIHE, VXIHE, VYIHE, VZIHE, ENIHE, TIHE
 DATA EM /9.1D-31/

C
 C Define the various excitation onset levels.

C
 EHE(1) = 19.8
 EHE(2) = 21.5
 EHE(3) = 24.5

C
 CALL ENERGY(VX, VY, VZ, VEL2, EN)
 VEL = SQRT(VEL2)
 IEN = EN
 ZZ = (EN - IEN) * 10.
 IF (ZZ .GE. 5) IEN = IEN + 1
 IF (EN .GE. 100) IEN = 100
 IF (IEN .LE. 1) IEN = 1
 SUMQ = QHE(IEN,2) + QHE(IEN,3) + QHE(IEN,4)
 CALL RANDOM(R2)
 DIVQ = SUMQ / QHE(IEN,1)

C
 C An elastic collision is assumed to occur if the random no. R2 is
 C greater than or equal to DIVQ.

C
 IF (R2 .GE. DIVQ) GO TO 50

C
 C In case of an inelastic collision determine which type it is.

C
 CHECK = 0.0
 J = 2
 10 CHECK = CHECK + (QHE(IEN,J)/QHE(IEN,1))
 IF (R2 .LT. CHECK) GO TO 20

C
 C If R2 is less than check this means that the level 'J' is excited.

C Otherwise check for level 'J+1'. ionisation occurs if $J = 4$.

C

$J = J + 1$

IF (J .EQ. 4) GO TO 40

GO TO 10

C

C Excitation to a higher level occurs.

C

20 JK = J - 1

EN = EN * EHE(JK)

C

IF (JK .NE. 1) GO TO 30

K1HE = K1HE + 1

GO TO 50

C

30 K2HE = K2HE + 1

GO TO 50

C

C Ionisation occurs.

C

40 EN = (EN * EHE(3)) / 2.0

C

C Store the position and velocity of ionised electrons. KI denotes the

C number of ionised electrons.

C

CALL NEWVEL(KIHE, VXIHE, VYIHE, VZIHE, XIHE, YIHE, ZIHE, ENIH

1 Y, Z, EN)

TIHE(KIHE) = TIME

50 IFLAG = 1

CALL NEWSTA(EN, X, Y, Z, VX, VY, VZ, IFLAG, &60)

C

60 RETURN 1

END

C

..... C

SUBROUTINE COLN2(X, Y, Z, VX, VY, VZ, EN, TIME,*)

..... C

C

C The aim of this subroutine is to determine which of the following

C types of collision is undergone by the electron with N2.

C

(i) Elastic

C

(ii) Vibrational excitation

C

(iii) Excitation to 6.22ev level

C

(iv) Excitation to 7.39ev level

C

(v) Excitation to 8.59ev level

C

(vi) Excitation to 17.1ev level

C

(vii) Ionisation with onset at 15.7 eV.

C

(viii) Diss. ions. with onset at 25.0 eV.

C

IMPLICIT REAL(A - H,O - Z)

DIMENSION XIHE(100), YIHE(100), ZIHE(100), VXIHE(100), VYIHE(100),

1 VZIHE(100), ENIHE(100), QHE(100,4), SPHE(101,81),

2 EHE(3), TIHE(100), SPN2(101,81), QN2(100,8),

3 SPCO2(101,81), QCO2(100,10)

COMMON /XSEC/ SPHE, QHE, SPN2, QN2, SPCO2, QCO2

COMMON /ARRAND/ DSEED

```
COMMON /CHE/ XIHE, YIHE, ZIHE, VXIHE, VYIHE, VZIHE, ENIHE, TIHE,
1 K1HE, K2HE, KIHE
DATA EM /9.1D-31/
```

C

C Define the various excitation onset levels.

```
EHE(1) = 19.8
```

```
EHE(2) = 21.5
```

```
EHE(3) = 24.5
```

C

```
CALL ENERGY(VX, VY, VZ, VEL2, EN)
```

```
VEL = SQRT(VEL2)
```

```
IEN = EN
```

```
ZZ = (EN - IEN) * 10.
```

```
IF (ZZ .GE. 5) IEN = IEN + 1
```

```
IF (EN .GE. 100) IEN = 100
```

```
IF (IEN .LE. 1) IEN = 1
```

```
SUMQ = QHE(IEN,2) + QHE(IEN,3) + QHE(IEN,4)
```

```
CALL RANDOM(R2)
```

```
DIVQ = SUMQ / QHE(IEN,1)
```

C

C An elastic collision is assumed to occur if the random no. R2 is

C greater than or equal to DIVQ.

```
IF (R2 .GE. DIVQ) GO TO 50
```

C In case of an inelastic collision determine which type it is.

C

```
CHECK = 0.0
```

```
J = 2
```

```
10 CHECK = CHECK + (QHE(IEN,J)/QHE(IEN,1))
```

```
IF (R2 .LT. CHECK) GO TO 20
```

C

C If R2 is less than check this means that the level 'J' is excited.

C Otherwise check for level 'j+1'. Ionisation occurs if j = 4.

C

```
J = J + 1
```

```
IF (J .EQ. 4) GO TO 40
```

```
GO TO 10
```

C

C Excitation to a higher level occurs.

C

```
20 JK = J - 1
```

```
EN = EN - EHE(JK)
```

C

```
IF (JK .NE. 1) GO TO 30
```

```
K1HE = K1HE + 1
```

```
GO TO 50
```

C

```
30 K2HE = K2HE + 1
```

```
GO TO 50
```

C

C Ionisation occurs.

```
40 EN = (EN - EHE(3)) / 2.0
```

C

C Store the position and velocity of ionised electrons. KI denotes the

C number of ionised electrons.

```

CALL NEWVEL(KIHE, VXIHE, VYIHE, VZIHE, XIHE, YIHE, ZIHE, ENIHE, X,
1  Y, Z, EN)
TIME(KIHE) = TIME
50 IFLAG = 1
CALL NEWSTA(EN, X, Y, Z, VX, VY, VZ, IFLAG, *60)
C
60 RETURN 1
END
C ..... C
SUBROUTINE COLN2(X, Y, Z, VX, VY, VZ, EN, TIME, *)
C ..... C
C
C The aim of this subroutine is to determine which of the following
C types of collision is undergone by the electron with n2.
C (i) Elastic
C (ii) Vibrational excitation
C (iii) Excitation to 6.22ev level
C (iv) Excitation to 7.39ev level
C (v) Excitation to 8.59ev level
C (vi) Excitation to 11.1ev level
C (vii) Ionisation with onset at 15.7 eV.
C (viii) Diss. Ionis. with onset at 25.0 eV.
C
C
C IMPLICIT REAL*8 (D-Z)
DIMENSION XIN2(100), YIN2(100), ZIN2(100), VXIN2(100), VYIN2(100),
1  VZIN2(100), ENIN2(100), X6N2(100), Y6N2(100), Z6N2(100),
2  VX6N2(100), VY6N2(100), VZ6N2(100), EN6N2(100), EN2(7),
3  TIN2(100), SPHE(101,81), QHE(100,4), SPN2(101,81),
4  QN2(100,8), SPCO2(101,81), QCO2(100,10)
C
COMMON /XSEC/ SPHE, QHE, SPN2, QN2, SPCO2, QCO2
COMMON /ARRAND/ DSEED*
COMMON /CN2/ XIN2, YIN2, ZIN2, VXIN2, VYIN2, VZIN2, ENIN2, TIN2,
1  X6N2, Y6N2, Z6N2, VX6N2, VY6N2, VZ6N2, EN6N2,
2  K1N2, K2N2, K3N2, K4N2, K5N2, K6N2, K1N2
DATA EM /9.1D-31/
C
C Define the various excitation onset levels.
EN2(1) = 1.5
EN2(2) = 6.22
EN2(3) = 7.39
EN2(4) = 8.59
EN2(5) = 11.1
EN2(6) = 15.7
EN2(7) = 25.0
C
CALL ENERGY(VX, VY, VZ, VEL2, EN)
VEL = SQRT(VEL2)
IEN = EN
ZZ = (EN - IEN) * 10.
IF (ZZ .GE. 5) IEN = IEN + 1
IF (EN .GE. 100) IEN = 100
IF (IEN .LE. 1) IEN = 1
SUMQ = QN2(IEN,2) + QN2(IEN,3) + QN2(IEN,4) + QN2(IEN,5) + QN2(
1IEN,6) + QN2(IEN,7) + QN2(IEN,8)
CALL RANDOM(R2)

```

$$DIVQ = SUMQ / QN2(IEN,1)$$

C
C An elastic collision is assumed to occur if the random no. R2 is
C greater than or equal to DIVQ.

C
C IF (R2 .GE. DIVQ) GO TO 110

C
C In case of an inelastic collision determine which type it is.

C
C CHECK = 0.0

C J = 2

C 10 CHECK = CHECK + (QN2(IEN,J)/QN2(IEN,1))

C IF (R2 .LT. CHECK) GO TO 20

C
C If R2 is less than CHECK this means that the level 'J' is excited.

C Otherwise check for level 'J+1'. Ionisation occurs if J = 7. Diss.

C Ionisation occurs if J=8.

C
C J = J + 1

C IF (J .EQ. 8) GO TO 20

C GO TO 10

C
C Excitation to a higher level occurs.

C
C 20 JK = J - 1

C IF (JK .EQ. 6 .OR. JK .EQ. 7) GO TO 30

C EN = EN - EN2(JK)

C GO TO 40

C 30 EN = (EN - EN2(JK)) / 2.

C GO TO 90

C
C 40 IF (JK .NE. 1) GO TO 50

C K1N2 = K1N2 + 1

C GO TO 110

C 50 IF (JK .NE. 2) GO TO 60

C K2N2 = K2N2 + 1

C GO TO 110

C 60 IF (JK .NE. 3) GO TO 70

C K3N2 = K3N2 + 1

C GO TO 110

C 70 IF (JK .NE. 4) GO TO 80

C K4N2 = K4N2 + 1

C GO TO 110

C 80 IF (JK .NE. 5) GO TO 90

C K5N2 = K5N2 + 1

C GO TO 110

C 90 IF (JK .NE. 6) GO TO 100

C CALL NEWVEL(KIN2, VXIN2, VYIN2, VZIN2, XIN2, YIN2, ZIN2, ENIN2, X,

C 1 Y, Z, EN)

C TIN2(KIN2) = TIME

C GO TO 110

C
C Dissociative ionisation occurs. K6 denotes the number of
C dissociative-ionised atoms of N2. Store the position and
C velocity of ionised electrons.

C


```
100 CALL NEWVEL(K6N2, VX6N2, VY6N2, VZ6N2, X6N2, Y6N2, Z6N2, EN6N2, X,
1 Y, Z, EN)
```

```
110 IFLAG = 2
```

```
CALL NEWSTA(EN, X, Y, Z, VX, VY, VZ, IFLAG, *120)
```

C

```
120 RETURN 1
```

```
END
```

C

```
..... C
SUBROUTINE COLCO2(X, Y, Z, VX, VY, VZ, EN, TIME*, *)
```

C

C

C The aim of this subroutine is to determine which of the following

C types of collision is undergone by the electron.

C

(i) Elastic

C

(ii) Vibrational excitation.

C

(iii) Excitation to 3.1 eV level.

C

(iv) Excitation to 6.1 eV level.

C

(v) Excitation to 7.0 eV level.

C

(vi) Excitation to 10.5 eV level.

C

(vii) Excitation to 11.5 eV level.

C

(viii) Ionisation with onset at 13.3 eV.

C

(ix) Diss. ions. with onset at 25.0 eV.

C

(x) Diss. attach. with onset at 3.0 eV.

C

```
IMPLICIT REAL(A - H, O - Z)
```

```
DIMENSION XICO2(100), YICO2(100), ZICO2(100), VXICO2(100),
```

```
1 YYICO2(100), VZICO2(100), ENICO2(100), X7CO2(100),
```

```
2 Y7CO2(100), Z7CO2(100), VX7CO2(100), VY7CO2(100),
```

```
3 VZ7CO2(100), EN7CO2(100), ECO2(9), TICO2(100),
```

```
4 SPHE(101,81), QHE(100,4), SPN2(101,81), QN2(100,8),
```

```
5 SPCO2(101,81), QCO2(100,10)
```

```
COMMON /XSEC/ SPHE, QHE, SPN2, QN2, SPCO2, QCO2
```

```
COMMON /ARRAND/ DSEED
```

```
COMMON /CCO2/ XICO2, YICO2, ZICO2, VXICO2, YYICO2, VZICO2, ENICO2,
```

```
1 X7CO2, Y7CO2, Z7CO2, VX7CO2, VY7CO2, VZ7CO2, EN7CO2,
```

```
2 TICO2, K1CO2, K2CO2, K3CO2, K4CO2, K5CO2, K6CO2, K7CO2,
```

```
3 K1CO2, K4CO2
```

```
DATA EM /9-AD-31/
```

C

C Define the various excitation onset levels.

```
ECO2(1) = 0.0
```

```
ECO2(2) = 3.1
```

```
ECO2(3) = 6.1
```

```
ECO2(4) = 7.0
```

```
ECO2(5) = 10.5
```

```
ECO2(6) = 11.5
```

```
ECO2(7) = 13.3
```

```
ECO2(8) = 25.0
```

```
ECO2(9) = 3.0
```

C

```
CALL ENERGY(VX, VY, VZ, VEL2, EN)
```

```
VEL = SQRT(VEL2)
```

```
IEN = EN
```

```
ZZ = (EN - IEN) * 10.
```

```
IF (ZZ .GE. 5) IEN = IEN + 1
```

```
IF (EN .GE. 100) IEN = 100
```

```

IF (IEN .LE. 1) IEN = 1
SUMQ = QCO2(IEN,2) + QCO2(IEN,3) + QCO2(IEN,4) + QCO2(IEN,5) +
IQCO2(IEN,6) + QCO2(IEN,7) + QCO2(IEN,8) + QCO2(IEN,9) + QCO2(IEN,
210)

```

```
CALL RANDOM(R2)
```

```
DIVQ = SUMQ / QCO2(IEN,1)
```

C
C An elastic collision is assumed to occur if the random no. R2 is
C greater than or equal to DIVQ.

```
IF (R2 .GE. DIVQ) GO TO 130
```

C
C In case of an inelastic collision determine which type it is.

```
CHECK = 0.0
```

```
J = 2
```

```
10 CHECK = CHECK + (QCO2(IEN,J)/QCO2(IEN,1))
```

```
IF (R2 .LT. CHECK) GO TO 20
```

C
C If R2 is less than CHECK this means that the level 'j' is excited.
C Otherwise check for level 'j+1'. Ionisation occurs if j = 8. Diss.
C ionisation occurs if j=9. Diss. att. occurs if j=10.

```
J = J + 1
```

```
IF (J .EQ. 10) GO TO 20
```

```
GO TO 10
```

C
C Excitation to a higher level occurs.

```
20 JK = J - 1
```

```
IF (JK .EQ. 7 .OR. JK .EQ. 8) GO TO 30
```

```
EN = EN * ECO2(JK)
```

```
GO TO 40
```

```
30 EN = (EN * ECO2(JK)) / 2.
```

```
GO TO 110
```

C
40 IF (JK .NE. 1) GO TO 50

```
K1CO2 = K1CO2 + 1
```

```
GO TO 130
```

50 IF (JK .NE. 2) GO TO 60

```
K2CO2 = K2CO2 + 1
```

```
GO TO 130
```

60 IF (JK .NE. 3) GO TO 70

```
K3CO2 = K3CO2 + 1
```

```
GO TO 130
```

70 IF (JK .NE. 4) GO TO 80

```
K4CO2 = K4CO2 + 1
```

```
GO TO 130
```

80 IF (JK .NE. 5) GO TO 90

```
K5CO2 = K5CO2 + 1
```

```
GO TO 130
```

90 IF (JK .NE. 6) GO TO 100

```
K6CO2 = K6CO2 + 1
```

```
GO TO 130
```

100 IF (JK .NE. 10) GO TO 110

```
KACO2 = KACO2 + 1
```

```

GO TO 150
110 IF (JK .NE. 7) GO TO 120
    CALL NEWVEL(KICO2, VXICO2, VYICO2, VZICO2, XICO2, YICO2, ZICO2,
    1 ENICO2, X, Y, Z, EN)
    TICO2(KICO2) = TIME
    GO TO 130
C
C Dissociative Ionisation occurs. K7 denotes the number of
C dissociative-ionised atoms of CO2. Store the position and
C velocity of ionised electrons.
C
120 CALL NEWVEL(K7CO2, VX7CO2, VY7CO2, VZ7CO2, X7CO2, Y7CO2, Z7CO2,
    1 EN7CO2, X, Y, Z, EN)
130 IFLAG = 3
    CALL NEWSTA(EN, X, Y, Z, VX, VY, VZ, IFLAG, *140)
C
140 RETURN 1
150 RETURN 2
    END
C ..... C
    SUBROUTINE NEWVEL(KI, VXI, VYI, VZI, XI, YI, ZI, ENI, X, Y, Z, EN)
C ..... C
C
C This subroutine calculates the velocity components of the
C secondary electron created by an excitation collision.
C
    IMPLICIT REAL(A - H,O - Z)
    DIMENSION VXI(100), VYI(100), VZI(100), ENI(100), XI(100),
    1 YI(100), ZI(100)
    COMMON /ARRAND/ DSEED
    DATA EM /9.1D-31/
    KI = KI + 1
    IF (EN .LE. 0.0) EN = 0
    CONST = 2.0 * EN * 1.6E-19 / EM
    CALL RANDOM(R1)
    CALL RANDOM(R2)
    CALL RANDOM(R3)
    RTOT = R1 + R2 + R3
    VXI(KI) = SQRT(CONST*R1/RTOT)
    VYI(KI) = SQRT(CONST*R2/RTOT)
    VZI(KI) = SQRT(CONST*R3/RTOT)
    CALL RANDOM(R11)
    CALL RANDOM(R21)
    CALL RANDOM(R31)
    IF (R11 .GE. 0.5) VXI(KI) = -VXI(KI)
    VXI(KI) = -VXI(KI)
    IF (R21 .GE. 0.5) VYI(KI) = -VYI(KI)
    VYI(KI) = -VYI(KI)
    IF (R31 .GE. 0.5) VZI(KI) = -VZI(KI)
    VZI(KI) = -VZI(KI)
    XI(KI) = X
    YI(KI) = Y
    ZI(KI) = Z
    ENI(KI) = EN
    RETURN
    END

```

```

C ..... C
C   SUBROUTINE NEWSTA(EN, X, Y, Z, VX, VY, VZ, IFLAG,*)
C ..... C
C
C The aim of this subroutine is to determine the state of the electron
C after a collision has occurred. Two random numbers R3 and R4 are used
C to determine the angles THETA and PHI respectively.
C
  IMPLICIT REAL(A - H,O - Z)
  DIMENSION SPHE(101,81), QHE(100,4), SPN2(101,81), QN2(100,8),
1     SPCO2(101,81), QCO2(100,10)
  COMMON /ARRAND/ DSEED
  COMMON /XSEC/ SPHE, QHE, SPN2, QN2, SPCO2, QCO2
  DATA EM /9.1D-31/
  CALL RANDOM(R3)
  Y1 = R3 / 0.0125
  IIX = X1
  IIX = (X1 - IIX) * 10.
  IF (Y1 .GE. 5) IIX = IIX + 1
  IIX = IIX + 1
  IEN = EN
  Z1 = (EN - IEN) * 10.
  IF (Z1 .GE. 5) IEN = IEN + 1
  IEN = IEN + 1
  IF (EN .GE. 101.) IEN = 101
  IF (IEN .LE. 1) IEN = 1
  IF (EN .LE. 0) EN = 0.00001
C
  IF (IFLAG .GE. 2) GO TO 10
  THETAC = SPHE(IEN,IIX) * 3.1415927 / 180.0
  GO TO 30
10 IF (IFLAG .EQ. 3) GO TO 20
  THETAC = SPN2(IEN,IIX) * 3.1415927 / 180.0
  GO TO 30
20 THETAC = SPCO2(IEN,IIX) * 3.1415927 / 180.0
C
30 CALL RANDOM(R4)
  PHIC = 2. * 3.1415927 * R4
  V1 = SQRT(VX*VX + VY*VY + VZ*VZ)
  V = SQRT(2. * EN * 1.6D-19 / EM)
  IF (V1 .EQ. 0.0) GO TO 40
  VZ11 = VZ / V1
  IF (VZ11 .GE. 1.0) VZ11 = 1.0
  THETA1 = ACOS(VZ11)
  GO TO 50
40 THETA1 = 0.0
50 PHII = FCNPHI(VX,VY)
  SINPI = SIN(PHII)
  COSPI = COS(PHII)
  SINPC = SIN(PHIC)
  COSPC = COS(PHIC)
  SINTI = SIN(THETA1)
  COSTI = COS(THETA1)
  SINTC = SIN(THETAC)
  COSTC = COS(THETAC)
  VX = V * (COSPI * COSTI * SINTC * COSPC - SINPI * SINTC * SINPC

```

```

1      + COSP1*SINT1*COSTC)
VY = V * (SINP1*COST1*SINTC*COSP1C + COSP1*SINT1*SIN1C
1      + SINP1*SINT1*COSTC)
VZ = V * (-SINT1*SINTC*COSP1C + COST1*COSTC)
RETURN 1
END

```

C

FUNCTION FCNPHI(VX, VY)

C

C

C FCNPHI calculates angle PHII (initial angle PHI) which the
C velocity vector just before collision makes on the X-Y plane
C with the X-axis.

C

```

IMPLICIT REAL(A-H,Q-Z)
IF (VX .EQ. 0.0) THEN
  IF (VY .GT. 0.0) THEN
    FCNPHI = 3.1415927/2.0
  ELSE
    FCNPHI = 3*3.1415927/2.0
  ENDIF
ELSE
  IF (VX .GT. 0.0) THEN
    FCNPHI = ATAN(VY/VX)
  ELSE
    FCNPHI = 3.1415927 + ATAN(VY/VX)
  ENDIF
ENDIF
RETURN
END

```

C

C

SUBROUTINE TIMER(X, Y, Z, VX, VY, VZ, S, T)

C

```

IMPLICIT REAL(A-H,O-Z)
REAL M, MU(19)
EXTERNAL F
COMMON /EDATA/ DC, VC, B0, MU, PRESS
COMMON /PARS/ A0, A1, A2, A3, A4, A5
DATA EM / 0.1D-31/, QE / -1.6D-19/
W = QE * H * EM
M = SQRT((W*W) - ((2*QE*VC)/(EM*DC*DC)))
B1 = -((2*QE*VC)/(M*EM*DC)) * (1 - (Z/DC)) + (W*VY) / M
WB = W * B1
DELTA = S
V = SQRT(VX*VX + VY*VY + VZ*VZ)
T = S / 1.33E6
IF (V .NE. 0.0) T = S / V
A0 = VX
A1 = -W * VZ / M
A2 = WB / M
A3 = VY
A4 = VZ
A5 = B1
A = 0.0
ACC = 1.0E-5

```

```

DXMAX = 3.0
USUM = S * M
B = M * X
CALL UNSIMP(F, A, B, ACC, USUM, ERROR, AREA, DXMAX, IFLAG)
B = B + ERROR
T = B / M
C      IFLAG = 1 for normal return.
C      = 2 if it is necessary to go to 30 levels or use a sub-
C      interval too small for machine word length. Error
C      may be unreliable in this case.
C      = 3 if more than 5000 function evaluations are
C      used. Rough approximations are used to complete
C      the computations and error is usually unreliable.
C      = 4 if the algorithm fails due to f(x) being
C      predominantly negative on some sub-interval.
      IF (IFLAG .EQ. 1) GO TO 30
      WRITE (6,10)
10  FORMAT (1X, 'IFLAG = 1 ----> NORMAL RETURN', /, 1X,
1     'IFLAG = 2 ----> NECESSARY TO GO TO 40 LEVELS OR USE A', /
2     '17X, 'SUB-INTERVAL TOO SMALL FOR MACHINE WORD', /, 17X,
3     'LENGTH. THE ANSWER RETURNED IS NOT CORRECT.', /, 1X,
4     'IFLAG = 3 ----> MORE THAN 5000 FUNCTION EVALUATIONS', /,
5     '1X, 'IFLAG = 4 ----> F(X) IS PREDOMINANTLY NEGATIVE ON', 1X,
6     'SOME SUB-INTERVAL')
      WRITE (6,20) IFLAG
20  FORMAT (1X, 'IFLAG = ', 14)
C      STOP
30  RETURN
      END
C ..... C
      FUNCTION F(X)
C ..... C
      IMPLICIT REAL(A - H,O - Z)
      COMMON /PARS/ A0, A1, A2, A3, A4, A5
      COSX = COS(X)
      SINX = SIN(X)
      Z1 = A0
      Z2 = (A1*SINX + A2*(COSX - 1.) + A3) ** 2
      Z3 = (A4*COSX + A5*SINX) ** 2
      F = SQRT(Z1 + Z2 + Z3)
      RETURN
      END
C ..... C
      SUBROUTINE UNSIMP(F, A, B, ACC, USUM, ERROR, AREA, DXMAX, IFLAG)
C ..... C
C
C  UNSIMP is an adaptive, iterative code based on Simpson's rule.
C  It is designed to evaluate the upper limit of integration required
C  to make the definite integral of a continuous non-negative function
C  close to a user specified sum.
C
C
C  F ---- Name of function to be integrated. The
C          function name f must appear in an external state-
C          ment in the calling program.
C

```

C A --- Lower limit of integration.
 C B --- Upper limit of integration. On entry this is set
 C to initialize the search. UNSIMP will search
 C for the upper limit which makes the definite
 C integral close to usum, the value
 C specified by the user. computation will be quicker
 C if the initial value of b given to the routine is an
 C underestimation.
 C ACC --- The desired accuracy of the final upper limit (B).
 C The code tries to make the error in B less than
 C $ACC * B$.
 C USUM --- The user-specified value of the integral of $f(x)$.
 C ERROR --- Estimated error of B. User may wish to extrapolate
 C by forming $B + ERROR$ to get what is often a more
 C accurate result, but not always.
 C AREA --- The calculated integral of $f(x)$ from $x=A$ to $x=B$,
 C where B represents the final value of B.
 C
 C DXMAX --- The maximum limit on the width of a
 C sub-interval to be used to yield
 C an acceptable value of the integral. For
 C periodic functions, DXMAX should be set
 C to the period (or smaller) to prevent
 C undesirable termination of the algorithm
 C in case of premature convergence of
 C Simpson's rule.
 C
 C IFLAG = 1 for normal return.
 C = 2 if it is necessary to go to 40 levels or use a sub-
 C interval too small for machine word length,
 C the answer returned is not correct.
 C = 3 if more than than 5000 function evaluations are
 C used.
 C the answer returned is not correct.
 C = 4 if the algorithm fails due to $f(x)$ being
 C predominantly negative on some sub-interval.
 C the answer returned is not correct.

DIMENSION LORR(40), FIT(40), F2T(40), F3T(40), DAT(40), ESIT(40),
 1 PSUM(40)
 REAL F, FIT, F2T, F3T, DAT, ESIT, PSUM, ACC, ALPHA, DA, D, A, B,
 1 EST, ESTL, ESTR, WT, DELSUM, USUM, SUM, AREA, PAREA, ERROR,
 2 DXMAX, PDIFF, DIFF, FV1, FV2, FV3, FV4, FV5, B2

C Set U to approximate the unit round-off of specific machine.
 C Here IBM 360/370 real.

C
 U = 2.220E-16
 FOURU = 4.0 * U
 IFLAG = 1
 KOUNT = 3
 LVL = 1
 PSUM(LVL) = 0.0
 ALPHA = A
 PAREA = 0.0

```

    PDIFF = 0.
C
10 LORR(LVL) = 1
    DA = B * ALPHA
    FV1 = F(ALPHA)
    FV3 = F(ALPHA + 0.5 * DA)
    FV5 = F(ALPHA + DA)
    WT = DA / 6.0
    EST = WT * (FV1 + 4.0 * FV3 + FV5)
C
C 'Basic Step'. Have estimate EST of integral on (ALPHA, ALPHA+DA)
C bisection and compute estimates on left and right half intervals.
C
    20 DX = 0.5 * DA
    FV2 = F(ALPHA + 0.5 * DX)
    FV4 = F(ALPHA + 1.5 * DX)
    KOUNT = KOUNT + 2
    WT = DX / 6.0
    ESTL = WT * (FV1 + 4.0 * FV2 + FV3)
    ESTR = WT * (FV3 + 4.0 * FV4 + FV5)
    SUM = ESTL + ESTR
    DIFF = EST - SUM
C
C If error is acceptable, go to 80. If interval is too small or
C too many levels or too many function evaluations, set a flag
C and go to 80 anyway.
C
    IF (SUM .LT. 0.) GO TO 110
    AREA = PAREA + SUM
    B2 = ALPHA + DA
    IF (ABS(ABS(USUM - AREA) * ABS(PDIFF)) + ABS(DIFF)) .GT. FV5 * ACC *
    (B2 - A)) GO TO 30
    ERROR = (USUM - AREA * (PDIFF + DIFF) / 15) / FV5
    B = B2
    RETURN
30 IF (ABS(USUM - AREA) .LE. ABS(PDIFF + DIFF)) GO TO 50
    IF (USUM .GT. AREA) GO TO 40
    PSUM(1) = PAREA
    LVL = 1
    LORR(LVL) = 1
    GO TO 50
40 IF (ABS(DIFF) .LE. FV5 * ACC * DA .AND. DA .LE. DXMAX) GO TO 60
50 IF (LVL .GE. 40) GO TO 90
    IF (ABS(DX) .LE. FOUR * ABS(ALPHA)) GO TO 90
    IF (KOUNT .GE. 5000) GO TO 100
C
C Here to raise level. Store information to process right half
C interval later. Initialise for 'basic step' so as to treat
C left half interval.
C
    LVL = LVL + 1
    SUM(LVL) = 0.
    LORR(LVL) = 0
    FIT(LVL) = FV3
    F2T(LVL) = FV4
    F3T(LVL) = FV5

```



```

DA = DX
DAT(LVL) = DX
EST = ESTL
ESTT(LVL) = ESTR
FV5 = FV3
FV3 = FV2
GO TO 20
C
C Accept approximate integral sum. If it was on a left interval go to 'move right'. If a right interval,
add results
C to finish at this level. Array LORR (mnemonic for left or
C right) tells whether left or right interval at each level.
C
60 PDIFF = PDIFF + DIFF
70 IF (LORR(LVL) .EQ. 0) GO TO 80
SUM = PSUM(LVL) + SUM
PAREA = PAREA + PSUM(LVL)
LVL = LVL - 1
IF (LVL .GE. 1) GO TO 70
LVL = 1
PSUM(LVL) = SUM
PAREA = SUM
ALPHA = ALPHA + DA
B = 2 * B - A
GO TO 10
C
C 'Move right'. Restore saved information to process right
C half interval.
C
80 PSUM(LVL) = SUM
PAREA = PAREA + SUM
LORR(LVL) = 1
ALPHA = ALPHA + DA
DA = DAT(LVL)
FV1 = FIT(LVL)
FV3 = F2T(LVL)
FV5 = F3T(LVL)
ES1 = ESTT(LVL)
GO TO 20
C
C Accept 'poor' value. Set appropriate flags.
C
90 IFLAG = 2
RETURN
100 IFLAG = 3
RETURN
110 IFLAG = 4
RETURN
END
C
C ..... C
C SUBROUTINE VELHE(11, 12, INEGHE, YIHE, ZIHE, TIHE, TOTVHE)
C ..... C
C
C This program calculates the discharge velocity
C (due to the Hall force) of the helium gas

```

```

C component in a laser gas mixture.
C
REAL MUHE, MU(19), YIHE(100), ZIHE(100), TIHE(100)
COMMON /EDATA/ DC, VC, BO, MU, PRESS
C
DO 60 I = 11, 12
  EHE = (2*VC/DC) * (1 - (ZIHE(I)/DC))
  IF (EHE .EQ. 0) GO TO 50
  EDIVP = EHE / PRESS
  IE = EDIVP / 1000
C
  IF (IE .GE. 1) GO TO 10
  MUHE = 0.85
  GO TO 40
10 IF (IE .GT. 10) GO TO 20
  MUHE = MU(IE)
  GO TO 40
20 IF (IE .GE. 100) GO TO 30
  IE = (IE/10.) + 9
  MUHE = MU(IE)
  GO TO 40
30 MUHE = 0.16
C
40 TIONHE = ZIHE(I) / (MUHE*EHE)
  TOTTHE = TIONHE + TIHE(I)
  HEVEL = YIHE(I) / TOTTHE
  TOTVHE = TOTVHE + HEVEL
  GO TO 60
50 INEGHE = INEGHE + 1
60 CONTINUE
C
RETURN
END

```

```

C
C ..... C
SUBROUTINE VELN2(11, 12, INEGN2, YIN2, ZIN2, TIN2, TOTVN2)
C ..... C

```

```

C This program calculates the discharge velocity
C (due to the Hall force) of the nitrogen gas
C component in a laser gas mixture.
C
REAL MUN2, MU(19), YIN2(100), ZIN2(100), TIN2(100)
COMMON /EDATA/ DC, VC, BO, MU, PRESS
C
DO 20 I = 11, 12
  EN2 = (2*VC/DC) * (1 - (ZIN2(I)/DC))
  IF (EN2 .EQ. 0) GO TO 10
C
  MUN2 = 0.2
  TIONN2 = ZIN2(I) / (MUN2*EN2)
  TOTTN2 = TIONN2 + TIN2(I)
  N2VEL = YIN2(I) / TOTTN2
  TOTVN2 = TOTVN2 + N2VEL
  GO TO 20
10 INEGN2 = INEGN2 + 1

```

20 CONTINUE

C

RETURN
END

C

C

..... C
SUBROUTINE VELCO2(11, 12, INEGCO, YICO2, ZICO2, TICO2, TOTVCO)
..... C

C

C

C

C

C

This program calculates the discharge velocity
(due to the Hall force) of the carbon-dioxide gas
component in a laser gas mixture.

C

REAL MUCO2, MU(19), YICO2(100), ZICO2(100), TICO2(100)
COMMON /EDATA/ DC, VC, B0, MU, PRESS

C

C

DO 20 I = 11, 12
ECO2 = (2.*VC/DC) * (1 - (ZICO2(I)/DC))
IF (ECO2 .EQ. 0) GO TO 10

C

MUCO2 = 0.073
TIONCO = ZICO2(1) / (MUCO2*ECO2)
TOTTCO = TIONCO + TICO2(1)
CO2VEL = YICO2(1) / TOTTCO
TOTVCO = TOTVCO + CO2VEL
GO TO 20

10 INEGCO = INEGCO + 1

20 CONTINUE

C

RETURN
END